Durham E-Theses

Seismic analysis of silica diagenetic boundaries: the North Sakhalin basin, Russian far east.

Meadows, David

How to cite:

Meadows, David (2009) *Seismic analysis of silica diagenetic boundaries: the North Sakhalin basin, Russian far east.*, Durham theses, Durham University. Available at Durham E-Theses Online: http://etheses.dur.ac.uk/1955/

Use policy

The full-text may be used and/or reproduced, and given to third parties in any format or medium, without prior permission or charge, for personal research or study, educational, or not-for-profit purposes provided that:

- a full bibliographic reference is made to the original source
- a link is made to the metadata record in Durham E-Theses
- the full-text is not changed in any way

The full-text must not be sold in any format or medium without the formal permission of the copyright holders.

Please consult the full Durham E-Theses policy for further details.

Academic Support Office, Durham University, University Office, Old Elvet, Durham DH1 3HP
e-mail: e-theses.admin@dur.ac.uk Tel: +44 0191 334 6107
http://etheses.dur.ac.uk

Seismic Analysis of Silica Diagenetic Boundaries: The North Sakhalin Basin, Russian Far East

David Meadows

Department of Earth Sciences

Durham University

The copyright of this thesis rests with the author or the university to which it was submitted. No quotation from it, or information derived from it may be published without the prior written consent of the author or university, and any information derived from it should be acknowledged.

ıbmitted to the University of Durham in partial fulfilment of the requirements for the degree of Doctor of Philosophy

2009

1 3 AUG 2009

BEST COPY AVAILABLE

Variable print quality

CONTAINS DISKETTE

Text cut off in original

Summary

The transformation of biogenic silica (opal-A) to cryptocrystalline opal-CT (cristobalite and tridymite) and subsequent transition of opal-CT to quartz are important diagenetic reactions that may occur in siliceous sediments within many sedimentary basins worldwide. These diagenetic transitions are basin-scale features and can have areal extents of $10^4 - 10^5$ km^2. These reactions can have a significant effect on the physical properties, especially porosity, seismic velocity and density, of the host sediment. The role played by silica diagenesis within sedimentary basins is poorly understood, but it is becoming apparent that these reactions could have significant implications for basin analysis in terms of the sedimentological and deformational history of the basin as well as for hydrocarbon exploration.

Seismic reflection data reveal two silica diagenetic boundaries located in the North Sakhalin Basin (NSB), offshore Sakhalin Island in the Russian Far East. These boundaries form distinctive high-amplitude seismic reflections that predominantly cross-cut Miocene stratigraphy. The boundaries represent the opal-A to opal-CT transition and the subsequent deeper opal-CT to quartz transition and cover an area of ~ 107000 km^2. The reflections represent diagenetic reaction fronts that advance through silica-rich host sediments during burial. The diagenetic boundaries develop a variety of morphologies. In the NSB these front geometries are probably the result of the interference of the diagenetic fronts with inclined and folded stratigraphy together with lateral changes in the composition and, therefore, depth of transformation of the sediment. This thesis defines criteria for the recognition of the 2D cross-sectional morphological elements and by so doing provides the basis for the objective description and categorization of diagenetic front geometry.

In many sedimentary basins the seismic reflections that mark the conversion of opal-A to opal-CT and the subsequent conversion of opal-CT to quartz, are parallel to the present-day seabed. As the reactions are, in part, thermally activated these boundaries have been proposed as potential isothermal markers and could have utility for hydrocarbon exploration. This thesis describes opal-A to opal-CT and opal-CT to quartz diagenetic boundaries using seismic data from the NSB that are not parallel to the present day seabed, but for ~ 80% of the area of the basin are parallel to an unconformity of Late Miocene age. The diagenetic boundaries are not parallel to the present day seabed, but may represent palaeo-isotherms that were parallel to the Late Miocene seabed. This characteristic is not unique and has been identified in other basins. It indicates that silica diagenetic boundaries do not make reliable

present day isotherms and therefore should be treated with caution in exploration campaigns. This thesis proposes that diagenetic boundaries which are not parallel to the seabed are not present day isotherms, but are palaeo-isotherms and propose several mechanisms that could be responsible for this palaeo-isothermal behaviour: (1) temperature decrease, such as a declining geothermal gradient, which will cause the rate of conversion to slow; (2) variations in the burial rate that will cause changes to the rate of conversion; (3) erosion of the overburden; and (4) a change in the rate of conversion as a result of variation in the physico-chemical factors influencing the silica diagenetic reactions.

A dramatic reduction in porosity, generally as much as 15-35%, is frequently associated with the fine-grained sediment within which the transition of opal-A to opal-CT occurs. Many of these silica diagenetic boundaries imaged on seismic reflection data show a variety of undulating morphologies. Where the diagenetic boundaries have variable relief, deformation of the overburden has been identified. Unusual stratal patterns are the result and these have recently been accounted for as a result of differential advancement of the diagenetic boundary, which leads to differential compaction and subsidence of the overburden. The hypothesis developed is that differential advancement of the diagenetic front simply causes differential compaction and folding of the strata above the opal-A to opal-CT boundary. This thesis tests this hypothesis and then uses knowledge of the relief of the diagenetic boundary and the folding above it, to make estimations of the magnitude of the porosity drop. This thesis applies this forward modelling technique to examples of boundaries from the NSB and from the Faeroe-Shetland, Vøring and Møre Basins from the Northeast Atlantic margin. This technique could be applied to some biogenic silica-rich successions in extreme latitudes where the lack of commercial or scientific drilling means that no other prior information on porosity-depth functions is available.

Note on Thesis Structure

The contents of the three core chapters of this thesis have either been published, in press or in review as papers in international journals. For each of these papers I am the lead author with my primary supervisor Prof. Richard J. Davies as co-author. With regards to the three papers that make up the core chapters, they are my own work with my primary supervisor providing constructive feedback, together with several journal reviewers, in order to improve the quality of the manuscripts. A paper entitled 'The suitability of silica diagenetic boundaries as isothermal markers: Examples from Offshore Sakhalin, Russian Far East', based upon Chapter 2, is currently in review with *Marine and Petroleum Geology*. A paper entitled 'Morphological development of basin-scale silica diagenetic fronts revealed with 2D seismic reflection data: offshore Sakhalin, Russian Far East', which Chapter 3 is based upon, was published in 2007 in the *Journal of the Geological Society* and is cited extensively throughout this thesis as Meadows & Davies (2007). A paper entitled 'Predicting porosity reduction due to silica diagenesis using seismic reflection data', based upon Chapter 4, was published in 2009 with *Marine and Petroleum Geology*. However, in this paper the relief model (see Chapter 4.5) is only mentioned briefly, but is described in more detail in the chapter.

Other than the seismic data, I have had very limited access to other forms of data to use in the thesis. Despite repeated requests to BP I have not had access to the well data for the NSB. However, BP has released an image (Fig. 1.10) showing the lithology, biogenic silica content and log (sonic, density and porosity) responses for one of the wells. BP has also released bottom hole temperature (BHT) data from the wells (Table 1.2) and the seismic stratigraphic interpretation for the NSB (Appendix II). Also BP has requested that the locations of these wells is kept confidential, hence they are not shown on the map of the NSB (Fig. 1.9).

Additional supporting information is provided in a series of appendices included with the thesis. Appendix I provides information on the seismic interpretation and processing methodology, as well as some additional regional seismic lines to help illustrate the tectono-stratigraphic setting of the NSB. Appendix II includes BP's seismic stratigraphic interpretation of the NSB, as well as some additional temperature data from onshore and offshore Sakhalin. Appendix III presents the results of some research into attempting to recreate the opal-A to opal-CT boundary using synthetic seismic and data from ODP sites. My secondary supervisor, Dr. Richard Hobbs, provided substantial assistance with the

generation and interpretation of the synthetic seismograms in Appendix III. Copies of the papers that make up the core chapter are provided in Appendix IV, which can be found on a CD at the back of this thesis. Also provided in Appendix IV is a paper by Davies *et al.* (2008) of which I am a co-author. This paper used some of the NSB dataset to illustrate fluid flow due to silica diagenesis (see Chapter 5.5.1).

Acknowledgements

I would like to thank my primary supervisor Prof. Richard J. Davies for all his support and greatly appreciate his input into this research. I would also like to thank my secondary supervisor Dr. Richard Hobbs for his opinions and greatly appreciate his assistance with the generation of synthetic seismograms (see Appendix III). I would like to thank Prof. Joe Cartwright (Cardiff University) for helpful discussions on the ideas presented in this thesis. I am also grateful to Prof. Neil R. Goulty (University of Durham) and Dr. Mads Huuse (University of Manchester) who examined my thesis. I gratefully acknowledge Gary Wilkinson and Dave Stevenson for valuable IT support. I would also like to thank Dr. Penny Widdison (Senior Tutor of Hatfield College, University of Durham) for providing pastoral support as my tutor during the course of my research.

I would like to acknowledge the moral support of my mother, Yvonne, and step-dad, Paul, over the course of this PhD. I also gratefully appreciate the moral support given to me by my friends, especially Claire Graham, Hamish Leese and Stephen Livingstone, over the past few years. I would like to thank Carole Coles, my A-level geology teacher at Portsmouth College, who cemented my interest in Earth Sciences and to Dr. Jim Hendry and John Whalley (University of Portsmouth), my tutors as an undergraduate, who encouraged me to apply to do a PhD and have continued to take an active interest in my progress.

I gratefully acknowledge NERC (Natural Environmental Research Council) for the provision of a NERC Industrial CASE award (NER/S/C/2005/14376), in conjunction with BP, which supports this research. I am very grateful to BP for supporting this research, through providing data, logistical support and part funding; in particular I would like to thank Ted Dunn, Philip Hirst, Jacek Jaminski, Andrew Lewis, Astrid Makowitz and Bryan Ritchie. I am very grateful to TGS-NOPEC and DMNG, who allowed for the release of the North Sakhalin Basin seismic datasets. StatoilHydro are thanked for permission to use data from the Vøring and Møre Basins and PGS are thanked for permission to used data from the Faeroe-Shetland Basin, which are used in Chapters 4 and 5. Schlumberger and Landmark are thanked for the use of seismic interpretation software. Landmark is also thanked for the use of *Promax*, a seismic data processing program used in Appendix III.

Table of Contents

List of Figures

List of Tables

Chapter 1: Introduction

1.1 Introduction to the thesis

1.1.1 Historical context

Seismic reflection data can be an important source of information for interpreting sedimentary basins. However, the use of seismic data as an aid to help understand the role of a host of diagenetic processes, which occur within the strata of many sedimentary basins, is arguably underrated as an analytical method. These diagenetic processes include the precipitation of cements in pore spaces and the conversion of clay minerals, such as the conversion of smectite to illite. These diagenetic processes can cause changes in the physical properties of the host sediment which in turn can be detected on seismic data. Identifying diagenesis on seismic data and recognising the controls on the diagenetic processes can be useful in terms of understanding the evolution of the host basin. This thesis focuses upon the use of seismic reflection data in identifying silica diagenetic reactions and their effects in sedimentary basins.

The transformation of biogenic silica (opal-A) to opal-CT and subsequent transition of opal-CT to quartz are important diagenetic reactions that can occur in siliceous sediments within sedimentary basins. The role played by silica diagenesis within sedimentary basins is poorly understood, but it is becoming apparent that these reactions could have significant implications for basin analysis in terms of the sedimentological and deformational history of the basin as well as for hydrocarbon exploration. These silica diagenetic transitions have previously been imaged on seismic reflection data from various basins worldwide. However, until recently, seismic data have not been used as an analytical tool for the interpretation of silica diagenetic boundaries. The purpose of this thesis is to increase the understanding of silica diagenetic boundaries using seismic reflection data as an important analytical tool.

1.1.2 Aims and objectives

The aims and objectives of the thesis are to (1) use 2D and 3D seismic reflection data to identify the silica diagenetic fronts and work out their morphology and areal extent; (2) understand the possible mechanisms and processes behind the development of the diagenetic boundaries; and (3) understand the role that these diagenetic processes can

potentially play within sedimentary basins, in terms of differential compaction and hydrocarbon exploration.

1.1.3 Methodology – seismic reflection data

The observations and interpretations in this thesis are almost exclusively made using seismic reflection data (see section 1.6). Seismic surveying is one of a series of useful analytical tools available in geology. The basic requirements for a seismic survey are a source of energy, a series of receivers and a layered subsurface geology. Seismic data use acoustic energy to image the subsurface geology and can be applied to onshore and offshore areas (Brown 2003). Seismic surveying involves three steps: data acquisition, processing and interpretation.

The seismic method relies upon changes in the acoustic properties of rock to perturb the sound waves as they are transmitted through the rock (Brown 2003). A signal is transmitted from the source down into the subsurface, where a fraction of this down-going transmitted energy is reflected at impedance boundaries beneath the surface upwards towards a receiver at ground/sea level (Fig. 1.1). Seismic surveying is largely concerned with using P-waves. When a wave from the source reaches a boundary between two media, such as a lithological or diagenetic boundary separating beds of different acoustic impedance (the product of density of the rock and its seismic velocity), then some of the acoustic energy is reflected back towards the surface where it is detected. The variations in the acoustic impedance contrast cause variations in the amplitudes of these reflections, i.e. a large difference in acoustic

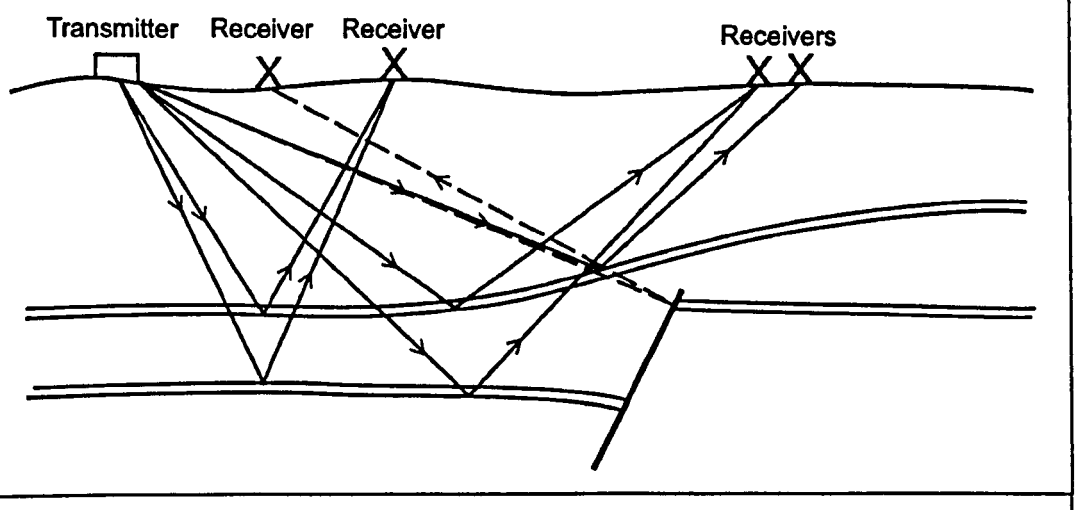

Fig. 1.1: A schematic diagram showing ray-paths between source and the receivers during seismic acquisition. (From: Gluyas & Swarbrick 2004)

impedance will lead to a high-amplitude reflection. The reflections created from different interfaces can then be used to build-up a picture of the subsurface geology. Normally many receivers are used, which give redundancy in the data that can be exploited in processing to enhance weak reflections. Knowing the geometry of the sources and receiver arrays together with the two-way travel time (t), i.e. the time taken for the signal to propagate down to the reflector and back to the surface, the data can be collated to yield seismic cross-sections in 2D and seismic volumes in 3D.

Acoustic energy is generated through a variety of sources; on land explosives or a machine to induce vibrations are used, while on water air-guns are commonly used that discharge high-pressure air to create an acoustic pulse in the water column and into the underlying sediment. Seismic energy returning to the surface, on land or sea, is collected by an array of receivers. Two-dimensional surveys use a linear array of receivers, while 3D surveys are acquired in a variety of patterns, such as grids and brick patterns, to build-up a more detailed picture of the subsurface than a 2D survey (e.g. Brown 2003). The processing of seismic data aims to enhance the useful seismic information relative to the interference/noise in the signal and place the seismic reflections in their correct x, y and t space. The stages of seismic processing are complicated and are not described in detail in this thesis. For more information see Yilmaz (1987). The seismic data used in the thesis have had pre-stack time migration applied to them during processing (see Appendix I). Migration is designed to restore seismic reflections to their proper x-y position – this is needed because inclined strata or the intersections of geological boundaries with faults can cause a distortion in the signal that returns from the reflector so the implicit assumption that the reflection point lies directly beneath the mid-point between the source and receiver is no longer valid (Brown 2003). The final step of seismic surveying is the interpretation of the processed data. The objective of this step is to generate a coherent geological story from an array of seismic reflections. At a simplistic level this involves tracing continuous reflections across 2D grids of seismic lines or throughout 3D data volumes (e.g. Brown 2003). However, due to the intuitive nature of interpretation and the resolution of the data, it is rarely possible to create an unambiguous geological interpretation of a seismic dataset.

One of the key issues when dealing with seismic data is that of resolution. According to Brown (2003) the resolution of the seismic data dictates in how much detail the subsurface geology can be imaged. There are two different types of

resolution associated with seismic data: horizontal and vertical. The vertical resolution can be defined as the minimum vertical distance between two interfaces needed to give rise to a single reflection that can be observed on a seismic section, this is known as the Rayleigh Criteria (Emery & Myers 1996). In a single noise-free seismic trace this is governed by the wavelength (λ) of the seismic signal. The shorter the wavelength, hence higher the frequency, the greater the vertical resolution. The limit of vertical resolution is ¼ λ. The spacing between the reflective interfaces decreases below the critical wavelength of the signal; interference begins to cause the formation of a composite wavelet with anomalous amplitudes. Reflections that are spaced more closely than ¼ λ have responses which begin to add constructively to produce a reflection with a high amplitude. This is known as the thin bed effect or 'tuning' (Emery & Myers 1996). The wavelength can be calculated using the following equation:

$$\lambda = V/F \qquad (1)$$

Where F is the frequency of the data, i.e. the number of peaks passing one point per second; V is the seismic velocity; and λ is the wavelength of the seismic signal. A normal seismic signal is not monochromatic (single frequency) so it is convention to use the dominant frequency and wavelength to work out the resolution.

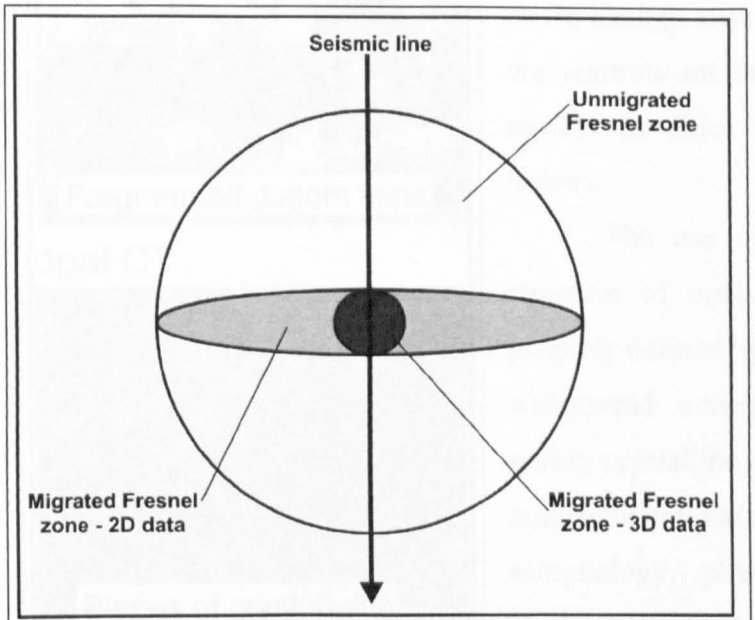

Fig. 1.2: A plan view of the focusing effect of migration in two and three dimensions. The Fresnel zone will be reduced to an ellipse perpendicular to the seismic line for 2-D migration and to a small circle by 3-D migration. (Modified from: Brown 2003)

Acoustic energy sent out from a source moves in three dimensions and spreads out over a large area, coming into contact with reflecting surfaces over discrete areas. The energy travels as waves and the region on the reflection where the seismic energy is reflected constructively is known as the Fresnel zone (Emery & Myers 1996). The horizontal resolution is determined by the radius of the Fresnel zone (Fig. 1.2), which itself depends on the

wavelength of the seismic wave and the depth of the reflection. On a buried horizon, all features with a lateral extent exceeding the Fresnel zone will be visible. The Fresnel radius is approximately equal to $V/2(t/F)^{0.5}$ where V is the seismic velocity, t is the two way travel time and F is the dominant frequency in the seismic data (Emery & Myers 1996). The procedure of migrating seismic data considerably enhances the horizontal resolution (Fig. 1.2). Migration improves the horizontal resolution to about ¼ λ (Emery & Myers 1996).

Seismic surveys enable entire stratigraphic horizons, including diagenetic boundaries, to be correlated over tens of thousands of kilometres across sedimentary basins (Cartwright & Huuse 2005). The methodology and database behind the seismic interpretation of silica diagenetic boundaries is described in section 1.6 as well as in Appendix I.

1.2 Silica diagenesis

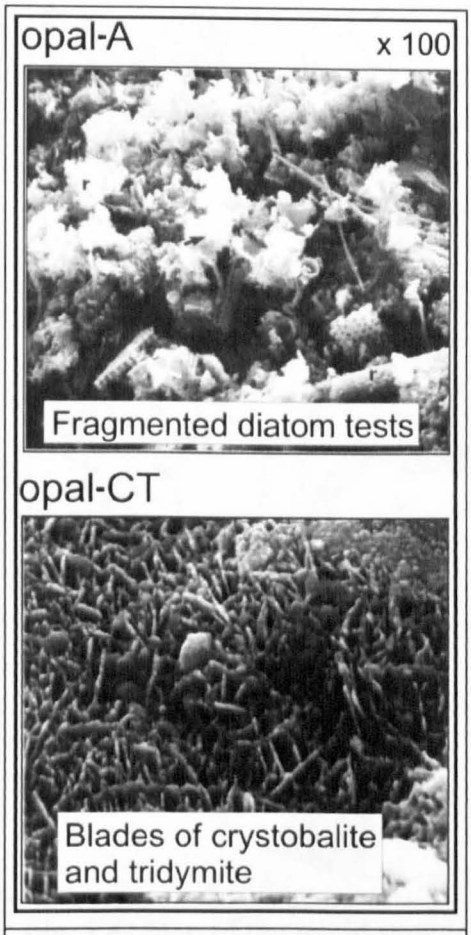

Fig. 1.3: SEM images of opal-A and opal-CT. (Modified from: Davies *et al.* 2008)

All the geochemical and geophysical aspects of the silica diagenetic conversion process have been studied to some extent over the past 50 years. These aspects range from defining the phase change sequence to the identification of the controls on the reaction rates. The main aspects of silica diagenesis are summarised below.

The use of the terms and crystalline structure of opal-A and opal-CT were first properly defined by Jones & Segnit (1971). The widespread occurrence of natural forms of poorly crystalline silica resulted in a confusing nomenclature based in different instances on morphology, physical properties or optical characteristics. In order to rationalise the classification of hydrous silicas, Jones & Segnit (1971) proposed a nomenclature based on the crystal structure (Fig. 1.3). The natural hydrous silicas were subdivided into three well defined structural groups: opal-C (well ordered

α-cristobalite), opal-CT (disordered α-cristobalite, α-tridymite) and opal-A (highly disordered, near amorphous) (Jones & Segnit 1971).

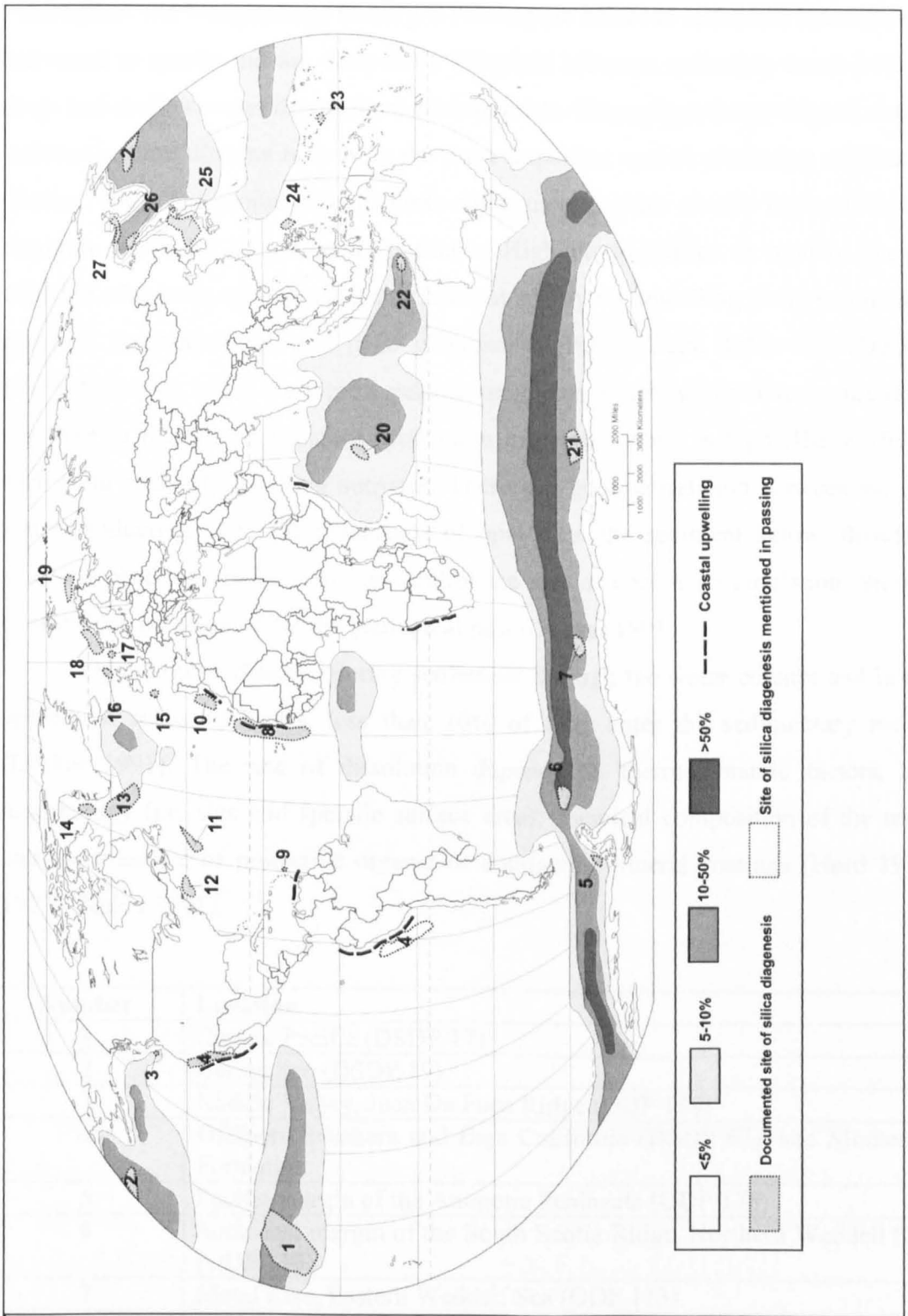

Fig. 1.4: Map of the world showing location of most of the known Palaeogene- and Neogene-age siliceous deposits. Mostly based on ODP/DSDP sites. Numbers refer to the list on Table 1.1. Map also shows the percentage of biogenic silica in pelagic sediments.

1.2.1 Origin of biogenic silica (opal-A)

Biogenic silica is an important constituent of marine sediments, particularly those of Palaeogene- and Neogene-age (most pre-Palaeogene siliceous sediments have already converted to quartz and are chert-rich). Biogenic siliceous sediments occur both in deep- and shallow-water depositional environments. Throughout the geological record radiolarians and diatoms have been the most important opal-A producing organisms (Hesse 1990). The productivity of these siliceous organisms closely responds to the changing advection of anorganic nutrients. High productivities in modern oceans coincide with areas of high anorganic nutrient supply by upwelling along continental margins, north-equatorial and polar divergences (Fig. 1.4 and Table 1.1) (Decker 1991). Siliceous oozes are typical pelagic sediments which accumulate on the deep sea floor in regions where silica production in surface water is high (Hesse 1990), such as in areas of upwelling nutrients. There is a good correlation between surface water productivity and the abundance of opal-A in the sediment below, therefore siliceous plankton productivity can control the rate of opal-A accumulation. Similar controls can be assumed for the geological past (Decker 1991).

Opaline tests dissolve during settlement through the water column and in the uppermost sediment layers, less than 10% of tests enter the sedimentary record (Decker 1991). The rate of dissolution depends on thermodynamic factors, test morphology (i.e. size and specific surface area), chemical composition of the tests, and the presence of protective organic or authigenic mineral coatings (Hurd 1972, 1973; Decker 1991).

Number	Location
1	Central Pacific (DSDP 17)
2	Bering Sea (DSDP 19)
3	Middle Valley, Juan De Fuca Ridge (ODP 139)
4	Offshore Southern and Baja California (DSDP 63), and Monterey Formation
5	Pacific margin of the Antarctic Peninsula (ODP 178)
6	Southeast margin of the South Scotia Ridge, Northern Weddell Sea (ODP 113)
7	Maud Rise, Eastern Weddell Sea (ODP 113)
8	Northwest Africa (DSDP 41)
9	Onshore and offshore Barbados
10	Eastern North Atlantic continental margin (DSDP 47 and 50)
11	Western North Atlantic Basin (DSDP 43)
12	Eastern North America continental slope and rise (DSDP 93 and

	95; ODP 150)
13	Labrador Sea (ODP 105)
14	Fylla prospect offshore West Greenland
15	Goban Spur area of the Northeast Atlantic (DSDP 80)
16	Faeroe-Shetland Basin (e.g. Davies 2005)
17	North Viking Graben – North Sea (Davies *et al.* 2006)
18	Vøring and Møre Basins (Davies & Cartwright 2007)
19	Barents Sea
20	Western Indian Ocean (ODP 115)
21	Kerguelen Plateau (ODP 120)
22	Argo Basin, North-eastern Indian Ocean (ODP 123)
23	Nauru Basin (DSDP 61)
24	Western Pacific (DSDP 31)
25	Sea of Japan (ODP 127/128; Lee *et al.* 2003) and Northern Japan (Tada & Iijima, 1983)
26	North Sakhalin Basin (Meadows & Davies 2007)
27	Basins of the Northern Sea of Okhotsk

Table 1.1: Table listing the locations of documented silica transitions that relate to the numbers on the map in figure 1.4.

1.2.2 Maturation sequence

Evidence from deep-sea sediments and from onshore outcrops, such as the Monterey Formation of California, supports the following overall diagenetic maturation sequence: opal-A (siliceous ooze) → opal-CT (porcellanite) → micro-quartz (chert) (Fig. 1.5 – path A). It has long been known that the silica phases are transformed from opal-A through opal-CT to quartz with an increase in burial temperature (e.g. Pisciotto 1981; Tada 1991). Opal-CT (cristobalite and tridymite) forms an intermediate metastable phase. Eventually, at higher temperatures (greater burial depth or higher heat flow) or with time opal-CT transforms to microcrystalline quartz, which is the stable silica phase in diagenetic environments (Kastner *et al.* 1977). Williams *et al.* (1985) suggested that direct transformation from opal-A to quartz was a possible transition pathway (Fig. 1.5 – path B) under extreme depositional and diagenetic conditions, where silica solubility allows quartz to form directly from opal-A. However, the intermediate opal-CT phase has been recognised in most diagenetic sequences in siliceous rocks (e.g. Hein *et al.* 1978; Tada & Iijima 1983).

1.2.3 Mechanism of phase changes

The transformation of opal-A to opal-CT and subsequent transition of opal-CT to quartz are dissolution-reprecipitation reactions. This interpretation of the reaction

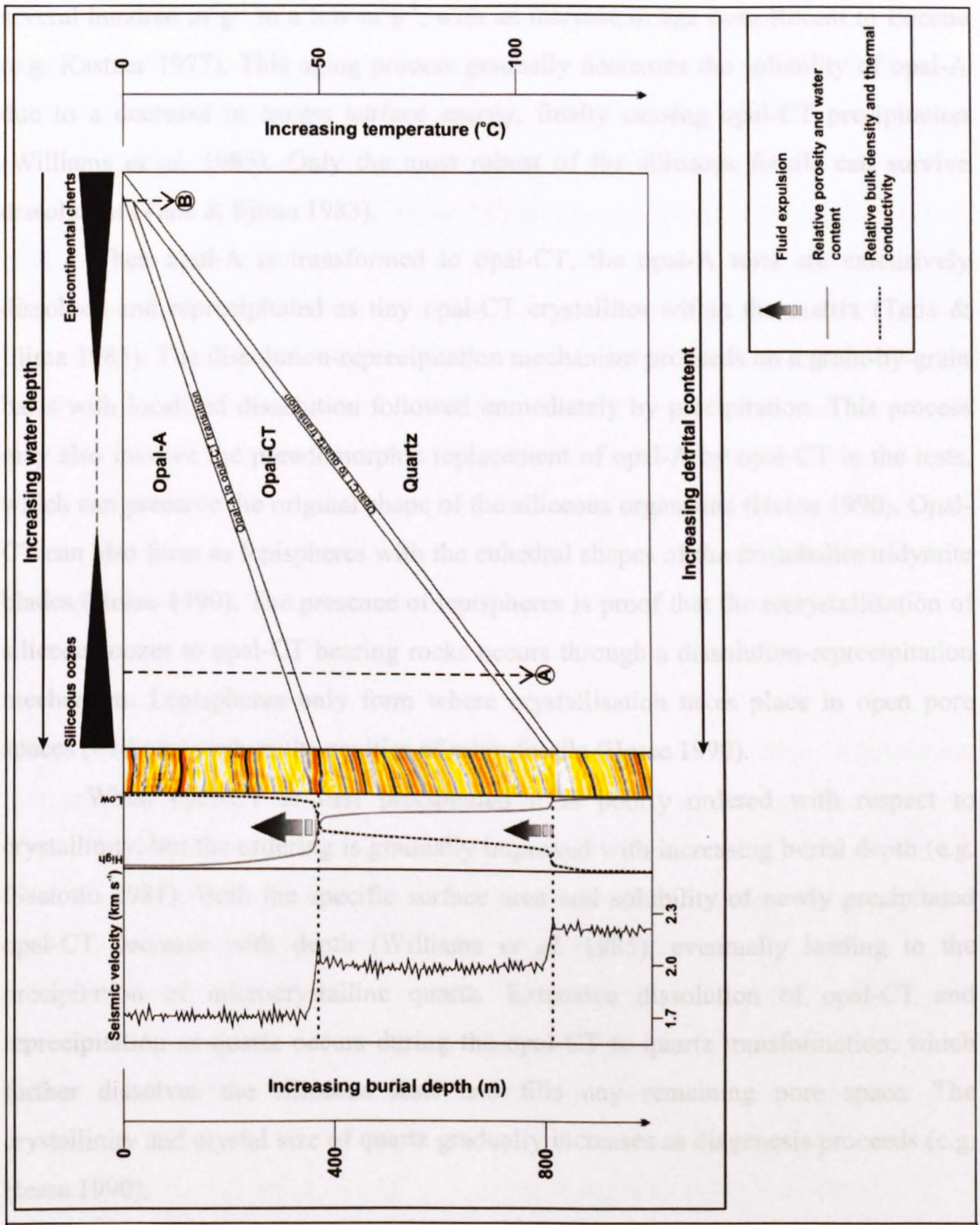

Fig. 1.5: Phase change diagram showing the idealised temperatures, burial depths and depositional environments. Also shown are the idealised relative physical property changes and seismic response associated with the transitions.

mechanism has been based on both oxygen isotope and petrographical evidence (e.g. Murata *et al.* 1977; Tada & Iijima 1983). The tests of the siliceous organisms in sediment can form an interlocking structure that has a high porosity, which collapses during the transformation to opal-CT as opal-A is dissolved and reprecipitated. In the opal-A zone there is a slow but progressive dissolution and weakening of the diatom and radiolarian tests (Tada 1991). The specific surface area of the tests decreases from

several hundred m^2g^{-1} to a few m^2g^{-1}, with an increase in age from Recent to Eocene (e.g. Kastner 1977). This aging process gradually decreases the solubility of opal-A due to a decrease in excess surface energy, finally causing opal-CT precipitation (Williams *et al.* 1985). Only the most robust of the siliceous fossils can survive dissolution (Tada & Iijima 1983).

When opal-A is transformed to opal-CT, the opal-A tests are extensively dissolved and reprecipitated as tiny opal-CT crystallites within the matrix (Tada & Iijima 1983). The dissolution-reprecipitation mechanism proceeds on a grain-by-grain basis with localised dissolution followed immediately by precipitation. This process may also involve the pseudomorphic replacement of opal-A by opal-CT in the tests, which can preserve the original shape of the siliceous organisms (Hesse 1990). Opal-CT can also form as lepispheres with the euhedral shapes of the cristobalite/tridymite blades (Hesse 1990). The presence of lepispheres is proof that the recrystallisation of siliceous oozes to opal-CT bearing rocks occurs through a dissolution-reprecipitation mechanism. Lepispheres only form where crystallisation takes place in open pore spaces (>10 μm) such as the cavities of microfossils (Hesse 1990).

When opal-CT is first precipitated it is poorly ordered with respect to crystallinity, but the ordering is gradually improved with increasing burial depth (e.g. Pisciotto 1981). Both the specific surface area and solubility of newly precipitated opal-CT decrease with depth (Williams *et al.* 1985), eventually leading to the precipitation of microcrystalline quartz. Extensive dissolution of opal-CT and reprecipitation as quartz occurs during the opal-CT to quartz transformation, which further dissolves the siliceous tests and fills any remaining pore space. The crystallinity and crystal size of quartz gradually increases as diagenesis proceeds (e.g. Hesse 1990).

The silica diagenetic transitions are examples of Ostwald processes, where the reactions are not single-step processes. Rather, it involves a series of dissolution-reprecipitation reactions as suggested theoretically by the kinetic model of Williams *et al.* (1985), which is based on surface-area effects. The relationship between specific surface area and solubility explains why opal-CT is required as an intermediate phase in the sequence of diagenetic transformations. Silicon solubility in equilibrium with opal-A of any specific surface area is normally too high for quartz to form directly from the dissolution of opal-A; hence quartz growth will be blocked as a less 'well-ordered' phase, opal-CT, will form instead (Williams & Crerar 1985; Williams *et al.*

1985; Hesse 1990). Quartz crystallisation is only possible when the 'equilibrium solubility' of opal-CT has been lowered sufficiently through Ostwald ripening (Williams *et al.* 1985; Hesse 1990). Opal-CT is a classic example of Ostwald's step rule that states, as a consequence of the crystallisation kinetics, that the transformation of an unstable to a stable mineral phase (at surface conditions) often requires one or more intermediate metastable phases (Morse & Casey 1988). Lowering the equilibrium solubility for dissolved silicon through Ostwald ripening of the opal-CT phase also counterbalances a solubility increase with rising temperature during burial; this is a prerequisite for quartz precipitation which would not occur if opal-CT solubility massively increased with temperature (Hesse 1990). The growth of a more highly ordered silica phase such as quartz is favoured by low silica supersaturation (Hesse 1990); hence the ordering process during burial of opal-CT works to produce such conditions and eventually enables quartz precipitation.

1.2.4 Controls on conversion

Silica phase transformations are affected by factors such as time, temperature, pressure, pore water chemistry and host rock lithology, with temperature and time (Fig. 1.6) being the main controls (e.g. Mizutani 1970; Kastner *et al.* 1977; Hein *et al.* 1978; Tada 1991). At hemipelagic sites with relatively high sedimentation rates, the reactions generally occur in younger sediments and at higher temperatures than at low sedimentation-rate pelagic sites (e.g. Tada 1991; Tribble *et al.* 1992). A combination of the above factors could lead to some transformations taking place at shallower burial depths and lower temperatures. The time required for the completion of each of the transformations within a single section with minor lithological variation is generally of the order of 0.1 to 1 Ma (e.g. Thein & von Rad 1987; Tada 1991).

Lithology can affect the rate and mode of transformation through its influence on pore water chemistry, porosity, permeability, detrital mineral concentration, fracture formation, and content and specific surface area of the silica phase(s). The rate of conversion of the opal-A to opal-CT is accelerated in calcareous siliceous sediments as a result of the enhancement of opal-CT nucleation by the presence of magnesium hydroxide as a nucleus (Kastner *et al.* 1977). Higher porosities and permeabilities that are associated with calcareous sediments compared with clayey siliceous sediments also seem to enhance the rate of conversion through opal-CT precipitation (Lancelot 1973). However, the presence of clay minerals tends to retard

the opal-A to opal-CT transformation (Isaacs 1982), through consuming dissolved magnesium (Kastner *et al.* 1977), by reducing the effective surface area by adsorbing cations or by covering the surfaces of siliceous particles (Tada 1991). The type of siliceous fossil may also have an effect on the timing of the opal-A to opal-CT conversion due to possible differences in their specific surface area (Williams *et al.* 1985).

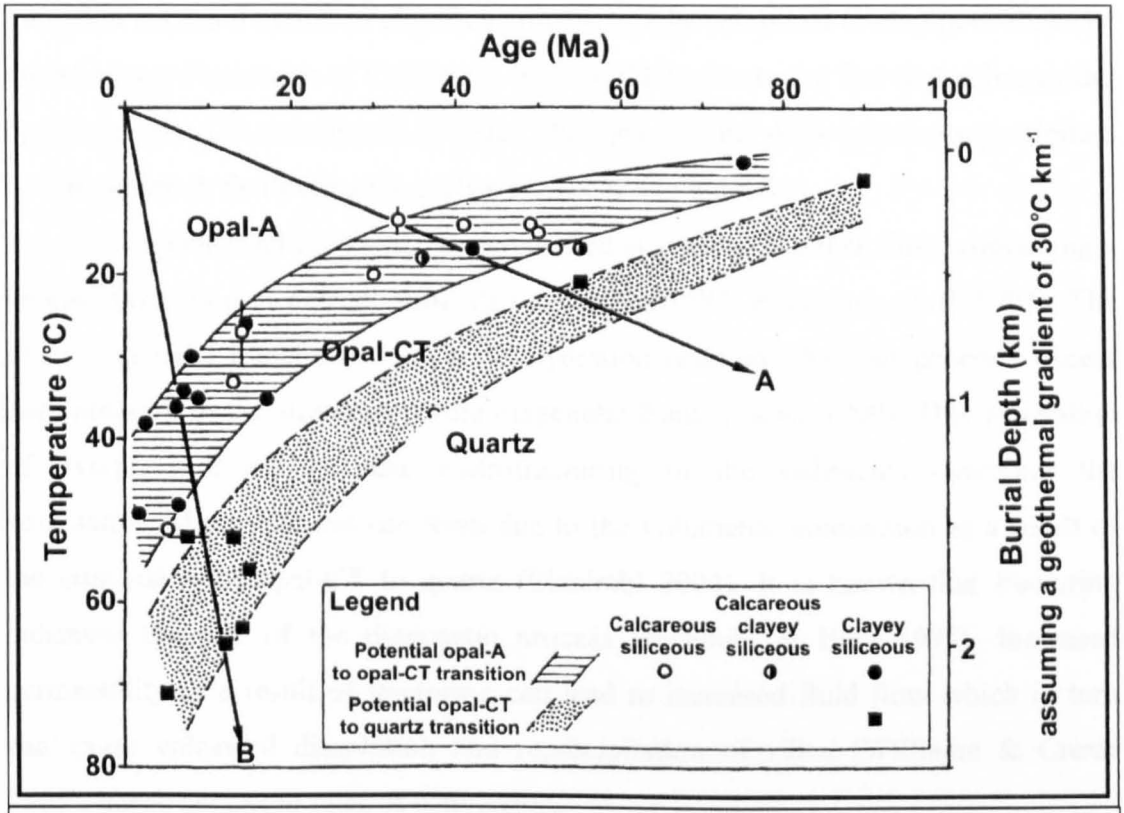

Fig. 1.6: Age-temperature relationship of the opal-A to opal-CT and opal-CT to quartz transformations within sediments of various lithologies from selected DSDP sites. Path A represents an age-temperature path for a low sedimentation rate and/or low geothermal gradient, whereas path B denotes a higher sedimentation rate and/or a higher geothermal gradient. (From: Tada 1991)

Tada (1991) observed no obvious difference in the timing of the first opal-CT precipitation between calcareous and clayey siliceous sediments subjected to the same temperatures. This observation is probably partly due to the uncertainty in the temperature estimation obscuring the effect of lithology (Tada 1991).

The opal-CT to quartz transformation tends to start earlier in chert concretions compared to surrounding siliceous chalks or calcareous porcellanites (Hesse 1990). The earlier formation of quartz within chert concretions could be related to the earlier diagenetic formation of opal-CT in these concretions which in turn could act as nucleation points for the conversion when they reach the diagenetic front, leading to

enhanced rates of diagenesis around the concretion. These concretions form above the diagenetic fronts due to favourable lithological and geochemical conditions, such as extremely low levels of detrital minerals (Bohrmann *et al.* 1994). Kastner *et al.* (1977) concluded that clay minerals present in the sediment also retard the rate of opal-CT to quartz conversion in a similar fashion to the effect they have on the opal-A to opal-CT transformation. In contrast, Isaacs (1982) observed that the opal-CT to quartz transition occurred earlier in clay-rich siliceous rocks compared to clay-poor rocks of the Monterey Formation of California. This could be due to the fact that although the opal-A to opal-CT transition is retarded, the opal-CT that does eventually precipitate is more ordered, facilitating the earlier conversion to quartz.

Sediments richer in silica are converted at a faster rate than those containing a greater proportion of detrital minerals (e.g. Isaacs 1982; Bohrmann *et al.* 1994). The silica diagenetic transformations are dehydration reactions that can generate excess pore pressure in the strata above the diagenetic fronts (Hesse 1990). This generation of overpressure could cause hydrofracturing in the sediments overlying the boundaries. Microfractures can form due to the volumetric contraction as a result of the conversion of opal-CT to quartz (Eichhubl 2004). It is known that fracturing enhances the rate of the diagenetic process (Eichhubl & Behl 1998). Increased permeability as a result of fracturing can lead to increased fluid flow which in turn can cause enhanced dissolution and reprecipitation of silica (Williams & Crerar 1985), hence enhanced rates of conversion.

The temperatures required for opal-A to opal-CT transformation can be highly variable, ranging from 2-56°C (Hein *et al.* 1978; Keller & Isaacs 1985; Nobes *et al.* 1992a; Bohrmann *et al.* 1994). The extremely low temperatures are related to siliceous oozes described by Bohrmann *et al.* (1994) along the Antarctic continental margin and are probably due to the exceedingly pure siliceous nature of these sediments. Temperatures needed for the opal-CT to quartz transition range from 46-110°C (Hesse 1990; Nobes *et al.* 1992a). The depths of conversion can vary significantly depending on heat flow, sedimentation rate and lithological effects. For example, the opal-A to opal-CT transformation generally occurs between 300-800 m, but can be shallower due to exceptional conditions (e.g. Bohrmann *et al.* 1994). The depths at which the transitions occur vary and depend on the temperature at which conversion is initiated.

1.3 Effects of silica diagenesis on acoustic and physical properties of sediments

The physical properties of sediments are influenced by compaction and diagenesis during burial. Changes in mineralogy, chemistry, density, porosity and microfabric can all affect the sediments' acoustic and electrical properties. The physical property changes that siliceous sediments undergo during diagenesis include marked porosity reduction, density increase, decrease in water content and an increase in thermal conductivity (Figs. 1.5 and 1.7). The compaction of siliceous rocks is closely related to silica phase transformations (Tada 1991). The majority of noncalcareous siliceous rocks lose their porosity mostly by mechanical compaction, but also by chemical compaction and reprecipitation associated with the opal-A to opal-CT transformation (Tada 1991).

Opal-A diatomites and radiolarites originally have an extremely high porosity due to abundant interskeletal pores. The changes in the physical properties are distinct across the opal-A to opal-CT boundary. The diagenetic alteration of biogenic opal-A to opal-CT causes a dramatic reduction of intra- and inter-skeletal porosity (15-35% decrease) allowing sediments to consolidate at depth (Langseth & Tamaki 1992; Volpi *et al.* 2003). The opal-CT to quartz transition results in a further, less dramatic, reduction as the remaining porosity is removed by chemical compaction (e.g. pressure-solution). The porosity loss can be sharp or gradual (Chaika & Dvorkin 2000; Chaika & Williams 2001) depending on clay mineral authigenesis. As a result of these physical property changes the analysis of silica diagenetic boundaries can be made difficult due to the fact that the transitions can overprint original depositional boundaries and pre-conversion deformational structures (Gutierrez-Alonso & Gross 1997).

Tribble *et al.* (1992) used sediments from the Japan Trench and offshore California to illustrate the dependence of physical properties on biogenic silica content. Increased opal-A content is linked with increased porosity but decreased grain density and compressional velocity. Variations with depth in opal-A concentration are therefore reflected in highly variable and, at times, inverse velocity-depth gradients (Tribble *et al.* 1992). Distinct changes in sediment microfabric, particularly in the porosity distribution as a result of the dissolution-reprecipitation reaction, accompany the phase transitions and contribute to a sharp velocity

discontinuity, even in relatively silica-poor sediments (Tribble *et al.* 1992), at the depth of the opal-A to opal-CT and opal-CT to quartz boundaries.

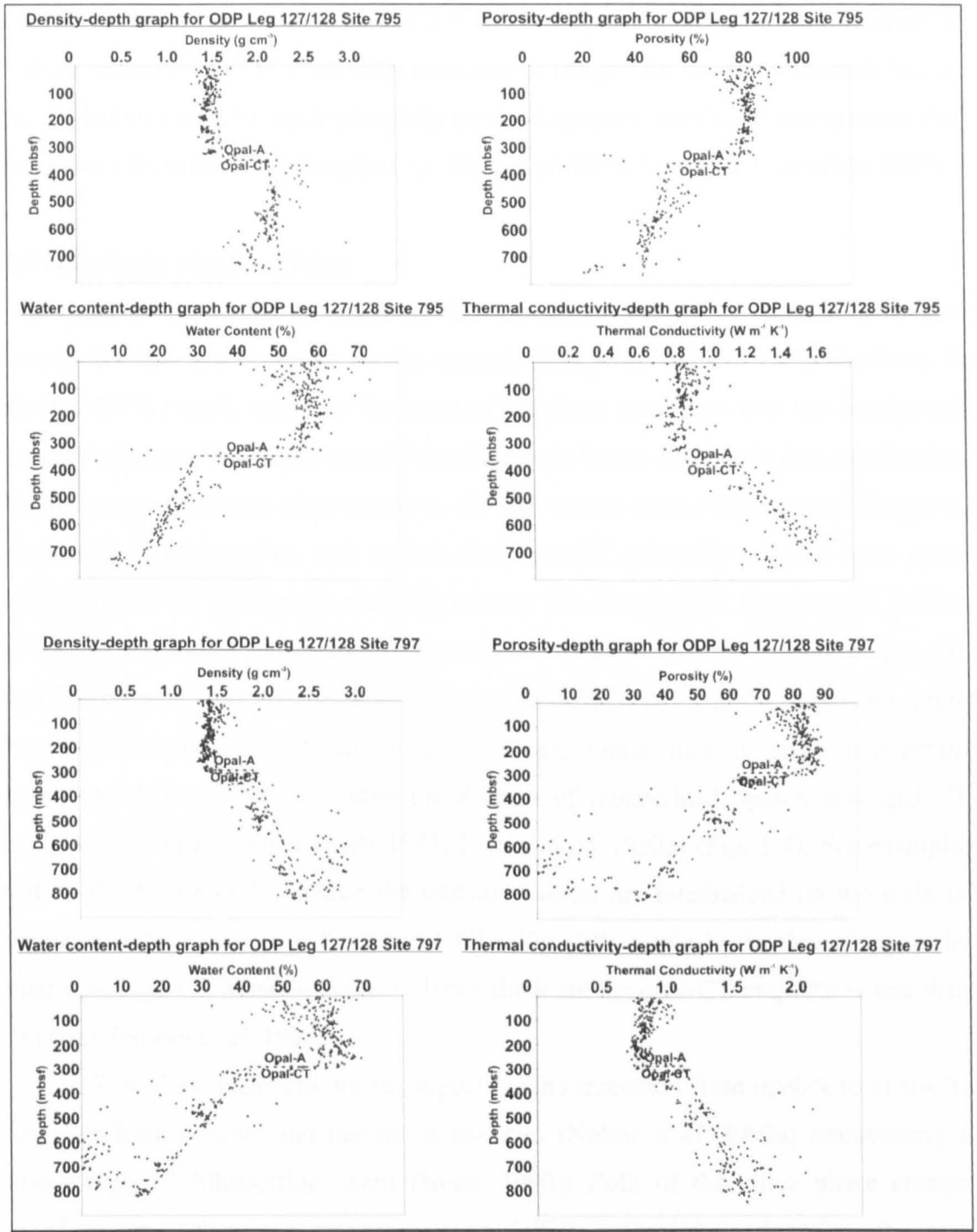

Fig. 1.7: Graphs detailing the main physical property changes (density, porosity, water content and thermal conductivity) associated with the opal-A to opal-CT transition. The data used are taken from ODP sources, in this case Sites 795 and 797 of ODP Leg 127/128 from the Sea of Japan.

The marked porosity decrease, and resultant increase in density and seismic velocity, across the silica diagenetic boundaries gives rise to a significant regional seismic reflection (Fig. 1.5) (e.g. Hein *et al.* 1978; Guerin & Goldberg 1996;

Meadows & Davies 2007). As a result of the acoustic impedance contrast these diagenetic fronts form positive polarity, high-amplitude seismic reflections (Davies & Cartwright 2002; Meadows & Davies 2007). The changes in the physical properties of marine sediments due to silica diagenesis can be imaged on seismic reflection data as two reflections (one for each phase change) and common amplitude terminations that can cross-cut inclined stratigraphy (e.g. Hein *et al.* 1978; Davies & Cartwright 2002).

1.4 Diagenetic reaction fronts

The diagenetic boundaries represent the top of an advancing reaction front and boundaries that are observed on the seismic data (e.g. Davies 2005; Meadows & Davies 2007) merely represent the onset of the phase transitions (i.e. the density and porosity change). The appearance of the diagenetic fronts on seismic data implies that the transition from one silica phase to another occurs over a few metres. However, diagenesis is progressive, and opal-A and opal-CT generally co-exist over some interval; opal-CT and quartz similarly overlap (Pisciotto 1981; Nobes *et al.* 1992a) (Fig. 1.8). Also most successions of biosiliceous rocks show interlayering of clay-rich and less clay-rich siliceous sediments (Tada 1991), therefore there is usually no single boundary between opal-A and opal-CT rocks; rather than a single conversion boundary, there is usually a transitional zone of interbedded opal-A and opal-CT rocks tens of metres thick (Tada 1991; Nobes *et al.* 1992a) (Fig. 1.8). For example, within the Monterey Formation the transition zones are interbedded on the scale of centimetres to metres (e.g. Compton 1991) (Fig. 1.8), while in the Sea of Japan the opal-A to opal-CT transition zone is 10m+ thick but the opal-CT to quartz is less than 1m thick (Nobes *et al.* 1992a).

The silica diagenetic fronts, especially the transition from opal-A to opal-CT, are significant seismic and thermal boundaries (Nobes *et al.* 1992a) representing a major regional lithification event (Hesse 1990). Both of the silica phase change reactions are reliant on temperature to initiate conversion; therefore the two boundaries are commonly parallel to one another. Temperature is one of the dominant controls on these reactions, therefore the two fronts have been considered to mark isotherms (Hein *et al.* 1978; Kuramoto *et al.* 1992; Nobes *et al.* 1992b; Lee *et al.* 2003) that can in some cases be parallel to the seabed (see Chapter 2).

Relatively speaking, transition zones advance upwards through the sedimentary section, or one could think of it as the sediment subsiding through the

transition which is located at a specific depth for any one lithology type, termed the depth of conversion (DOC – Eichhubl & Boles 1998). The transition zones are reaction fronts, which are defined as a layer of reaction that propagates through a

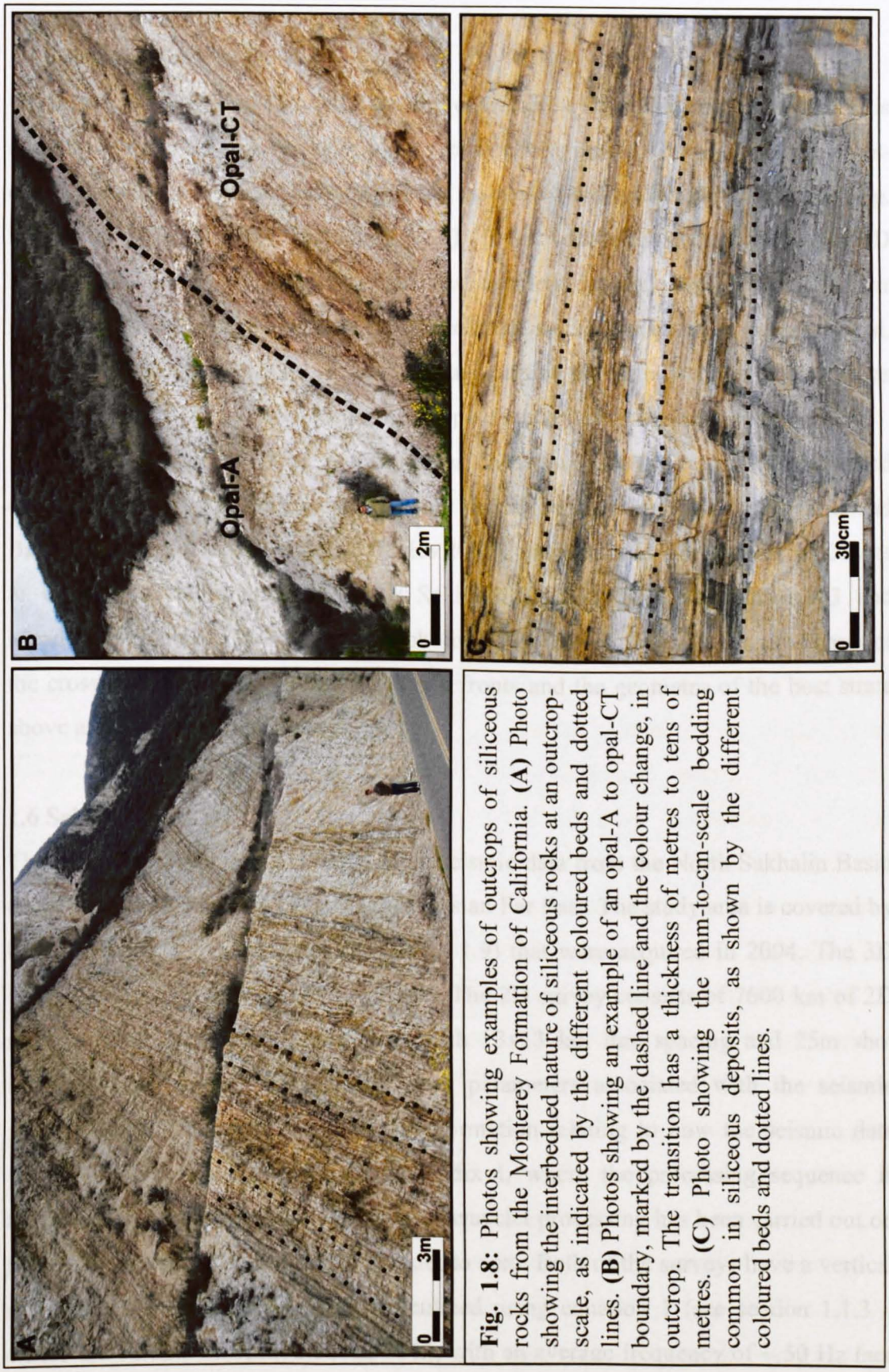

Fig. 1.8: Photos showing examples of outcrops of siliceous rocks from the Monterey Formation of California. **(A)** Photo showing the interbedded nature of siliceous rocks at an outcrop-scale, as indicated by the different coloured beds and dotted lines. **(B)** Photos showing an example of an opal-A to opal-CT boundary, marked by the dashed line and the colour change, in outcrop. The transition has a thickness of metres to tens of metres. **(C)** Photo showing the mm-to-cm-scale bedding common in siliceous deposits, as shown by the different coloured beds and dotted lines.

chemical mixture, converting the initial reactants to final products (Scott 1994). Reaction fronts and the processes by which they form are widely studied, since they are found in chemical, biological and geological systems.

1.5 Seismic reflection studies

Using seismic reflection data to image and characterise silica diagenetic boundaries is a relatively recent development (e.g. Davies & Cartwright 2002), although the cross-cutting seismic reflections have long been associated with silica phase changes (e.g. Hein *et al.* 1978; Thein & von Rad 1987). The advent of high quality 2D and 3D seismic data from around the world has enabled detailed descriptions of their morphologies and has revealed an insight into the mechanisms of front advancement. The term 'front advancement' is used throughout this thesis to describe the processes by which the diagenetic boundaries move up-section relative to the host strata.

The diagenetic front morphologies that have so far been described and explained have been identified on seismic reflection data from the Faeroe-Shetland Basin (Davies & Cartwright 2002; Davies 2005), the Møre and Vøring Basins (Davies & Cartwright 2007) and the North Sakhalin Basin (NSB) (see Chapter 3 and Meadows & Davies 2007). These morphologies have been recognised on the basis of the cross-sectional forms of the diagenetic fronts and the geometry of the host strata above and below the boundaries.

1.6 Seismic database

The majority of this thesis is based upon seismic data from the North Sakhalin Basin (NSB), offshore Sakhalin Island in the Russian Far East. The study area is covered by both a 2D and a 3D seismic survey (Fig. 1.9) that were acquired in 2004. The 3D seismic data cover an area of ~2400 km^2. The 2D survey consists of 7600 km of 2D multi-channel seismic reflection data, with 13x13 km line spacing and 25m shot interval. Information regarding the other parameters associated with the seismic surveys can be found in Appendix I. Information relating to how the seismic data were processed can be found in Appendix I, where the processing sequence is outlined. However, it is unknown whether wavelet processing has been carried out on these data to convert the effective wavelet to zero. Both of the surveys have a vertical resolution of ~ 10 m, which was calculated using equation 1 (see section 1.1.3 – where the vertical resolution equals ¼ λ), with an average frequency of ~ 50 Hz (see

Appendix I) and assuming a seismic velocity of 2000 m s^{-1} (see below). Both surveys image the diagenetic fronts; however, it is the 2D survey that provides the best images for interpretation which are used in the thesis. This is probably because the 2D survey images a larger part of the basin; hence providing more examples of the front geometry. However, the 3D dataset does provide some useful images of the opal-A to opal-CT boundary (e.g. Fig. 2.3), but rarely images the opal-CT to quartz boundary. The silica boundaries are probably less well developed in the 3D survey because this survey is located in the centre of the basin (Fig. 1.9) and the development of the boundaries is influenced by detrital sediments (see Chapter 3.5).

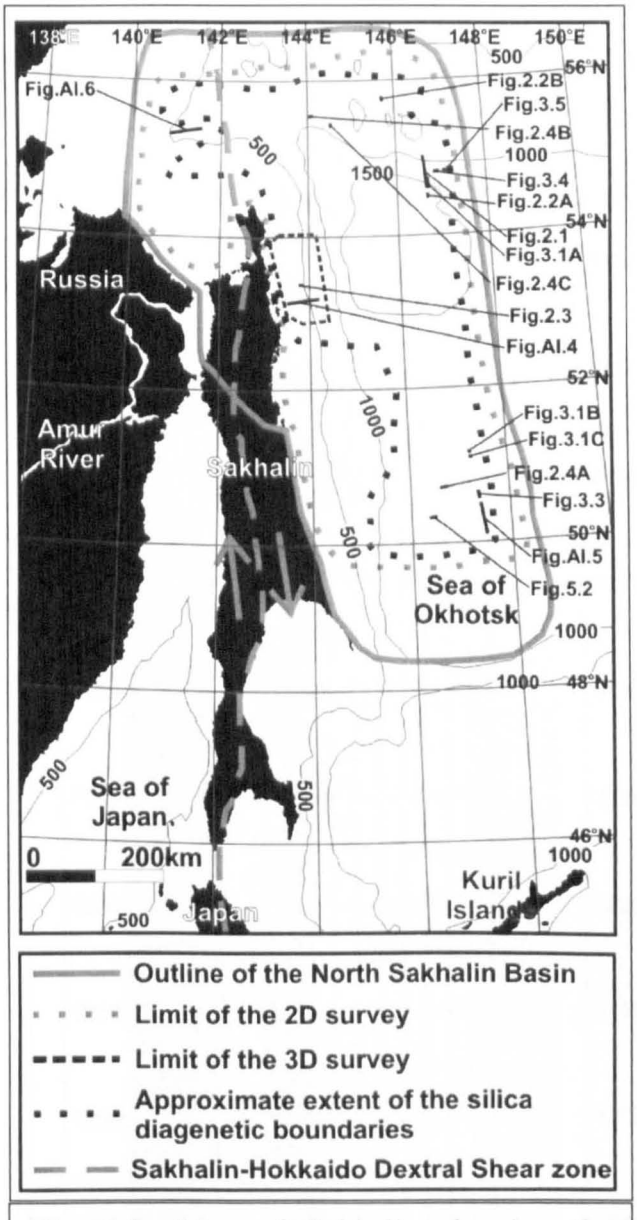

Fig. 1.9: Map of Sakhalin showing the location of the NSB. Bathymetry (thin black lines) shown in metres. Locations of subsequent figures from Chapters 2, 3, 5 and Appendix I that use images from the seismic dataset (see section 1.6) are indicated.

Seismic character alone is insufficient to constrain the origin of the high-amplitude, cross-cutting reflection events. However, lithological calibration of the seismic data are provided by offshore drilling, which indicates that these reflections are coincident with the transitions of opal-A to opal-CT and of opal-CT to quartz. I have not had access to wells from the NSB, despite repeated requests to BP. However, an image showing the lithology, biogenic silica content and log responses of one of these wells was released by BP (Fig. 1.10), though the raw data associated with the well was not. The neutron porosity, bulk density and sonic logs in figure 1.10 were obtained through LWD (logging while drilling). The positions of the silica diagenetic boundaries are identified by a combination of log response (Fig.

1.10), percentage of biogenic silica in the well cuttings through smear slide analysis (Fig. 1.10) and confirmed by seismic response (e.g. Fig. 2.1).

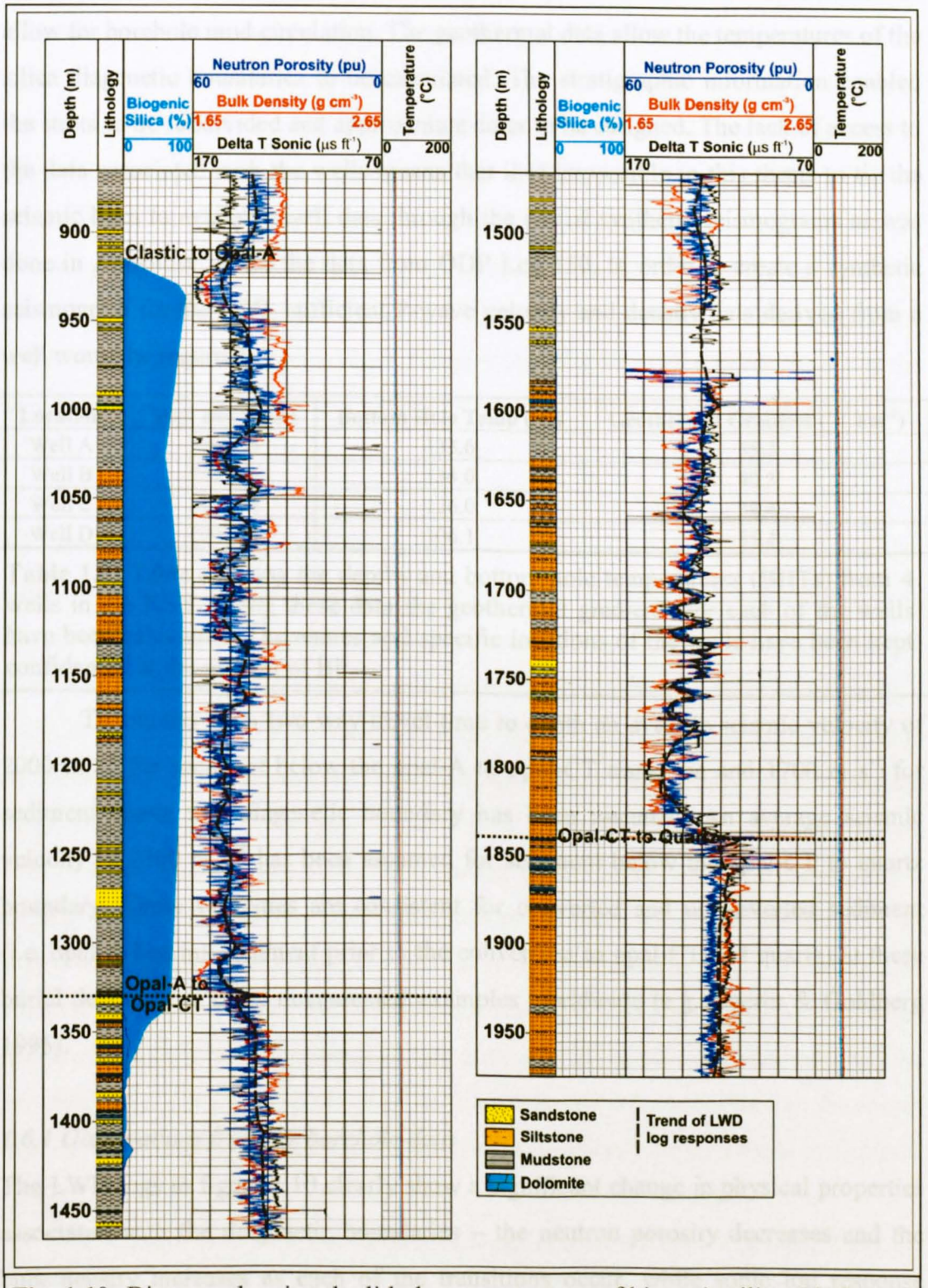

Fig. 1.10: Diagram showing the lithology, percentage of biogenic silica, LWD logs and temperature data for Well B (see Table 1.2) in the NSB. The temperature graph uses the bottom hole temperature. The percentage of biogenic silica is calculated by rig site smear slide analysis of cuttings from the well. The depth scale is in metres below sea level.

BP did provide limited data which relate to the geothermal gradient and the stratigraphy of the basin (see Appendix II). The bottom hole temperatures (BHTs) shown in table 1.2 are measured from the base of the wells and have been corrected to allow for borehole mud circulation. The geothermal data allow the temperatures of the silica diagenetic boundaries to be calculated. The stratigraphic information enabled the strata to be subdivided and approximate dates to be assigned. The lack of access to the data associated with the wells means that it is impossible in this thesis to tie the seismic lines to available well data through the use of synthetic seismograms as was done in Appendix III for the data from ODP Leg 150. In order to create a synthetic seismogram for the NSB, sufficient P-wave velocity and density data derived from a well would be required.

Location	Well Depth (m)	Bottom Hole Temp (°C)	Geothermal Gradient (°C km^{-1})
Well A	3795.45	133.6	35.2
Well B	3325.06	134.0	40.3
Well C	3199.94	126.0	39.4
Well D	2997.17	106.1	35.4

Table 1.2: Table showing the depths and bottom hole temperatures (BHTs) from 4 wells in the NSB. Using these data the geothermal gradients for each of the wells have been calculated. The names and specific locations of the wells have been kept confidential at the request of BP.

To convert from two-way-travel time to depth an average seismic velocity of 2000 m s^{-1} for sediment below the opal-A to opal-CT transition and 1700 m s^{-1} for sediment above this diagenetic boundary has been assumed. An average seismic velocity of 2300 m s^{-1} has been assumed for sediment below the opal-CT to quartz boundary. These velocities are consistent for converted and unconverted sediment (i.e. opal-A-bearing sediment prior to the conversion to opal-CT and quartz) at these burial depths from other documented examples worldwide (e.g. Guerin & Goldberg 1996).

1.6.1 Observations from the borehole data

The LWD logs in figure 1.10 clearly show a significant change in physical properties associated with the diagenetic boundaries – the neutron porosity decreases and the bulk density increases as each of the transitions occur, while sonic log response decreases as the sediment is compacted as a result of the changes in density and porosity. The sonic log decreases from ~150 μs ft^{-1} above the opal-A to opal-CT boundary to ~125 μs ft^{-1} below the boundary. The bulk density increases from ~1.75 g

cm^{-3} above the opal-A to opal-CT boundary to ~2.05 g cm^{-3} below the boundary, while the porosity decreases from ~50 pu (porosity units) above the opal-A to opal-CT boundary to ~35 pu below the boundary. The sonic log decreases from ~125 μs ft^{-1} above the opal-CT to quartz boundary to ~110 μs ft^{-1} below the boundary. The bulk density increases from ~2.05 g cm^{-3} above the opal-CT to quartz boundary to ~2.25 g cm^{-3} below the boundary, while the porosity decreases from ~35 pu (porosity units) above the opal-CT to quartz boundary to ~25 pu below the boundary. The data from the wells indicate that the reflections identified on seismic data are coincident with the transitions of opal-A to opal-CT and of opal-CT to quartz. The sediment becomes diatomaceous at ~925 m below sea level (Fig. 1.10). The percentage of biogenic silica in the diatomaceous sediment ranges between 60-90%, this value rapidly drops at the opal-A to opal-CT boundary to a value of <5% within 50 m below the boundary (Fig. 1.10).

1.7 Geological setting of the NSB

Sakhalin Island is located along the western margin of the Sea of Okhotsk (Fig. 1.9). The Sea of Okhotsk is a relatively shallow marginal sea forming the north-western margin of the Pacific Ocean. The sea has an average depth of ~ 820 m, reaching ~ 3400 m at its deepest point near the Kuril Islands. It is an area where biogenic siliceous sediments accumulated during the Miocene, which were overlain by deltaic sediments during the Pliocene (Tull 1997). Pelagic and hemi-pelagic marine sedimentation in the NSB, particularly during the Miocene, included diatomaceous organic-carbon rich siliceous mudstones, siltstones, marls and sandstones (Fig. 1.10), which were deposited in a restricted to basinal environment (Ritchie *et al.* 2006). It is within these rocks that the silica transitions are most likely to occur. The siliceous shales and diatomites are common in the basins of the Sea of Okhotsk, because the marginal sea represents a clastic-poor, sediment starved area, with much of the runoff towards the Arctic due to Eocene uplift of the areas around the sea (Karlo & Gebhard 2006).

The study area is located within the North Sakhalin Basin, which is a deep (up to 12 km), Tertiary strike-slip downwarp associated with a major north-south trending dextral strike-slip fault system, known as the Sakhalin-Hokkaido Dextral Shear Zone (Fig. 1.9), that formed as a result of Neogene displacement (Khvedchuk 1993; Worrall *et al.* 1996; Lindquist 2000; Weaver *et al.* 2004). The stratigraphy of the NSB

is outlined in Fig. 1.11. The basin fill unconformably overlies a Cretaceous to Palaeocene basement accretionary complex. This in turn is overlain by Oligocene syn-rift deposits and Miocene diatomaceous siliciclastic marine sediments, together with thick successions of deltaic sediments that accumulated in the Late Miocene-Pliocene (Tull 1997). These deltaic sediments are thought to have been deposited by the eastward-prograding palaeo-Amur River system (Lindquist 2000). The wells provide BHTs from which the geothermal gradient can be calculated (Table 1.2). Using the BHTs the calculated geothermal gradient in the NSB ranges between 35 and 40°C km^{-1} (see Table 1.2).

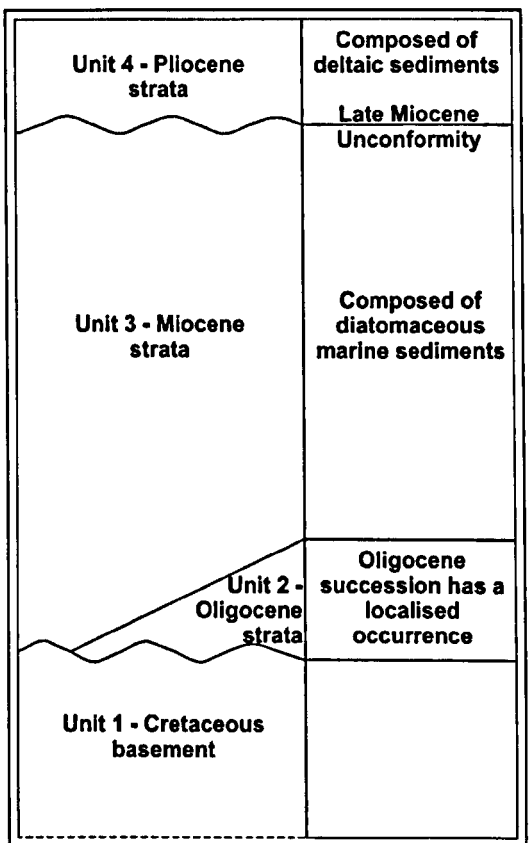

Fig. 1.11: Stratigraphic column showing the stratigraphy of the NSB. Based upon BP stratigraphic data (see Appendix II), the literature and observations from the seismic dataset (see Fig. 2.1).

Sakhalin has had a complicated geological evolution and has been affected by several phases of Cretaceous and Tertiary deformation which were caused by the complex interaction of plates in the north-western Pacific region. During the Mesozoic, Sakhalin was part of an offshore passive continental margin, but Aptian to Palaeocene plate collision resulted in subduction. The timing of the cessation of subduction is currently poorly constrained, but estimates range from Late Mesozoic to Early Cenozoic (Worrall *et al.* 1996; Weaver *et al.* 2004). There was a change in tectonic regime from subduction to strike-slip in the Tertiary that generated a series of basins to the east of Sakhalin. Early Tertiary transtension provided the accommodation space for deltaic progradation from the palaeo-Amur and its distributaries, with very high sedimentation rates of up to 500-800 m Ma^{-1} (Tull 1997). An episode of lateral compression during the Late Miocene resulted in erosion and the development of an unconformity on top of which the Pliocene deltaic sediments were deposited (Lindquist 2000). Sakhalin had become an island by 3Ma (Early Pliocene) as a result of the propagation of the strike-slip fault

system northwards; this resulted in the deflection of the Amur delta to the north (Brettle & Bessa 2006).

The diagenetic boundaries are hosted within Miocene and Pliocene sediments. There was also an episode of Late Pliocene tectonism and orogenic inversion that resulted in significant geologically recent folding and thrusting, and the modification of pre-existing structures as well as in significant amounts of erosion in the NSB (Tull 1997). The folds are orientated northwest-southeast and have a wavelength of 0.5-2 km.

1.8 Format of the thesis

The main part of this study concentrates on the silica diagenetic boundaries located in the North Sakhalin Basin. Chapter 1 provides an overview of what is currently known about the aspects of silica diagenesis. Chapters 2 and 3 give an in depth description of the silica diagenetic boundaries located within the North Sakhalin Basin, providing an account of their morphologies and position within the strata. Chapter 4 presents a new approach to estimating the porosity reduction associated with the opal-A to opal-CT transition using differential compaction and seismic data. Finally, Chapters 5 and 6 discuss the findings and present the overall conclusions of this thesis.

Chapter 2: The Silica Diagenetic Boundaries of the North Sakhalin Basin - Parallel Relationship of the Diagenetic Boundaries to the Late Miocene Unconformity

2.1 Introduction

Reflections that cross-cut stratigraphy and that are approximately parallel to the seabed are known from many continental margin settings. They are sometimes referred to as bottom simulating reflectors and are usually attributed to the base of gas hydrates or due to the conversion of opaline silica. Silica diagenetic boundaries are readily distinguished from hydrate-related boundaries because they generally occur at greater depths and have a positive acoustic impedance contrast as opposed to the negative impedance contrast of the hydrate base (Hein *et al.* 1978; Berndt *et al.* 2004).

This chapter deals with the terms isotherm or isothermal marker and thermal marker, as well as with their palaeo-equivalents. Each of these terms has a specific definition (e.g. Hein *et al.* 1978; Andrews-Speed *et al.* 1984; Kuramoto *et al.* 1992 and references therein): an isotherm is a boundary that can be traced across a basin, which will give a specific temperature for that point in the strata, while a thermal marker cannot be traced and can only be used in one location, such as in a well. Palaeo-isotherms and palaeo-thermal markers have the same definitions as their present day counterparts, but can only be used as temperature indicator at a specific point in the past, i.e. they cannot be used to give the present day temperature at that point or boundary in the strata. This chapter primarily deals with isotherms and palaeo-isotherms.

It is thought that because temperature is one of the dominant controls on the silica reactions that the opal-A to opal-CT diagenetic boundary may be isothermal marking a specific temperature at which the reaction occurred over extensive areas of basins (Hein *et al.* 1978; Kuramoto *et al.* 1992; Lee *et al.* 2003). This has been used as an explanation for the tendency of the opal-A to opal-CT reflection to also be parallel to the present day seabed, assuming the basin has a uniform geothermal gradient and that the reaction occurs at a single temperature. However, the thermal structure of a basin need not be parallel to the seabed and variations in heat flow caused by large-scale fluid movements in the subsurface may result in isotherms that are not parallel to the seabed (Andrews-

Speed *et al.* 1984). Many documented silica diagenetic boundaries are parallel to the present day seabed (e.g. Hein *et al.* 1978; Volpi *et al.* 2003), however others are not (e.g. Brekke *et al.* 1999; Davies & Cartwright 2002; Meadows & Davies 2007). Instead they are parallel to prominent unconformities. This chapter examines in detail the silica diagenetic boundaries from the North Sakhalin Basin (NSB), which show a high-degree of parallelism with the Late Miocene unconformity. The stratigraphy of the NSB is outlined in Chapter 1.7, figure 1.11.

Opal-A to opal-CT boundaries have also tentatively been used as low-temperature present day thermal markers to help reconstruct the thermal history of the basin in order to determine source rock maturity and the timing of the maturation (e.g. Brekke *et al.* 1999). They also have been considered useful for estimating the general trend of heat flow in a basin (Kuramoto *et al.* 1992; Lee *et al.* 2003). As a result of their tendency to follow unconformities the boundaries have even been proposed as potential palaeothermometers (e.g. Kuramoto *et al.* 1992).

The aim of this chapter is to examine the stratigraphic position of silica transformation boundaries in relation to the seabed and major unconformity surfaces, consider factors that control this and, through these seismic-based observations, question the suitability of silica diagenetic boundaries as isothermal markers.

2.2 Geological setting and database

The seismic database used in this chapter and the geological setting of the NSB are described in detail in Chapters 1.6 and 1.7 respectively.

2.3 Seismic stratigraphic observations

For the purposes of this study, the succession has been informally subdivided into four units primarily based upon seismic reflection amplitude, continuity and discordance, together with lithological and stratigraphic correlation provided by BP (see Appendix II). As a result of the lack of access to well data the ages listed below are approximate and are based upon published literature (Tull 1997; Lindquist 2000) and the stratigraphic data derived from the wells (see Appendix II). The seismic stratigraphy (Fig. 2.1) consists of a Cretaceous basement overlain by Oligocene, Miocene and Pliocene successions (Tull 1997; Lindquist 2000).

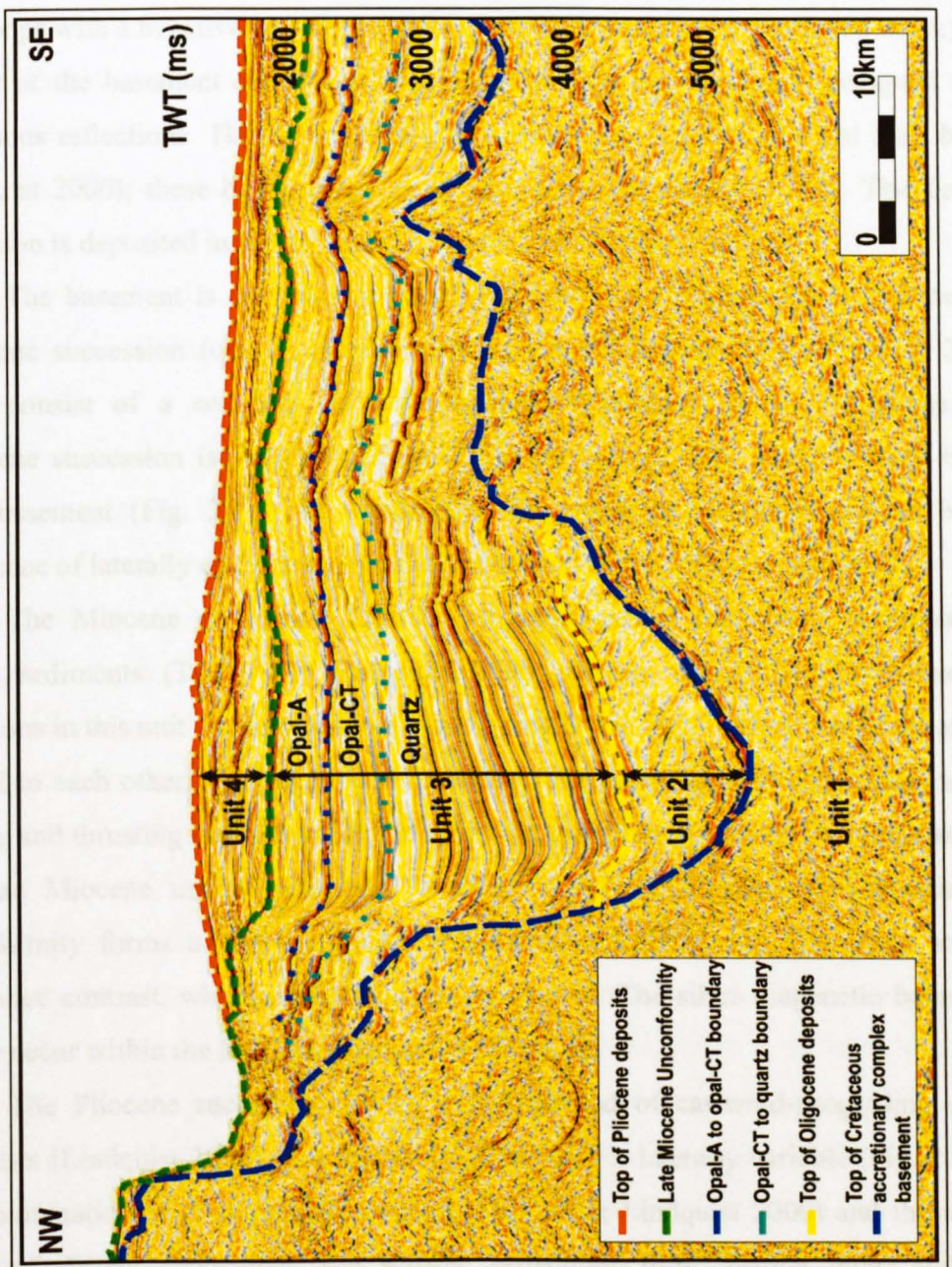

Fig. 2.1: Seismic line showing the main stratigraphic subdivisions discussed in the text and the position of the silica diagenetic boundaries. The stratigraphic succession is subdivided into a Cretaceous basement (unit 1), Oligocene syn-rift deposits (unit 2), Miocene siliciclastic, diatomaceous marine sediments (unit 3) and Pliocene deltaic sediments (unit 4). Note the southeastward progradation of the Pliocene deposits and the parallel relationship of the Late Miocene unconformity with the silica diagenetic boundaries. The same horizon colour convention is used throughout Chapters 2 and 3.

The basement (unit 1) consists of a Cretaceous accretionary complex, the top of this succession forms a semi-continuous high-amplitude seismic reflection consisting of three loops with a negative-positive-negative amplitude pattern (i.e. black-red-black). The interior of the basement consists of a series of mainly low-amplitude disrupted semi-continuous reflections. The basement has been rifted into a series of tilted fault blocks (Lindquist 2000); these highs occasionally reach the present day seabed. The Tertiary succession is deposited in the depressions between the blocks (Fig. 2.1).

The basement is overlain by both Oligocene and Miocene age sediments. The Oligocene succession (unit 2) is composed of syn-rift deposits (Ritchie *et al.* 2006), which consist of a sequence of low-amplitude disrupted seismic reflections. The Oligocene succession is only present locally at the base of depressions formed by the rifted basement (Fig. 2.1). The top of the Oligocene succession is marked by the occurrence of laterally continuous, parallel reflections of the Miocene succession.

The Miocene succession (unit 3) is composed of siliciclastic, diatomaceous marine sediments (Tull 1997; Lindquist 2000; Ritchie *et al.* 2006). The seismic reflections in this unit are laterally continuous, range from high- to low-amplitude and are parallel to each other. The succession has been deformed (Fig. 2.1) by folding, normal faulting and thrusting (not shown in Fig. 2.1). The top of the succession is represented by the Late Miocene unconformity on to which the Pliocene succession onlaps. The unconformity forms a high-amplitude, continuous reflection with a positive acoustic impedance contrast, which is the same as the seabed. The silica diagenetic boundaries mainly occur within the Miocene succession (Fig. 2.1).

The Pliocene succession (unit 4) is composed of eastward-prograding deltaic sediments (Lindquist 2000). The thickness of this unit is laterally variable (Fig. 2.1) due to a combination of post-Pliocene erosion (Tull 1997; Lindquist 2000) and the uneven nature of deltaic deposition. The seismic reflections form distinct high- and low-amplitude progradational 'packages' and clinoforms, which have onlapping and downlapping relationships with each other and with the Late Miocene unconformity (Fig. 2.1). Parts of the Pliocene succession show evidence of being affected by only minor deformation, while most of the succession remains unaffected. There are also minor Pleistocene and Holocene deposits (Lindquist 2000), which have been grouped with the

Pliocene succession in this study because they are too thin on the seismic lines to be classed as a separate unit.

2.4 Interpretation of seismic stratigraphy

On the basis of the observations the stratigraphy is subdivided into Cretaceous, Oligocene, Miocene and Pliocene stratigraphic units with an important unconformity dated by its position in the stratigraphy, on the basis of the pattern of the seismic reflections, as being Late Miocene in age. These ages are approximate and are based upon published literature (Tull 1997; Lindquist 2000) and the stratigraphic data (Appendix II).

The boundary that forms the top of the Miocene succession consists of a high-amplitude, continuous reflection, which has a positive acoustic impedance contrast on to which the Pliocene succession onlaps (marked 1, Fig. 2.2). The stratal reflections of the Late Miocene succession are truncated at this boundary (marked 2, Fig. 2.2). This feature is interpreted to be a break in sedimentation and subsequent erosion that occurred during the Late Miocene, which marked a change in depositional setting from marine to deltaic (Tull 1997). This break in sedimentation also coincided with the propagation of the dextral strike-slip fault system northwards during the Late Miocene to Early Pliocene (Brettle & Bessa 2006). This break in sedimentation, together with erosion, led to the development of an unconformity during the Late Miocene.

Currently the well data for the basin has not been released, but BP's own seismic stratigraphic interpretation, see Appendix II, indicates that there is an unconformity at this point in the succession, but the biostratigraphic data are not sufficient to indicate how long the period of erosion and non-deposition lasted. Throughout much of the seismically surveyed parts of the NSB the Pliocene succession unconformably overlies the Miocene succession, but there are instances where the successions are conformable, i.e. the unconformity becomes a correlative conformity. The Late Miocene unconformity is located approximately between <50-1000 m below the present day seabed. The lithologies present in the Miocene strata include diatomaceous organic-carbon rich siliceous mudrocks together with some sandstones, marls and cherts (Tull 1997; Lindquist 2000; Richie *et al.* 2006). Pliocene lithologies consist of deltaic sandstones and some mudstones with limited biosiliceous content (Tull 1997; Lindquist 2000).

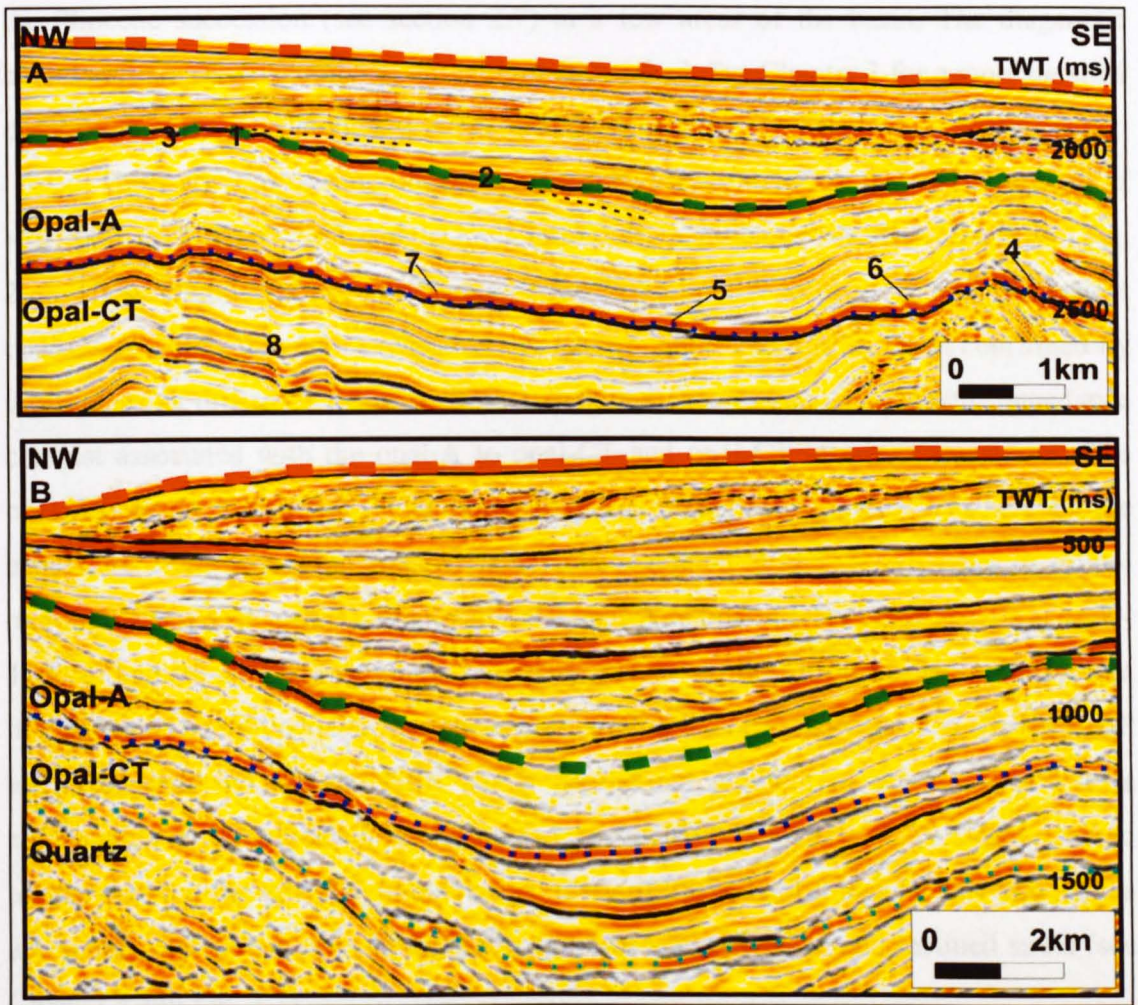

Fig. 2.2: Seismic lines showing the Late Miocene unconformity close-up. **(A)** The overlying Pliocene deltaic sediments have an onlapping relationship to the unconformity (1), while the top of the Miocene succession shows some minor evidence of erosional truncation (2). The unconformity reflection has an irregular, erosive appearance (3), which truncates the underlying sediments. Note the parallel relationship with the diagenetic boundaries. This seismic line also shows some of the morphological features of the diagenetic boundaries: serrated patterns (4), cross-cutting of stratigraphy (5), attached wings (6) and less well developed attached wings (7) – see Chapter 3. Also note the faulting (8). **(B)** Another example of the diagenetic boundaries showing a parallel relationship to the Late Miocene unconformity.

2.5 Diagenetic fronts: General characteristics

The diagenetic fronts are not observed in the Cretaceous basement or in Oligocene-age sediments and where the basement forms fault blocks the boundaries terminate. The diagenetic boundaries are generally observed to cross-cut the Miocene succession, but the opal-A to opal-CT front also cross-cuts the Late Miocene Unconformity and passes into

the Pliocene succession (see section 2.7) in a few areas of the basin. The diagenetic boundaries are rarely parallel to the present day seabed. See Chapter 3 for a more detailed description of the morphology of the diagenetic fronts.

There are two seismic boundaries separated by 300-400 m that cover an area of ~107,000 km^2, which form single high-amplitude, continuous seismic reflections (Fig. 2.2). These boundaries have been interpreted to be opal-A to opal-CT and subsequent opal-CT to quartz transitions (Meadows & Davies 2007) and this has been confirmed by the four wells drilled in the area. Both reflections show a positive acoustic impedance contrast associated with the opal-A to opal-CT and opal-CT to quartz transitions. The opal-A to opal-CT and opal-CT to quartz boundaries are mostly parallel to each other, the exceptions being where the boundaries have been altered by the various types of frontal morphology (see Chapter 3). Regionally, the opal-A to opal-CT boundary occurs at ~500-1400 m and the opal-CT to quartz boundary occurs at ~800-1900 m below the present day seabed. The shallowest occurrences are found in the near-shore parts of the NSB. BP well data indicate that the NSB has a geothermal gradient of 35-40°C km^{-1}. This corresponds to temperatures at the opal-A to opal-CT boundary of 17.5-49°C and to temperatures at the opal-CT to quartz boundary of 28-76°C (Table 2.1). The boundaries are mainly concordant with stratigraphy, but cross-cut deformed and inclined strata (see Chapter 3 and Fig. 2.2).

Location	A-CT Depth (m)	A-CT Temp (°C)	CT-Qtz Depth (m)	CT-Qtz Temp (°C)	Geothermal gradient (°C km^{-1})
Sakhalin (NSB)	500	17.5 – 20	800	28 – 32	37.5 ± 2.5
Sakhalin (NSB)	800	28 – 32	1100	38.5 – 44	37.5 ± 2.5
Sakhalin (NSB)	1400	49 – 56	1900	66.5 – 76	37.5 ± 2.5

Table 2.1: Table showing the depths and temperatures associated with the silica diagenetic boundaries in the NSB. The depths of the boundaries were taken from the seismic data and the temperatures were calculated using the highest and lowest geothermal gradients from Table 1.2.

The diagenetic fronts are rarely parallel to the seabed, unlike many other silica transitions (e.g. Hein *et al.* 1978). Instead in most areas they are parallel to the Late Miocene Unconformity (Figs. 2.1, 2.2 and 2.3). Figure 2.3 also shows how the change in

porosity of the sediment caused by the transition influences the inclination of the strata above and below the boundary.

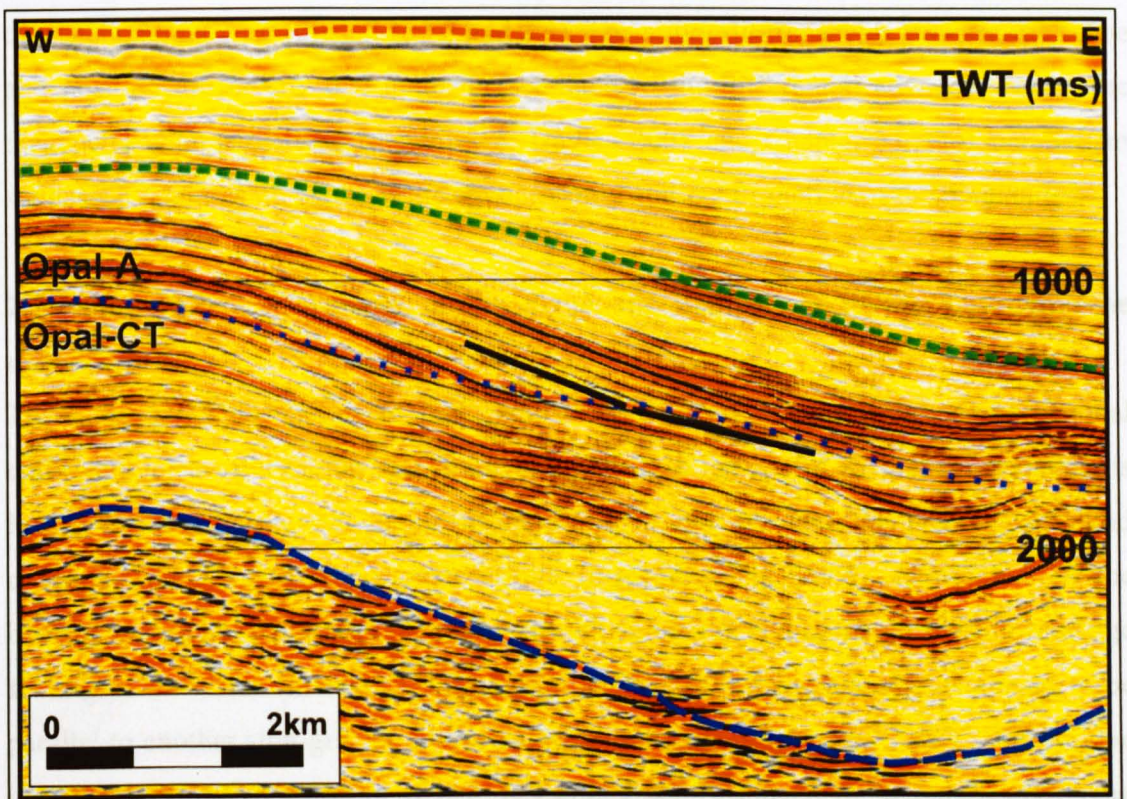

Fig. 2.3: Seismic line showing the opal-A to opal-CT boundary (purple dotted line). Note that the boundary shows a high degree of parallelism to the Late Miocene unconformity (green dashed line). Note that the inclination of the strata changes as they pass through the boundary (indicated by the solid black lines). The strata are more steeply inclined above the boundary than it is below the boundary.

2.6 Parallel relationship of the diagenetic boundaries to the Late Miocene unconformity

Over ~ 80% of the area covered by the silica diagenetic boundaries, which cover an area of ~107000 km^2, show a high degree of parallelism with the Late Miocene unconformity (Figs. 2.1, 2.2 and 2.3). The parallel relationship with the unconformity extends to both the opal-A to opal-CT and opal-CT to quartz diagenetic boundaries. The opal-A to opal-CT boundary is located ~300-400 m below the unconformity, while the opal-CT to quartz boundary is ~600-800 m below. The examples in figures 2.1, 2.2 and 2.3 show that there is a close match between the geometry and position of the Late Miocene unconformity and that of the silica diagenetic boundaries. Where there are highs in the Late Miocene

unconformity there are also highs in the position of the silica diagenetic boundaries; conversely lows in the position of the unconformity are matched by lows in the diagenetic boundaries (Figs. 2.1, 2.2 and 2.3). The minor discrepancies between the shape and position are mostly due to features related to the differential advancement of the diagenetic boundaries (see Meadows & Davies 2007 and Chapter 3). This parallelism suggests a relationship between the unconformity and the formation of the boundaries.

2.7 Non-parallel relationship of the diagenetic boundaries to the Late Miocene unconformity

There are some exceptions to this parallel relationship usually where compressional deformation has affected the host strata. In figure 2.4A the opal-A to opal-CT boundary is hosted in the Pliocene syn-compressional fill of a syncline (marked 1, Fig. 2.4A) and cross-cuts the Late Miocene unconformity (marked 2, Fig. 2.4A). In figure 2.4B the boundaries are not parallel to the deformed unconformity and cross-cut the Pliocene age folding of the strata (marked 3, Fig. 2.4B). In figure 2.4B the boundaries appear to be parallel to another stratigraphic horizon (green-grey dashed line, Fig. 2.4B). This horizon is probably Mid-Late Pliocene in age. In figure 2.4C the diagenetic boundaries cross-cut anticlinal folding of the strata, which it is only slightly affected by (marked 4, Fig. 2.4C). Where there is a low in the Late Miocene unconformity (marked 5, Fig. 2.4C) the diagenetic boundaries do not maintain a parallel relationship with that stratigraphic horizon. However, where the parallel relationship with the Late Miocene unconformity does not occur, the diagenetic boundaries are not parallel to the present day seabed.

Fig. 2.4 (next page): Seismic lines showing examples where the silica diagenetic boundaries lose their parallel relationship with the Late Miocene unconformity. **(A)** Folding has allowed syn-compressional upward migration of the boundaries within the trough of a syncline (1). The opal-A to opal-CT boundary has advanced into the Pliocene syn-compressional fill above the unconformity, cross-cutting the limbs of the syncline (2). Note that the boundaries largely retain their parallel relationship with the unconformity within the crests of the anticlines. **(B)** The silica diagenetic boundaries are not parallel to the deformed Late Miocene unconformity, but cross-cut the Pliocene-age folding (3) of the Miocene strata. The boundaries appear to be parallel to another stratigraphic horizon (grey-green dashed line), which is probably Middle to Late Pliocene in age and undeformed. **(C)** Another example where the diagenetic boundaries are no longer parallel to the Late Miocene unconformity.

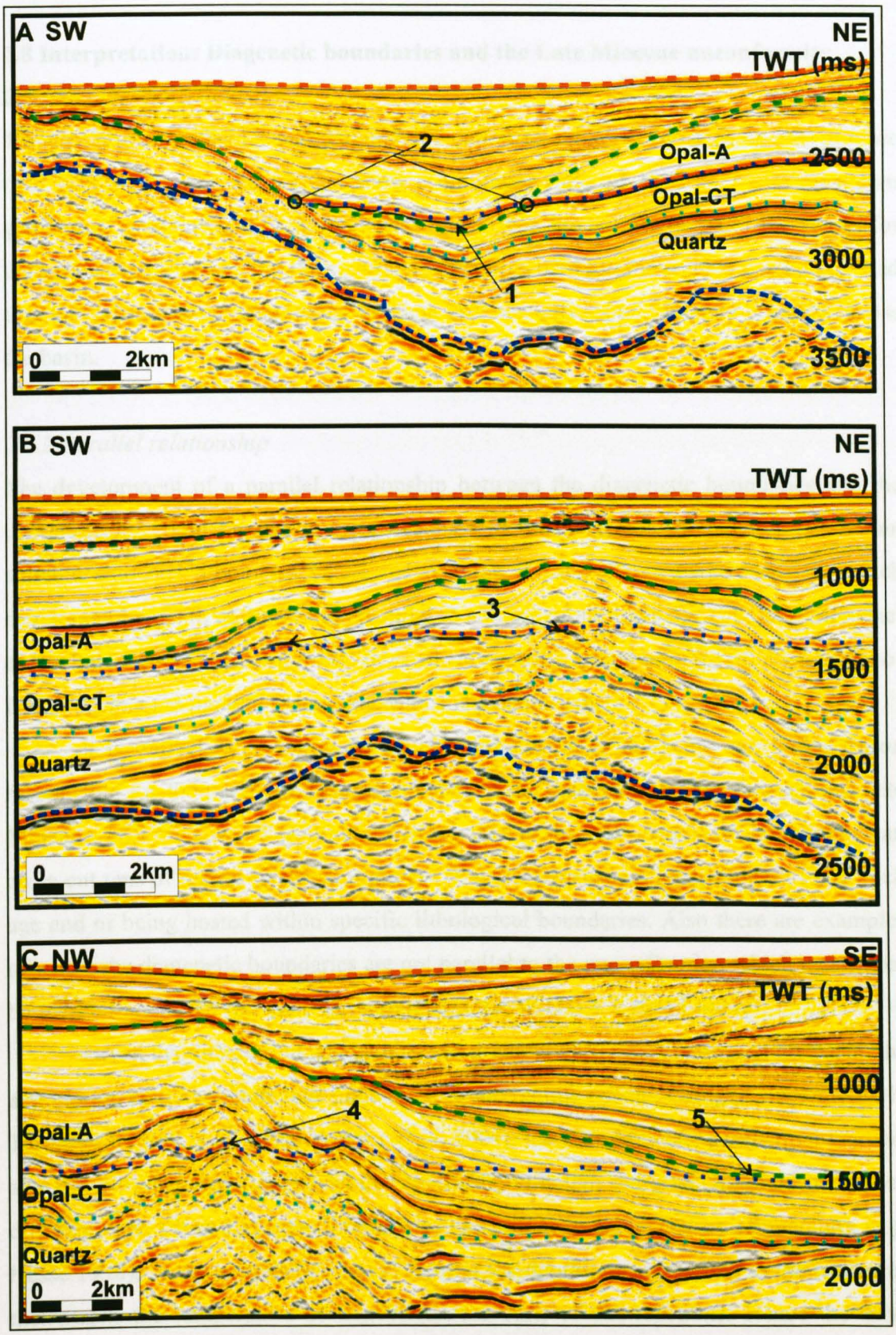
A SW
NE
TWT (ms)
2
Opal-A
2500
Opal-CT
Quartz
3000
1
0
2km
3500
B SW
NE
TWT (ms)
1000
3
Opal-A
1500
Opal-CT
Quartz
2000
0
2km
2500
C NW
SE
TWT (ms)
1000
4
5
Opal-A
1500
Opal-CT
Quartz
2000
0
2km

2.8 Interpretation: Diagenetic boundaries and the Late Miocene unconformity

2.8.1 Geothermal gradient

The geothermal gradient is based upon BHT data from the wells covering an area of more than 10000 km^2. The wells either show a minimum value of 35°C km^{-1} or a maximum geothermal gradient of 40°C km^{-1} (Table 1.2). Given the narrow range of the values for the geothermal gradient and the significant distances between the wells it can be assumed that the values for the geothermal gradient are, spatially, approximately constant across the basin.

2.8.2 Parallel relationship

The development of a parallel relationship between the diagenetic boundaries and the unconformity could be due to two reasons: (1) the diagenetic boundaries are within suitable siliceous lithologies where the reaction is more likely to be initiated, which develop at the depth of conversion parallel to and are of the same age (i.e. Late Miocene) as the Late Miocene unconformity; or (2) the diagenetic boundaries are following palaeo-isotherms that are parallel to the Late Miocene palaeo-seabed.

It is unlikely that following suitable lithologies of the same age is the reason responsible for the parallel relationship between the diagenetic boundaries and the Late Miocene unconformity. The main basis for this is that the diagenetic boundaries can cross-cut tens of metres of the stratigraphy (Fig. 2.2), hence are independent of host rock age and of being hosted within specific lithological boundaries. Also there are examples of where the diagenetic boundaries are not parallel to the unconformity, which means that boundaries are not of the same age throughout the NSB (i.e. Late Miocene).

Given that the present day geothermal gradient does not vary around the basin, the assumption could be made that since the tectonic regime has not changed since the Early Tertiary (Worrall *et al.* 1996; Weaver *et al.* 2004), the Late Miocene geothermal gradient also did not vary significantly around the basin, although the gradient could have been different. The silica diagenetic boundaries are primarily controlled by temperature (e.g. Hesse 1990), so the boundaries should form at the depths corresponding to the isotherms that match the temperature of conversion for each of the reactions. Hence the most probable and simplest reason for the parallel relationship of the diagenetic boundaries

with the Late Miocene unconformity results from the diagenetic boundaries following an isotherm parallel to the Late Miocene seabed. The diagenetic boundaries are rarely parallel to the present day seabed, but may represent palaeo-isotherms that are parallel to the Late Miocene palaeo-seabed.

2.8.3 Non-parallel relationship

In some parts of the basin the diagenetic boundaries are not parallel to the Late Miocene unconformity. Where this relationship occurs the boundaries are not parallel to the present day seabed either; therefore it can be proposed that they are not following present day isotherms. In these examples the boundaries can be parallel to Pliocene stratigraphy (e.g. Fig. 2.4B). Therefore the boundaries may be following palaeo-isotherms parallel to a palaeo-seabed that is Pliocene in age.

This could have several explanations, which relate to the timing and mechanisms that affect the rate of conversion at the diagenetic boundaries. This suggests that there could be a more fundamental relationship between diagenetic boundary equilibrium and the prevailing lithological and geothermal conditions. It is important to note that the opal-CT to quartz boundary is parallel to the opal-A to opal-CT boundary, this probably indicates that changes to the rate of conversion at the diagenetic boundaries occurred at the same time. These transitions would have different reaction kinetics, but they have been affected by the same event or factors.

2.9 Explanation for the stratigraphic position of the diagenetic boundaries

2.9.1 Palaeo-isothermal diagenetic boundaries

It has been observed that conversion in the NSB occurs at different depths and therefore temperatures (Table 2.1), based upon the overall geothermal gradient of the NSB. There is no identifiable systematic pattern to the changes in diagenetic boundary depths across the basin, i.e. the deviations in the depths of the boundaries do not relate to the basin geometry, such as the seafloor bathymetry or variations in the height of the basement. For example, the diagenetic boundaries in the NSB, especially large-scale boundary morphologies such as multi-kilometre scale depressions, have previously been identified as being independent of the effects of highs in the basement (see Meadows & Davies 2007). It is also unlikely that variations in seafloor temperatures, which would only vary

very slightly, would have a significant influence on the positions of the diagenetic boundaries. Assuming that temperature is the principal factor controlling conversion and that the isotherms are parallel to the contemporaneous seabed, one would expect the boundaries to occur at similar depths across the basin. Therefore, at least in the present day NSB, it can be proposed that the diagenetic boundaries are not present day isothermal boundaries. These are termed palaeo-isothermal boundaries.

2.9.2 Influences on the rate of conversion

Mizutani (1970) related the rate of conversion at the silica diagenetic boundaries to a dependence on temperature. However, Williams *et al.* (1985) suggested that temperature, together with other physical parameters, may not be as important as previously thought in the process of silica diagenetic alteration. The relationship between solubility and surface area or particle size (i.e. lithologic effects) would be sufficient to explain simple opal-A to opal-CT to quartz transformations (Williams *et al.* 1985). If this is the case then the diagenetic boundaries do not necessarily represent some single maximum temperature, but instead represent a cumulative time/temperature threshold. The primary effect of temperature may be simply to increase the rates of reaction, allowing transformations to occur earlier than they otherwise would. For example, the Monterey Formation is still diatomaceous in many areas and has only undergone transformation where it has been buried to sufficient depths for temperature to act to increase the rate of dissolution and reprecipitation (e.g. Keller & Isaacs 1985). If the kinetic view of Williams *et al.* (1985) is correct it would mean that the overall temperature history, in conjunction with lithologic effects, and not just the maximum palaeo-temperature will determine the position of the diagenetic boundaries within the strata.

2.9.3 Mechanisms for palaeo-isothermal behaviour

This chapter outlines four possible mechanisms that could cause a change in the relative rate of conversion at the diagenetic fronts, which will affect the stratigraphic position of the boundaries and their development into palaeo-isothermal boundaries (Fig. 2.5). These mechanisms are (1) a decrease in temperature, e.g. caused by a declining geothermal gradient, which would cause the rate of conversion to slow; (2) a decreasing burial rate, which causes the rate of conversion to decrease; (3) erosion of the overburden, which

would produce a similar effect to a decrease in temperature and a decreasing burial rate; and (4) change in the rate of conversion hence the rate the front advances due to the physico-chemical factors varying in the strata, such as variations in lithology.

A decrease in temperature (Fig. 2.5B), such as through a declining geothermal gradient, would cause a reduction in the rate of conversion at the diagenetic boundary. A decrease in temperature would leave the boundaries at depths no longer corresponding to the temperatures required for conversion, i.e. the DOC (depth of conversion) would be deeper in already converted sediment. This rapid reduction in the rate of conversion would leave the boundaries following palaeo-isotherms parallel to the palaeo-seabed prior to the reduction in temperature. A rapid decrease in the burial rate (Fig. 2.5C) will result in the strata not being buried and subsiding through the DOC as fast as before. This means the diagenetic boundaries would rapidly slow their upward migration through the subsiding strata, resulting in a significant decrease in the rate of conversion. This decrease in the rate of conversion could be significant enough to cause the diagenetic boundaries to no longer maintain a parallel relationship to the present day seabed and to follow the palaeo-seabed prior to the decrease in burial rate (Fig. 2.5C). Erosion of the overburden (Fig. 2.5D) would result in a decrease in the rate of conversion as removal of the overlying sediment results in deeper DOCs, in a similar way to a decrease in temperature. Varying physico-chemical factors, such as the silica content of the sediment can also have an effect on the rate of conversion (Fig. 2.5E). These factors may be more important than the effect of temperature (e.g. Williams *et al.* 1985) over localised rather than basinal distances. For example, strata with a high silica content will cause the rate of conversion to increase, although this will not result in palaeo-isothermal boundaries as the high rate of conversion would enable the boundaries to follow isotherms parallel to the present day seabed. However, a low silica content in the sediment will inhibit the rate of conversion meaning the boundaries would no longer be able to follow isotherms parallel to the contemporaneous seabed, but become palaeo-isotherms that could be parallel to a palaeo-seabed.

However, without evidence of the precise conditions operating in a basin it is not possible to tell if one of the above mechanisms is dominant or whether it is a combination of the mechanisms that is responsible for the relative decrease in the rate of conversion and to the development of palaeo-isothermal boundaries. It would also require the strata

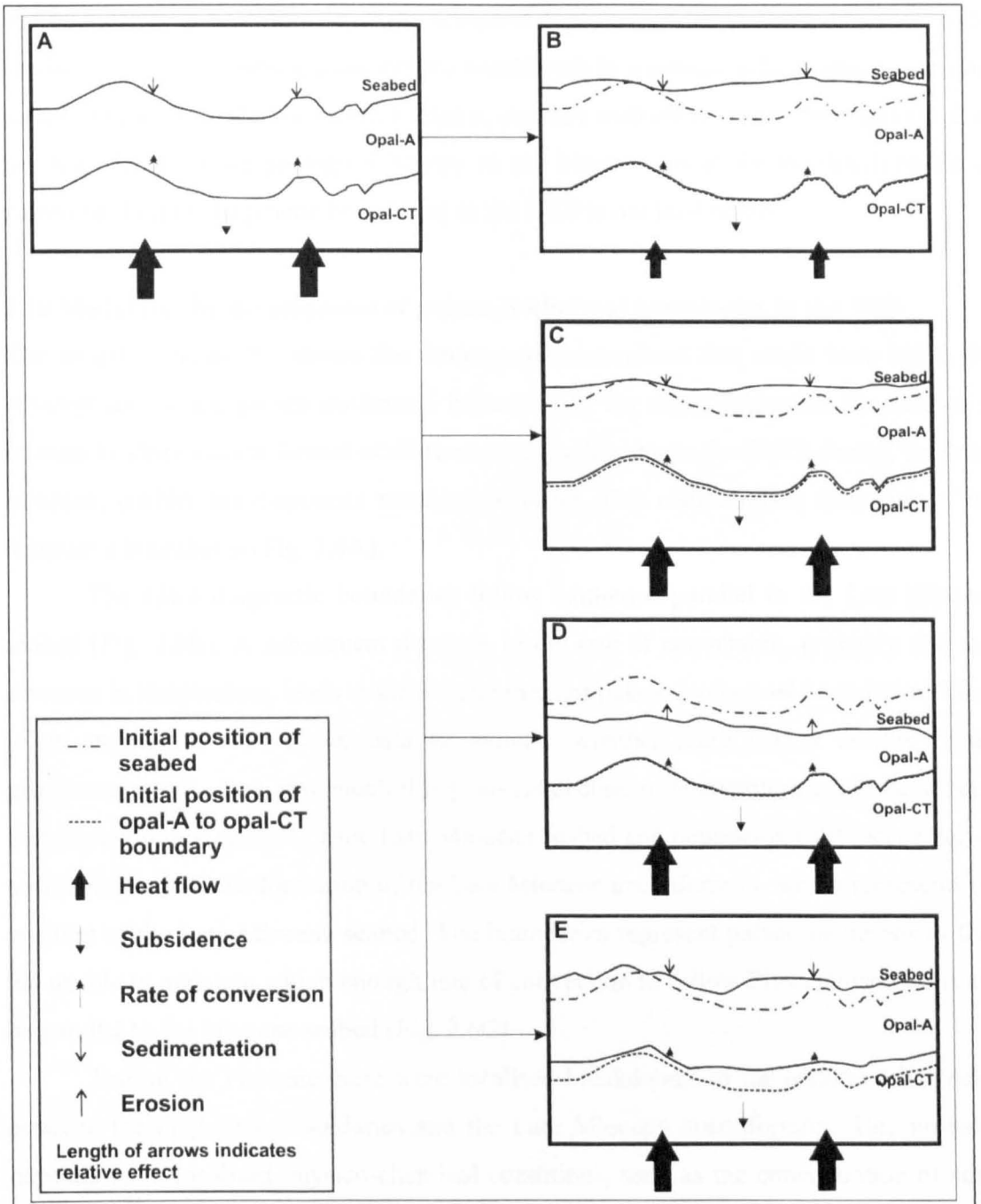

Fig. 2.5: Schematic diagram showing the various mechanisms that could lead to the development of palaeo-isothermal diagenetic boundaries. **(A)** Diagenetic boundary is in equilibrium with the prevailing conditions within the basin and develops as an isothermal boundary. **(B)** Declining geothermal gradient leads to a decrease in the rate of conversion. **(C)** A rapid decline in burial rate causes the rate of conversion to decrease. **(D)** Erosion of the overburden leads to a decrease in the temperature at the boundary, hence to a decrease in the rate of conversion. **(E)** A change in the physico-chemical conditions within the strata leads to a change in the rate of conversion.

and boundaries to be deformed or the sediment deposited above the boundaries not to be parallel to them to produce a discernible breakdown in a parallel relationship on seismic data. Using some of the above mechanisms, together with observations from seismic data and knowledge of the geological history of the basin, a model for the development of palaeo-isothermal diagenetic boundaries in the NSB is outlined below.

2.10 Model for the development of palaeo-isothermal boundaries in the NSB

The model in figure 2.6 shows the timing and mechanisms that could have led to the development of the palaeo-isothermal behaviour of the silica diagenetic boundaries in relation to other events. Burial of diatomaceous sediments to the DOC, during the Mid-Miocene, enables the diagenetic reactions to occur. This results in the formation of the diagenetic boundaries (Fig. 2.6A).

The silica diagenetic boundaries follow isotherms parallel to the Late Miocene seabed (Fig. 2.6B). A subsequent decrease in the rate of conversion, probably due to a decrease in temperature, leads to the development of palaeo-isothermal boundaries. There is no supporting temperature data to indicate whether there was a decline in the geothermal gradient or how much this possible decline in temperature could have been. Subsequent minor erosion of the Late Miocene seabed and deposition of Pliocene deltaic sediments leads to the formation of the Late Miocene unconformity, which represents the position of the Late Miocene seabed. The boundaries represent palaeo-isotherms as they are unable to maintain a high enough rate of conversion to follow Pliocene isotherms and be parallel to the Pliocene seabed (Fig. 2.6C).

During the Pliocene there were localised breakdowns in the parallel relationship between the diagenetic boundaries and the Late Miocene unconformity. This probably depends upon localised physico-chemical conditions, such as the concentration of silica in the sediment, or localised variations in heat flow which varied the rate of conversion at that point relative to other parts of the boundaries. This enables a high enough rate of conversion to continue in isolated areas (Fig. 2.6C), which results in these areas following Pliocene isotherms parallel to the Pliocene seabed.

During the Mid-Late Pliocene (Fig. 2.6D), deformation resulted in uplift and NW-SE trending folding of the strata, including the Late Miocene unconformity. Pliocene

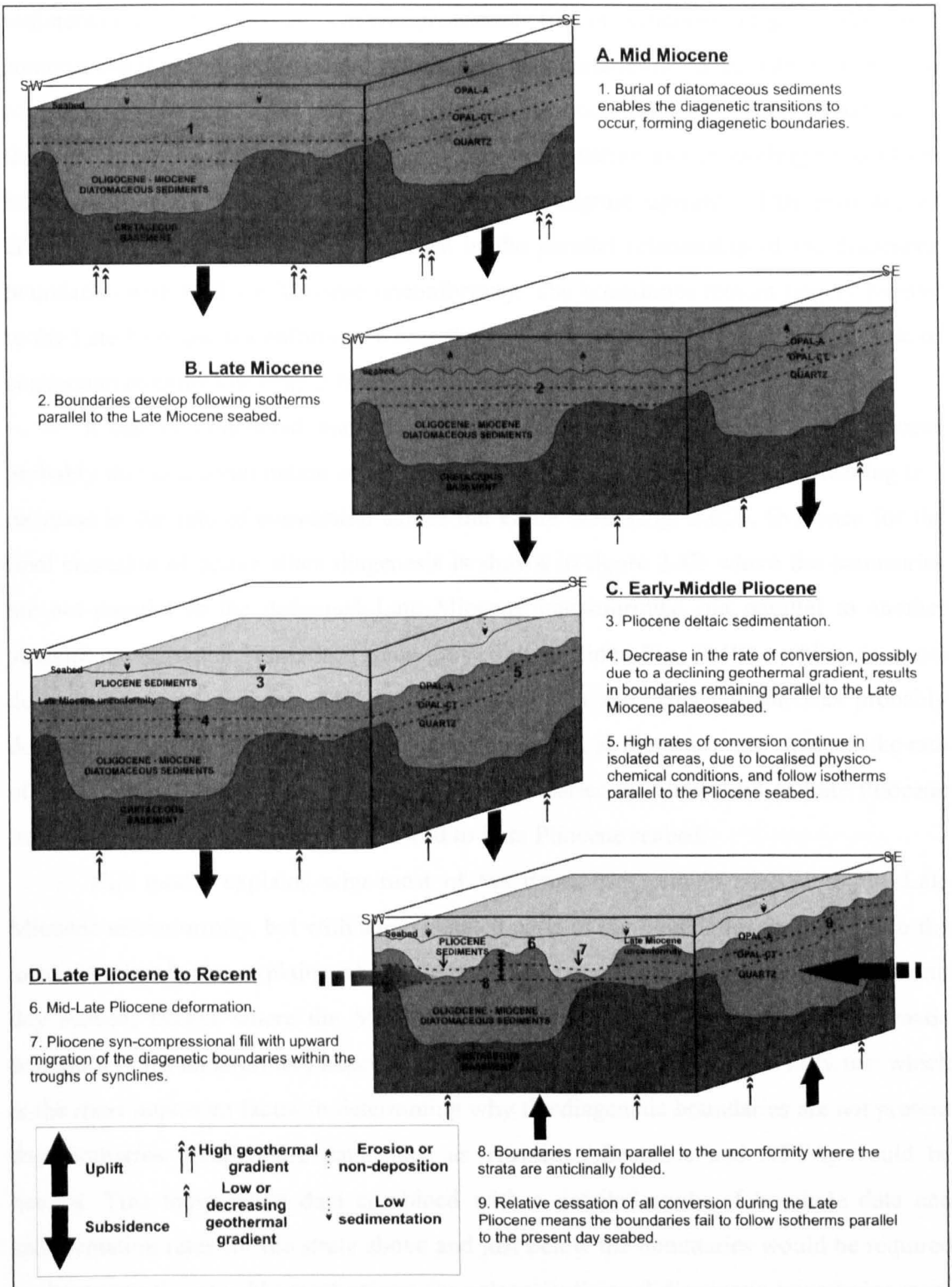

Fig. 2.6: Model showing the development of the silica diagenetic boundaries relative to other events. See text in the figure for further explanation.

sedimentation continued as syn-compressional fill in synclines (Fig. 2.6D). Syn-compressional upward migration of the diagenetic boundaries occurred within the troughs of the synclines (Figs. 2.4A and 2.6D), because the boundaries have been folded below the DOC meaning the rate of conversion increases relative to surrounding parts of the boundary to allow that part of the boundary to migrate upwards. This provides an alternative mechanism for the breakdown in the parallel relationship of the diagenetic boundaries with the Late Miocene unconformity. The boundaries remain largely parallel to the Late Miocene unconformity where the strata are anticlinally folded and the rate of conversion remains low (Fig. 2.6D).

It can be concluded that all active conversion ceased after the Late Pliocene probably due to a combination of uplift and a declining geothermal gradient leading to a decrease in the rate of conversion across the entire NSB (Fig. 2.6D). Evidence for the final cessation of active silica diagenesis is shown in figure 2.4B where the boundaries are not parallel to the deformed Late Miocene unconformity, but parallel to another younger stratigraphic horizon (green-grey dashed line, Fig. 2.4B), which is post-deformational and probably Mid to Late Pliocene in age. This horizon was probably deposited soon after the episode of deformation ended, as there was still time for the rate of conversion at certain isolated parts of the boundaries to follow Mid to Late Pliocene isotherms, hence parallelism with the Mid to Late Pliocene seabed.

This model explains why most of the boundaries remain parallel to the Late Miocene unconformity, but with some isolated parts of the boundaries not parallel to the unconformity. It also explains why no parts of the boundaries are parallel to the present day seabed, except where the Miocene and Pliocene strata, including the diagenetic boundaries, are undeformed; hence remaining parallel to the seabed. To fully test which is the most important factor in determining why the diagenetic boundaries are not present day isotherms, temperature data, such as vitrinite reflectance and AFTA, would be needed. This temperature data combined with a detailed study of borehole data and sedimentation rates for the strata above and just below the boundaries would be required to determine the possible mechanisms for palaeo-isothermal diagenetic boundaries more precisely.

2.11 Discussion

2.11.1 Implications for hydrocarbon exploration

There are several examples of where the silica diagenetic boundaries are parallel to the seabed and are thought to be isotherms that could be used as present day or palaeo-temperature markers within a basin (e.g. Hein *et al.* 1978; Nobes *et al.* 1992a; Davies & Cartwright 2002; Lee *et al.* 2003). Hein *et al.* (1978) suggested that the opal-A to opal-CT boundary, which is parallel to the present day seabed in the Bering Sea, is a time transgressive boundary and not hosted by a lithology of a single age. This boundary may mark an isotherm related to the depth of burial and the local geothermal gradient (i.e. the temperature recorded is that required to transform the opal-A to opal-CT in the area). Hein *et al.* (1978) noted that the diagenetic boundary moved up-section keeping pace with the upward migrating thermal boundary during ongoing burial, hence the opal-A to opal-CT boundary should remain at a sub-bottom depth of 550-650 m. Therefore, as long as the silica diagenetic boundaries remain in equilibrium with the prevailing conditions they will develop as isothermal boundaries parallel to the present day seabed. Hence, such isothermal boundaries could be used in basin analysis as temperature markers (i.e. the temperature of conversion) from which the geothermal gradient could be calculated. However, if the rate of conversion is affected by changes in conditions within the basin, then boundaries are no longer in equilibrium with the thermal conditions and will cease to be isotherms parallel to the present day seabed. This is the case in the NSB and in the Faeroe-Shetland Basin (see Davies & Cartwright 2002) where the boundaries appear to be palaeo-isotherms parallel to a palaeo-seabed. In this situation the boundaries could not be used as present day temperature markers as the position of the boundaries in the strata would no longer correspond to the original temperature of conversion. Therefore, the use of silica diagenetic boundaries as temperature markers is highly dependent on their identification as present day isotherms or palaeo-isotherms. For example, in the Vøring and Møre Basins the opal-A to opal-CT boundary is parallel to a Pliocene unconformity (Brekke *et al.* 1999); hence the boundary would not be a present day isotherm and could not be used as a temperature indicator within these basins. However, in those basins the opal-A to opal-CT boundary has been considered as an absolute thermal marker indicating the maximum temperature reached during burial (Brekke *et al.* 1999; Brekke 2002). The opal-A to opal-CT boundaries in those basins would no longer correspond to

the temperature it originally formed at, but would be a palaeo-isotherm parallel to the Pliocene palaeo-seabed. Therefore, any attempt to determine the thermal maturity of such basins using the opal-A to opal-CT boundary as a present day isothermal marker would lead to significant errors and could result in potential source rocks being categorised as under or overmature and entire basins possibly being written off as potential hydrocarbon reserves. Diagenetic boundaries could be useful temperature indicators, especially in Arctic exploration, if given enough time to acquire equilibrium with the prevailing conditions in a basin, but they are easily disrupted by changing conditions and become palaeo-isotherms as shown by the parallel relationship of some boundaries to unconformities.

2.11.2 Remaining questions and uncertainties

Most of the mechanisms for the formation of parallel relationships of the diagenetic boundaries with specific stratigraphic horizons other than the seabed remain speculative in the absence of additional detailed borehole data. Hence, with respect to the NSB and many other basins where these palaeo-isothermal diagenetic boundaries have been observed, multiple scientific drilling, sampling and examination of such phenomena would be required.

2.12 Conclusions

Through seismic stratigraphic analysis it is found that the silica diagenetic boundaries in the NSB show a high degree of parallelism to the Late Miocene unconformity and are not parallel to the present day seabed and probably represent palaeo-isotherms parallel to the Late Miocene seabed. It can be concluded that diagenetic boundaries that are not parallel to the seabed do not make good present day isothermal markers, but have the potential to be used as palaeo-isotherms. The tendency for the diagenetic boundaries to track an unconformity has been identified in other basins and indicates that the boundaries do not make suitable present day isotherms and therefore should be treated with caution in exploration campaigns. The reasons why some silica diagenetic boundaries develop parallel relationships with certain stratigraphic horizons, such as unconformities, and cease to be present day isotherms are poorly understood. However, the diagenetic

boundaries could probably be used as present day thermal markers as long as the depth of the boundary below the present day seabed and the geothermal gradient are known.

There are four possible mechanisms that could be responsible for the present day palaeo-isothermal behaviour of diagenetic boundaries, which cause changes in the rate of conversion (see section 2.9.3). The four mechanisms are (1) temperature decrease, such as a declining geothermal gradient, which will cause the rate of conversion to slow; (2) decreasing burial rate with respect to the rate of conversion; (3) erosion of the overburden; and (4) a change in the rate of conversion as a result of variation in the physico-chemical factors influencing the silica diagenetic reactions. These mechanisms are not exclusive and, therefore, it is possible that they work in combination with each other to produce palaeo-isothermal diagenetic boundaries.

The possible explanation for the development of palaeo-isothermal boundaries in the NSB relies upon the silica diagenetic boundaries forming during the Middle to Late Miocene. These boundaries develop following isotherms parallel to the Late Miocene seabed, which subsequently becomes the Late Miocene unconformity. During the Early Pliocene there is a dramatic reduction in the rate of conversion at the boundaries. This is most likely due to a decreasing geothermal gradient. The boundaries represent palaeo-isotherms as they are unable to maintain a high enough rate of conversion to follow Pliocene isotherms and be parallel to the Pliocene seabed. During the Pliocene there were localised breakdowns in the parallel relationship between the diagenetic boundaries and the Late Miocene unconformity. This results from variations in the rate of conversion at points along the boundaries. This enables a high enough rate of conversion to be maintained in isolated areas. All active conversion ceases by the Mid-Late Pliocene meaning the rate of conversion is not high enough for any parts of the diagenetic boundaries to follow isotherms parallel to the present day seabed.

However, due to a lack of supporting evidence, such as well data, for basins where the diagenetic boundaries exhibit palaeo-isothermal behaviour means that the mechanisms proposed remain speculative. The precise mechanisms for this phenomenon will be specific for each basin studied and the explanations given here are only the most likely possibilities. Much more research is required in this area in order to more specifically identify the causes behind palaeo-isothermal diagenetic boundaries. The

reasons for this phenomenon could be of importance for hydrocarbon exploration in terms of increased knowledge of basin evolution and the conditions within basins.

Chapter 3: The Silica Diagenetic Boundaries of the North Sakhalin Basin - Morphological Development of Basin-Scale Silica Diagenetic Fronts

3.1 Introduction

The opal-A to opal-CT conversion usually occurs within the first 1000 m of burial and changes the sediments' physical properties, such as acoustic velocity and density (e.g. Guerin & Goldberg 1996). This conversion is commonly recognised on seismic reflection data. Opal-CT is subsequently converted to quartz and this can also give rise to a seismic reflection, albeit generally less obvious on seismic data. Therefore, these silica transition boundaries (herein termed 'diagenetic fronts or boundaries') can often be imaged with seismic reflection data and mapped over areas of up to 10^5 km^2. Recent research has found that diagenetic fronts can develop complex and variable 3D forms (e.g. Davies 2005). But little is known about how diagenetic fronts advance at kilometre- to basin-scale and the role and interplay between chemical and physical processes (e.g. hydrofracturing) is uncertain.

The aim of this chapter is to describe an array of new and recently described opal-A to opal-CT diagenetic front geometries as well as the first descriptions of an opal-CT to quartz boundary using seismic reflection data from offshore Sakhalin, far eastern Russia. Objective criteria for the cross-sectional recognition of the variety of morphological forms are defined to allow for a standard categorisation of frontal geometries in different sedimentary basins worldwide. The chapter then explores the potential linked chemical and physical processes that could account for the formation of the geometries, in order to further our understanding of the controls on large-scale diagenetic front advancement. The diagenetic boundaries identified within the North Sakhalin Basin (NSB) have different morphologies from those previously described in other basins, such as the Faeroe-Shetland Basin (e.g. Davies 2005). The key features between the two contrasting sets of morphologies are compared and contrasted in order to gain a greater understanding of the mechanisms of conversion and advancement of the diagenetic boundaries.

3.2 Geological setting and database

The seismic database used in this chapter and the geological setting of the NSB are described in detail in Chapters 1.6 and 1.7 respectively.

3.3 Diagenetic fronts: General characteristics

Two seismic boundaries have been identified that are separated by 300-400 m, which cover an area of ~107,000 km^2 and form single high-amplitude, continuous seismic reflections (Fig. 3.1). The interpretation of the boundaries as silica transitions is supported by the positive polarity and high amplitude of the two reflections (Fig. 3.1A), which is consistent with them being diagenetic boundaries where density and acoustic velocity increase. The opal-CT to quartz boundary is generally of lower amplitude than the opal-A to opal-CT boundary (Fig. 3.1A). The polarity of the diagenetic boundaries is identical to those of the seabed and the Late Miocene unconformity. The upper reflection is also very similar to an opal-A to opal-CT boundary in the Faeroe-Shetland Basin proven by drilling (e.g. Davies & Cartwright 2002). Therefore in the remainder of this chapter the upper seismic reflection is termed the opal-A to opal-CT boundary and the lower reflection is termed the opal-CT to quartz boundary.

The boundaries are generally parallel to each other, with only localised variations in this relationship. Regionally, the opal-A to opal-CT boundary occurs at ~500-1400 m and the opal-CT to quartz boundary occurs at ~800-1900 m below the present day seabed. The shallowest occurrences relative to the seabed are found along the margins and in the near-shore parts of the NSB. The fronts are mainly concordant with stratigraphy, but cross-cut deformed and inclined strata (marked 1, Fig. 3.1A).

In most areas of the basin the diagenetic fronts are parallel to the Late Miocene Unconformity (Fig. 3.1A and Chapter 2.6). The reflections are mainly concordant with stratigraphy, but cross-cut deformed and inclined strata (Fig. 3.1). The diagenetic reflections are mostly observed to cross-cut the Miocene succession, but the opal-A to opal-CT boundary in a few examples cross-cuts the Late Miocene unconformity and passes through the Pliocene succession (see Chapter 2). Lastly, the diagenetic fronts are not obvious on all 2D seismic lines and on others they only occur across part of the line.

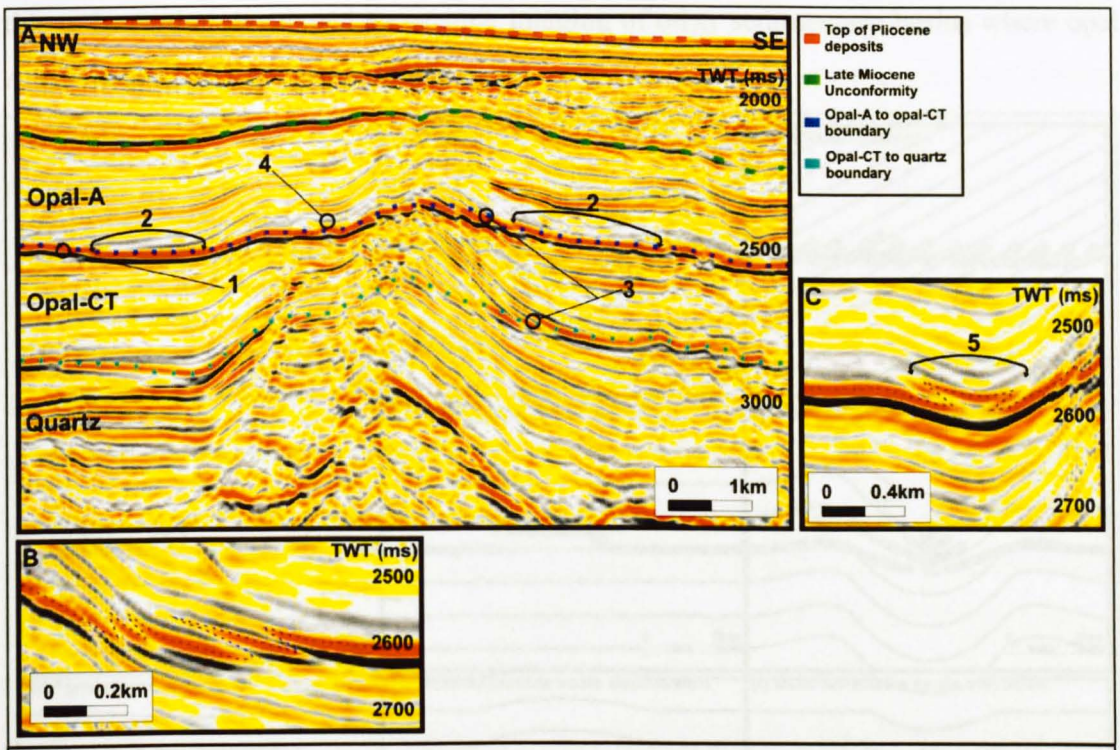

Fig. 3.1: (**A**) Seismic line showing the characteristics of the silica diagenetic fronts. (1) Cross-cutting of inclined strata; (2) Planar fronts; (3) Serrated pattern; (4) Attached wing. (**B**) Close-up of a serrated pattern in the opal-A to opal-CT front. Note the 'saw-tooth' shape of the front as it cross-cuts inclined stratigraphy. (**C**) Close-up of an attached wing in the opal-A to opal-CT front. Note the concave shape and the upward tapering edges of the feature. Also note the differential subsidence (5) of the wing's centre and of the overlying sediment.

3.4 Diagenetic front morphologies

This thesis has adopted some of the nomenclature proposed by Davies & Cartwright (2002) and Davies (2005) and expands upon it, describing and providing objective criteria for the recognition of several new morphological features. These morphological features are almost always better developed on the opal-A to opal-CT front than on the opal-CT to quartz front. The following description starts by describing the simplest front morphologies before analysing the more complex forms. The cross-sectional geometry of host strata above and below the diagenetic front and the cross-sectional form of the fronts allows for a simple and objective nomenclature to be proposed for the NSB examples. In order for this classification to be useful and objective a simple recognition criteria has been devised. Eight categories are defined here (Fig. 3.2) but it is reasonable to expect

this to be further developed by seismic imaging of other sedimentary basins where opal-A-rich sediments have accumulated.

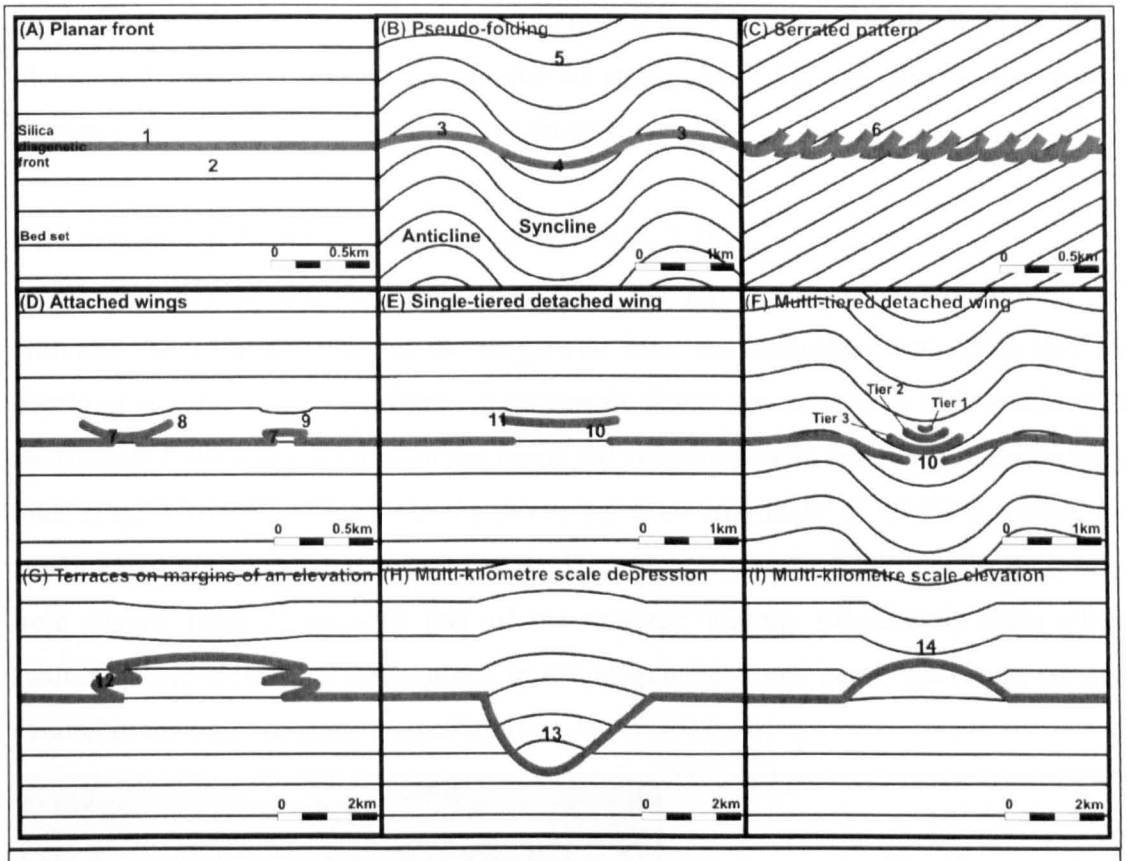

Fig. 3.2: Schematic diagram summarising the key seismic attributes of the various morphological features (**A-I**). (1) Lack of frontal relief; (2) Track stratigraphy; (3) Pseudo-antiform; (4) Pseudo-synform; (5) Front is parallel to a higher stratal reflection; (6) Up-dip 'saw-tooth' pattern of front as it cross-cuts inclined stratigraphy; (7) Base attached to main diagenetic front; (8) Concave-upward shape with tapering margins; (9) Flat to dome shape; (10) Base detached from main diagenetic front; (11) Slight concave-upward to elongate shape; (12) Terrace; (13) Gentle antiformal folding; (14) Downward flexure of overlying sediment.

3.4.1 Distribution of diagenetic front morphologies

The frontal morphologies associated with the silica diagenetic boundaries occur throughout the basin fill where these boundaries have been identified. However, the morphologies are more commonly developed along the easternmost margin of the NSB (Fig. 1.9), i.e. the more distal and deeper marine areas. Multi-kilometre scale depressions and elevations (see below) are almost exclusively formed in this area of the basin.

3.4.2 Planar fronts (Fig. 3.2A)

Planar fronts are featureless regions of the diagenetic fronts that are located between other morphological features (marked 2, Fig. 3.1A). They can be planar over multi-kilometre distances. They can be parallel to stratigraphy, but can also have a planar geometry where they cross-cut stratal reflections.

3.4.3 Apparent folding of the diagenetic fronts (Fig. 3.2B)

At a regional scale, the diagenetic fronts take the form of a series of antiforms and synforms. These undulations in the diagenetic front are coincident with folds that are clearly of tectonic origin. Synforms in diagenetic fronts are coincident with synclines in the tectonic folds and antiforms in the fronts are coincident with anticlines in the tectonic folds (Fig. 3.3A). The 'folds' in the fronts have an amplitude of 20-50 m versus the amplitude of the folded strata of 50-150 m. The amplitude of the folding in the diagenetic front ranges from 25 to 45% that of the tectonic folding. On seismic lines where synformal and antiformal undulations in the diagenetic fronts occur the fronts are also parallel to the Late Miocene unconformity.

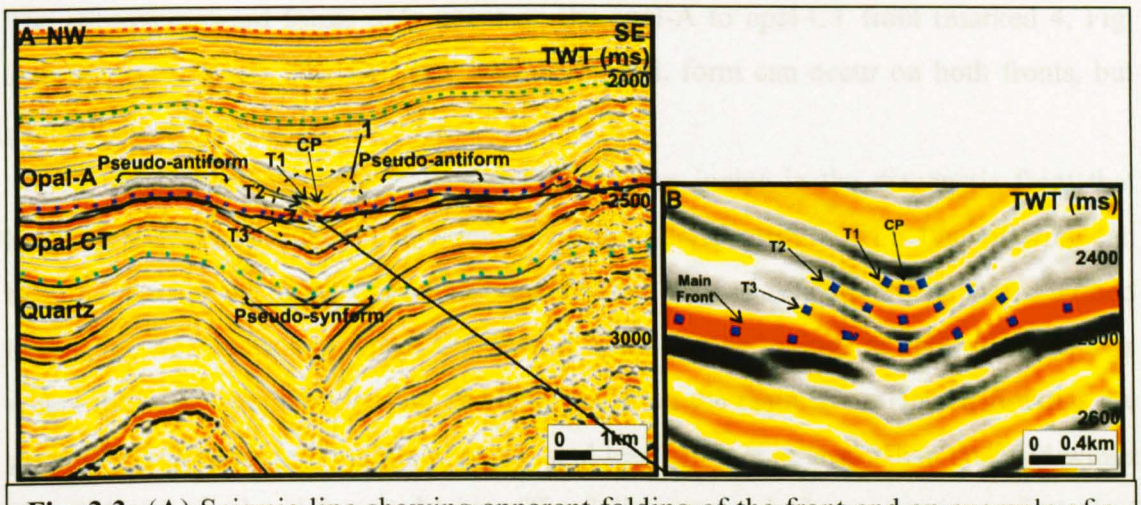

Fig. 3.3: (**A**) Seismic line showing apparent folding of the front and an example of a multi-tiered detached wing that has formed in the trough of a syncline (1) that has been cross-cut by the opal-A to opal-CT boundary. Also note the Late Miocene unconformity (green dashed line) 'drapes' the deformed Miocene strata and that the apparent folding of the diagenetic fronts tracks the unconformity. (**B**) Close-up of the multi-tiered detached wing. T1= tier 1, T2= tier 2, T3= tier 3 and CP= central peak.

3.4.4 Serrated pattern (Fig. 3.2C)

These are asymmetrical saw-tooth to stair-step patterns that only occur where the diagenetic fronts cross-cut inclined and deformed stratigraphy (marked 3, Fig. 3.1A and Fig. 3.1B). The 'teeth' are between 10 and 50 m in height. Their angle is the same as the inclination of the strata that the front cross-cuts. The width of the serrated patterns is equal to the lateral extent of inclined strata that the fronts pass through. Similar features have been described previously by Davies & Cartwright (2002) and Davies (2005).

3.4.5 Wings (Fig. 3.2D, E and F)

Wings are concave-upwards to elongate features in cross-sectional view. Two types of wings have been identified: attached and detached wings. They are differentiated by shape, size and their spatial relationship to the main diagenetic front above which they form.

Attached wings (Fig. 3.2D) are flat to concave-upward forms, with margins or 'wings' that point away upward from the main front. The bases of these wings are attached to the main front. Attached wings are commonly up to ~ 0.3 - 0.8 km in length. The concave-upward forms only occur on the opal-A to opal-CT front (marked 4, Fig. 3.1A and Fig. 3.1C). The flat, less well developed, form can occur on both fronts, but generally lack the wings.

Detached wings (Fig. 3.2E and F) are sharp jumps in the diagenetic front that have slight concave-upward and elongate cross-sectional profiles. This type of wing can be composed of up to three progressively smaller stacked reflections which are termed tiers (Fig. 3.3). Detached wings are distinct from attached wings as they form regions where the front becomes elevated and detached from the main front. Detached wings are generally larger in size – but not always – and less concave in shape than attached wings (Fig. 3.4). Single-tiered detached wings (Fig. 3.4) appear to be larger versions of attached wings that have separated from the main front. Multi-tiered detached wings (Fig. 3.3B) in this study tend to form in the troughs of synclines (marked 1, Fig. 3.3A). The highest tier of a detached wing can show evidence for a central peak, which marks the highest level of advancement of the feature and diagenetic front (marked CP, Fig. 3.3B). Detached wings are normally between 0.8-2 km in length.

3.4.6 Terraces (Fig. 3.2G)

These are regions of the diagenetic front that have stair-step cross-sectional profiles. Terraces are distinguished from serrated patterns as terraces form on the margins of larger morphological features (Figs. 3.4 and 3.5). For example, Davies (2005) identified terraces that formed on the margins of elevated regions of the front that formed a ridge network. This term is applied in the same way here. Terraces are generally 0.25-1 km in length. Wings and terraces are phenomena that generally occur at scales of ≤ 2 km.

3.4.7 Multi-kilometre scale depressions (Fig. 3.2H)

The diagenetic front forms a trough-like feature (marked 1, Fig. 3.4) that has terraced margins (marked 2, Fig. 3.4) extending into the depression (marked 3, Fig. 3.4). The depressions are between 3-5 km in width and 150-250 m in depth. In many cases the depression in the opal-A to opal-CT diagenetic front is deep enough for it to almost merge with the opal-CT to quartz front, which shows no evidence of downward deflection. Where depressions are identified the stratigraphy above the depressed diagenetic front shows evidence for a gentle antiformal fold (marked 4, Fig. 3.4). No depressions have so far been identified along the opal-CT to quartz boundary.

3.4.8 Multi-kilometre scale elevations (Fig. 3.2I)

Elevations in the diagenetic front are multi-kilometre scale regions of the front that have preferentially advanced upwards relative to the surrounding regions of the front (marked 1, Fig. 3.5). They form arch shapes that cross-cut stratigraphy, hence forming an area of converted sediment in younger stratigraphy. Stratal reflections extend from the outer margins of the elevations producing terraces (marked 2, Fig. 3.5). The examples that have been identified are ~ 4-5 km wide and 50-150 m in height. Where elevations are identified the stratigraphy above the elevated diagenetic front shows evidence for a gentle synformal fold (marked 3, Fig. 3.5). The opal-CT to quartz boundary does not show the same upward deflection.

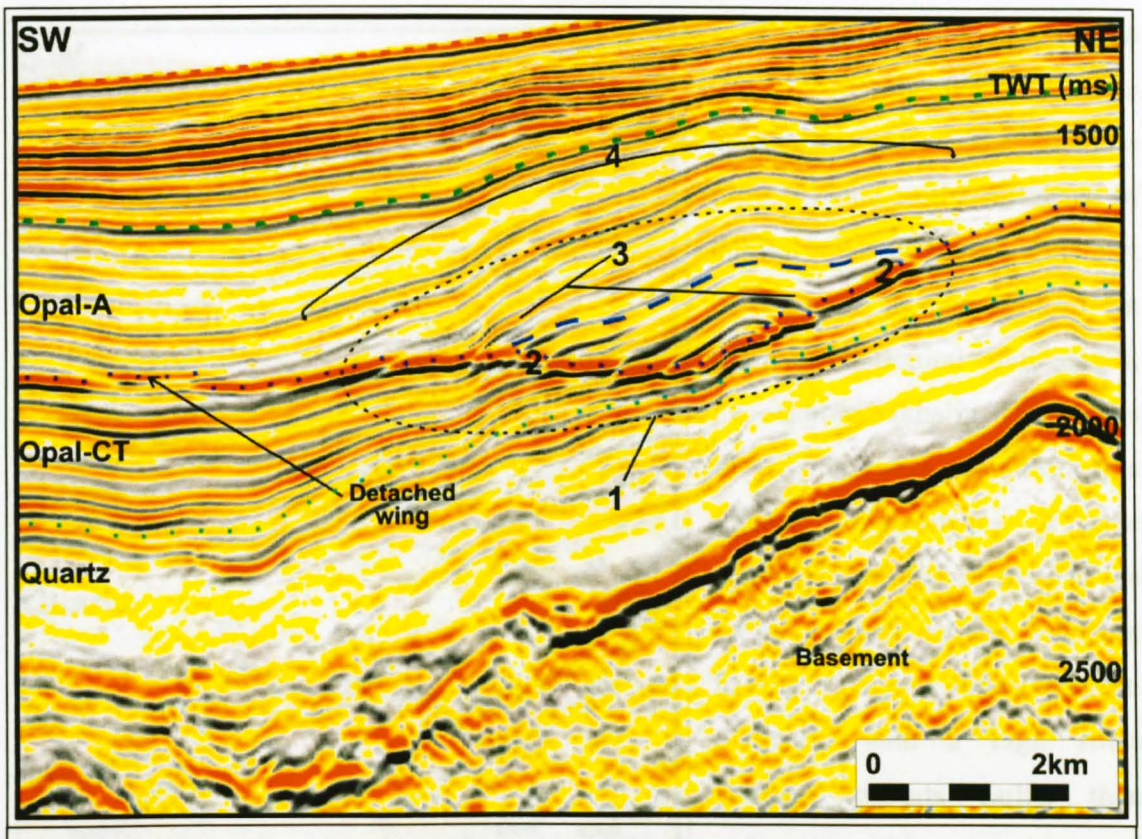

Fig. 3.4: Seismic line showing an example of a multi-kilometre scale depression in the opal-A to opal-CT front (1). The depression has terraced margins (2), which can form discontinuous, high-amplitude reflections that extend from the main diagenetic front (3). Note that the strata above the depression forms an antiformal fold (4). Note how the opal-CT to quartz boundary has almost merged with the opal-A to opal-CT boundary – the opal-CT to quartz boundary is not clear in this image, but the boundary can be traced with accuracy both sides of this screenshot. The opal-A to opal-CT boundary also shows an example of a single-tiered detached wing.

3.5 Evolution of front morphology

Seismic tuning is occurring at reflection discordances but it cannot account for the geometries of the various morphologies observed. This is because the features identified are larger in size than the resolution of the data, which is ~ 10 m, hence they are not artefacts created by the acquisition and processing of the data. Although seismic tuning may play a role in the seismic amplitudes observed in regions where wings, terraces and serrated patterns form, these features are considered to be real and not seismic artefacts.

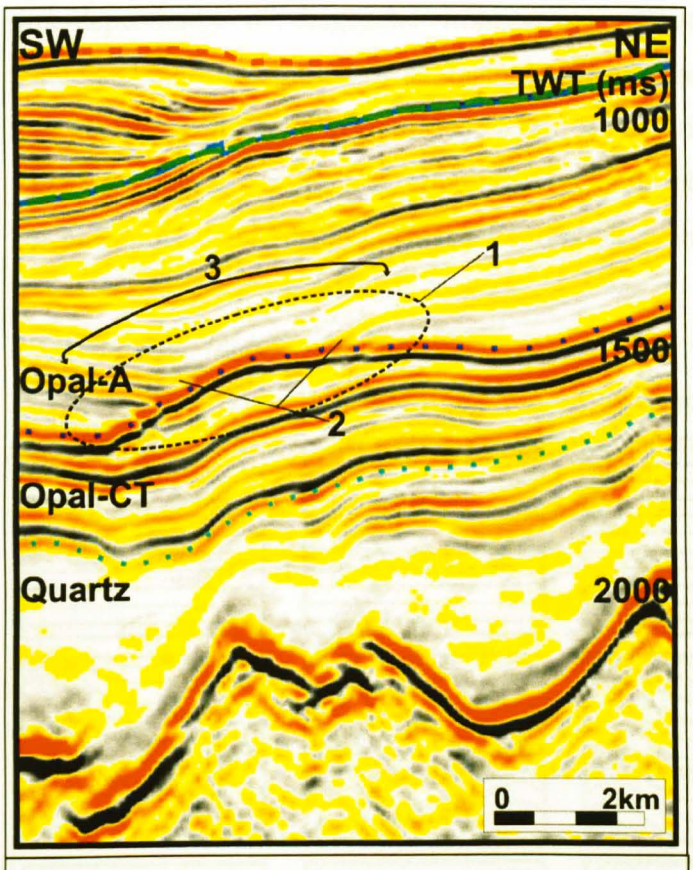

Fig. 3.5: Seismic line showing an example of a multi-kilometre scale elevation (1) in the opal-A to opal-CT front. The elevation has terraced margins (2) that extend from the main diagenetic front. Note the downward flexure of the sediments above the elevation (3).

The concentration of the frontal morphologies in the eastern margin of the basin is probably due to the influence of detrital mineral content. This part of the basin is more distal from the possible detrital source areas, i.e. onshore Sakhalin. This means the diatom ooze would form a greater component of the sediment in the distal areas of the basin, leading to the sediment having a higher silica content. Sediment with a high silica content converts earlier than sediment with an increased detrital component (Isaacs 1981), but silica-rich sediment might also allow greater potential for the various morphologies to develop. Another explanation is that the diagenetic fronts and their associated morphologies are better imaged in the eastern part of the basin.

It is apparent from the examples of the various frontal morphologies that the opal-A to opal-CT front behaves differently from the opal-CT to quartz front. Most of the geometries are poorly developed and less common along the opal-CT to quartz front, while multi-kilometre scale depressions and elevations have not been observed along this boundary. This is probably due to the smaller magnitude of the physical property changes, especially the porosity drop, associated with the opal-CT to quartz transition. This could lead to the development of features that are only just above or even below the seismic resolution of the data, hence are not as obvious on the seismic data.

In the following interpretation it is important to bear in mind that seismically imaged patterns are a snapshot of front advancement, with examples revealing the likely

time-dependency of diagenetic front cross-sectional development. Diagenetic front patterns should be thought of as dynamic phenomena that evolve over time periods of thousands to millions of years (Tada 1991). This section starts by briefly considering the apparent folding of the fronts and the parallel relationship with the Late Miocene Unconformity before dealing with each morphology in turn.

3.5.1 Apparent folding of the diagenetic fronts

There are three possible explanations for why the fronts appear to be folded (Fig. 3.6).

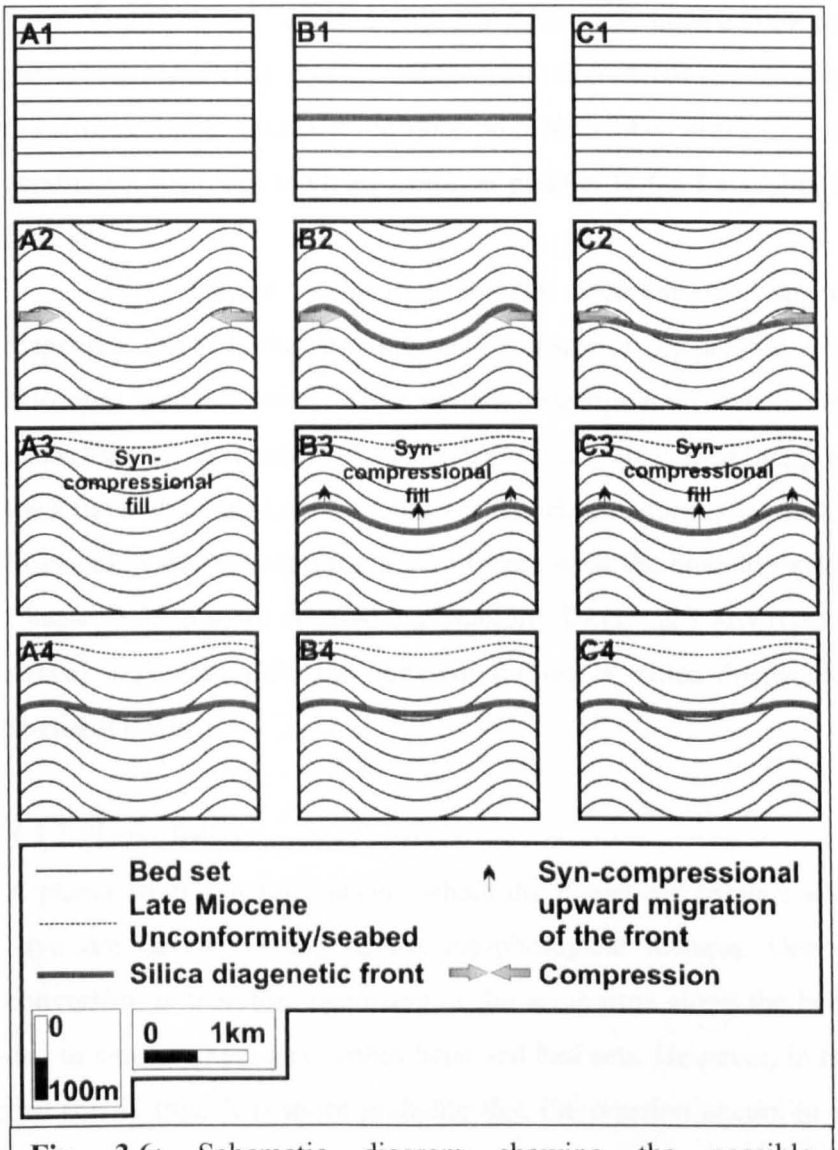

Fig. 3.6: Schematic diagram showing the possible explanations for the apparent folding of the diagenetic fronts with respect to their parallel relationship to the Late Miocene Unconformity (see text for explanation).

For example, the diagenetic fronts could have advanced to their present position after the folding (Fig. 3.6A1-4). Since the Late Miocene unconformity formed above the syn-compressional sedimentary fill of the folds, it forms an undulating surface with the same wavelength as the tectonic folds but a lower fold amplitude (Fig. 3.6A3). As the reactions are principally controlled by temperature the fronts should be parallel to isotherms

and these will often be parallel to the contemporaneous seabed (the Late Miocene Unconformity) (Fig. 3.6A4). Therefore the fronts may simply develop the same undulating relief as the Late Miocene Unconformity. Alternatively the diagenetic fronts could form before the folding (Fig. 3.6B1-4) and during an episode of lateral compression both the strata and the fronts are deformed (Fig. 3.6B2). Syn-compressional sediments are then deposited mantling the folds. Again the diagenetic fronts will probably advance to develop a parallel relationship with the contemporaneous seabed and thereby develop an undulating morphology (Fig. 3.6B3) that tracks the Late Miocene Unconformity (Fig. 3.6B4). Lastly the fronts may have advanced near to the end of the shortening phase (Fig. 3.6C2) and therefore underwent less shortening (Fig. 3.6C3). Once the fronts have regained equilibrium, with the prevailing thermal and chemical conditions, they will track an isotherm parallel to the Late Miocene Unconformity (Fig. 3.6C4).

The preferred explanation for the occurrence of apparent folding along the diagenetic fronts is that it is probably a result of the parallel relationship with the Late Miocene Unconformity. This specific stratigraphic relationship indicates that the unconformity represented the seabed, and that rather than being folded the fronts simply track the undulating Late Miocene seabed. Hence, during the Late Miocene the diagenetic fronts advanced maintaining a parallelism with the contemporaneous palaeoseabed (see Chapter 2 for a more detailed explanation). Davies & Cartwright (2002) proposed a very similar explanation for the apparent folding of silica diagenetic fronts in the Faeroe-Shetland Basin.

3.5.2 Planar fronts

A planar front generally occurs where the diagenetic fronts track stratal boundaries and have not developed any of the morphological features. One could assume that the conversion is therefore occurring at the same time along the beds and bed sets perhaps due to similar chemistry within beds and bed sets. However, in reality it is very unlikely that this is true. It is more probable that the reaction occurs in some parts of a bed set first, with the front advancing laterally parallel to bedding until the bed sets are converted. In other words, some sort of differential vertical advancement of the diagenetic front is likely to occur followed by lateral advancement of the front. This

progressive lateral advancement along bed sets would lead to diagenetic fronts being parallel to stratal reflections and would, therefore, inherit the stratigraphic architecture (Fig. 3.7). This is consistent with some of the known controls on conversion (sediment age, detrital mineral content, and the host rock chemistry), which locally are likely to be

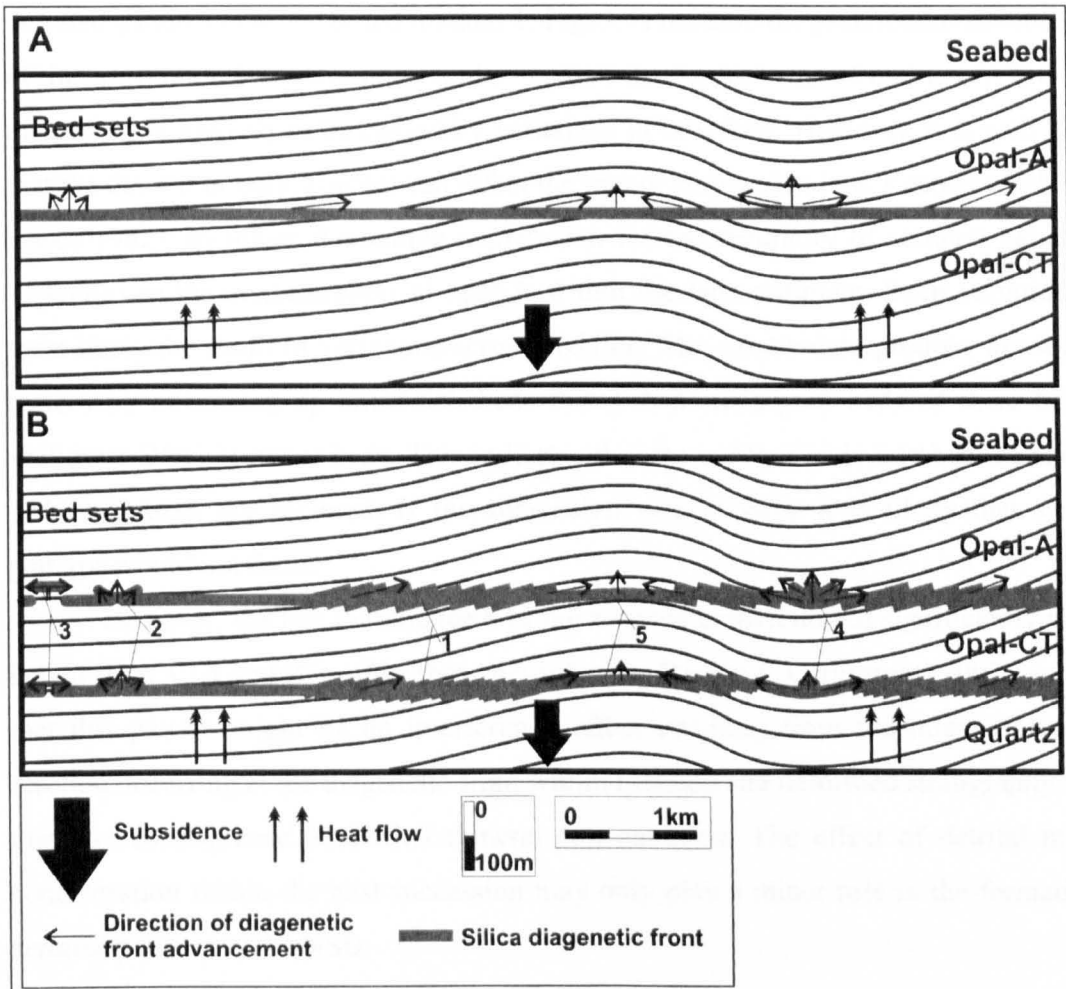

Fig. 3.7: Schematic diagram showing the mechanisms of silica diagenetic boundary development in terms of direction of front advancement and inclination of the strata. (**A**) A combination of temperature and burial cause biogenic silica-rich strata to reach the DOC where the sediment is transformed from opal-A to opal-CT, forming a diagenetic front. (**B**) In inclined strata the front advances along silica-rich bed sets forming serrated patterns (1). In predominantly horizontal strata attached wings (2) and single-tiered detached wings (3) can form. In folded strata, multi-tiered detached wings can develop in the troughs of synclines (4). However, in the crests of anticlines no detached wings form and the front cross-cuts the fold (5) with serrated patterns forming where the front cuts the limbs of the fold. Note that the morphological features are less well developed on the opal-CT to quartz diagenetic boundary.

similar within any one bed or bed set, hence leading to lateral advancement, but vary significantly across bedding if the succession is heterogeneous (Davies 2005).

3.5.3 Serrated pattern

Serrated patterns (Fig. 3.1B and marked 1, Fig. 3.7) indicate the preferential advancement of the conversion boundary at a regular separation of a few tens of metres. At this scale the pattern is unlikely to be caused by variations in heat flow. However, it is well known that the detrital mineral content can affect the rate of conversion (e.g. Kastner *et al.* 1977; Isaacs 1982); therefore the simple explanation for the regularity of serrated patterns is variations in the concentration of opal-A within the host sediment. Such variations are most likely the result of variations across bedding. The front would produce the serrated pattern by advancing up silica-rich beds faster than silica-poor beds or there being a shallower DOC in richer beds. This indicates that the succession is interbedded and that bedding planes are inclined. If the succession was massive it is likely that serrated patterns would not form.

However, the fact that the teeth of the serrated pattern do not significantly vary in height (Fig. 3.1A and B), unlike those described by Davies & Cartwright (2002), suggests that this pattern might be an interference effect resulting from the interaction of the reaction occurring at the diagenetic front within inclined and deformed stratigraphy rather than the consequence of detrital mineral concentration. The effect of detrital mineral concentration within the host succession may only play a minor role in the formation of serrated patterns in the NSB.

3.5.4 Wings

Attached wings (marked 2, Fig. 3.7) describe localised concave- and dome-shaped features that form in stratal reflections above the main level of the diagenetic front, but are still attached to the front. The term 'attached' relates to the appearance of the feature on seismic data. They are localised regions where overburden beds and bed sets have started to undergo conversion, but this conversion has not yet advanced laterally along that bed or bed set. The ideal concave shape of an attached wing probably forms as a result of differential subsidence of the central part of the wing, which has undergone

conversion before the edges. The tapering edges of a concave-shape wing most likely represent the leading edge of the reaction front.

Detached wings form for exactly the same reasons as attached wings, but prefer to use this term to indicate that the feature has completely detached from the diagenetic front. The term detached refers to the spatial relationship, in seismic data, to the main diagenetic front that the wing has formed above. It is probable that single-tiered detached wings (marked 3, Fig. 3.7) are more evolved forms of attached wings, which signify that the conversion has started to advance laterally along a bed or bed set above the main diagenetic front. As wings advance laterally and convert more sediment one would expect them to flatten out as a result of progressive differential compaction and subsidence. The dominance of lateral advancement and progressive differential subsidence means the detached wing does not exhibit the concave-shape of an attached wing, but still does show the tapering edges that represent the leading edge of the reaction.

A multi-tiered detached wing can form in the trough of a syncline (Fig. 3.3 and marked 4, Fig. 3.7). The front advances through multiple beds and bed sets that have been folded below the DOC leading to the conversion of several bed sets. This occurs progressively as the front advances both laterally along the limbs and directly upwards from the hinge zone, perhaps due to fracture generation causing enhanced diagenesis in the trough of the syncline (see section 3.6.2 below). The conversion process of the bed sets in the trough of the syncline is time-dependent and would lead to a set of increasingly smaller detached wings stacking one on top of another, with the central peak indicating the highest and most recent stratal level the front has reached (hence least converted bed set). The concave-shape is similar to that of attached wings, but is probably due to a combination of the front following the inclination of the bed sets in the trough of the syncline and some differential subsidence at the centres of the individual tiers.

3.5.5 Terraces

Terraces form in conjunction with kilometre scale depressions and elevations in the diagenetic front; hence these are explained below along with the larger features.

3.5.6 Depressions and elevations in the diagenetic front

The potential mechanisms for causing depressions and elevations are dealt with together. The multi-kilometre scale depressions (marked 1, Fig. 3.8) in the opal-A to opal-CT diagenetic front have to be consistent with the absence of a depression in the opal-CT to quartz boundary. This would probably rule out lateral variations in heat flow as you would expect to see a depression in the opal-CT to quartz boundary. Hence, the formation of depressions in the diagenetic front are primarily due to the direction and rate of diagenetic front advancement, with the inclination of the strata having little or no influence (Fig. 3.8). There are two possible hypotheses for these features. Firstly, depressions could form due to variations in host lithology geochemistry (e.g. silica, detrital and carbonate content and pore water chemistry). For example, there may be regions that have low concentrations of biogenic silica (marked SPZ, Fig. 3.8). This would slow the rate of front advancement (ROFA) relative to adjacent successions. This impeded section of the front forms the depression in the front as ROFA outside of the silica-poor zone is not impeded.

It is also plausible that the rheology of the sediment is different; it may not be conducive for the development of hydrofractures, which may be important for enhancing the rates of diagenesis (see Eichhubl & Boles 1998). Therefore, a depression may form where ROFA is inhibited by reduced hydrofracture formation. Gross (1995) suggested that the fracture style within the Monterey Formation, California, depended upon the mineralogical composition of the host lithology. For example, opening-mode veins tended to form in more brittle units such as diagenetic opal-CT beds, while faults were more common in beds rich in opal-A and 'weak' detrital minerals (e.g. clays). Hence the mechanical properties of the host lithology can influence the type and extent of fracture formation.

The depression caused by the restriction of the opal-A to opal-CT front can lead to the opal-CT to quartz front that has not been impeded to almost merge with the opal-A to opal-CT front. Terraces (marked 2, Fig. 3.8), form within the trough of the depression as the front attempts to regain equilibrium with the prevailing burial and geothermal conditions by trying to advance laterally through the fracture- or silica-poor sediment and close the depression to form a planar front.

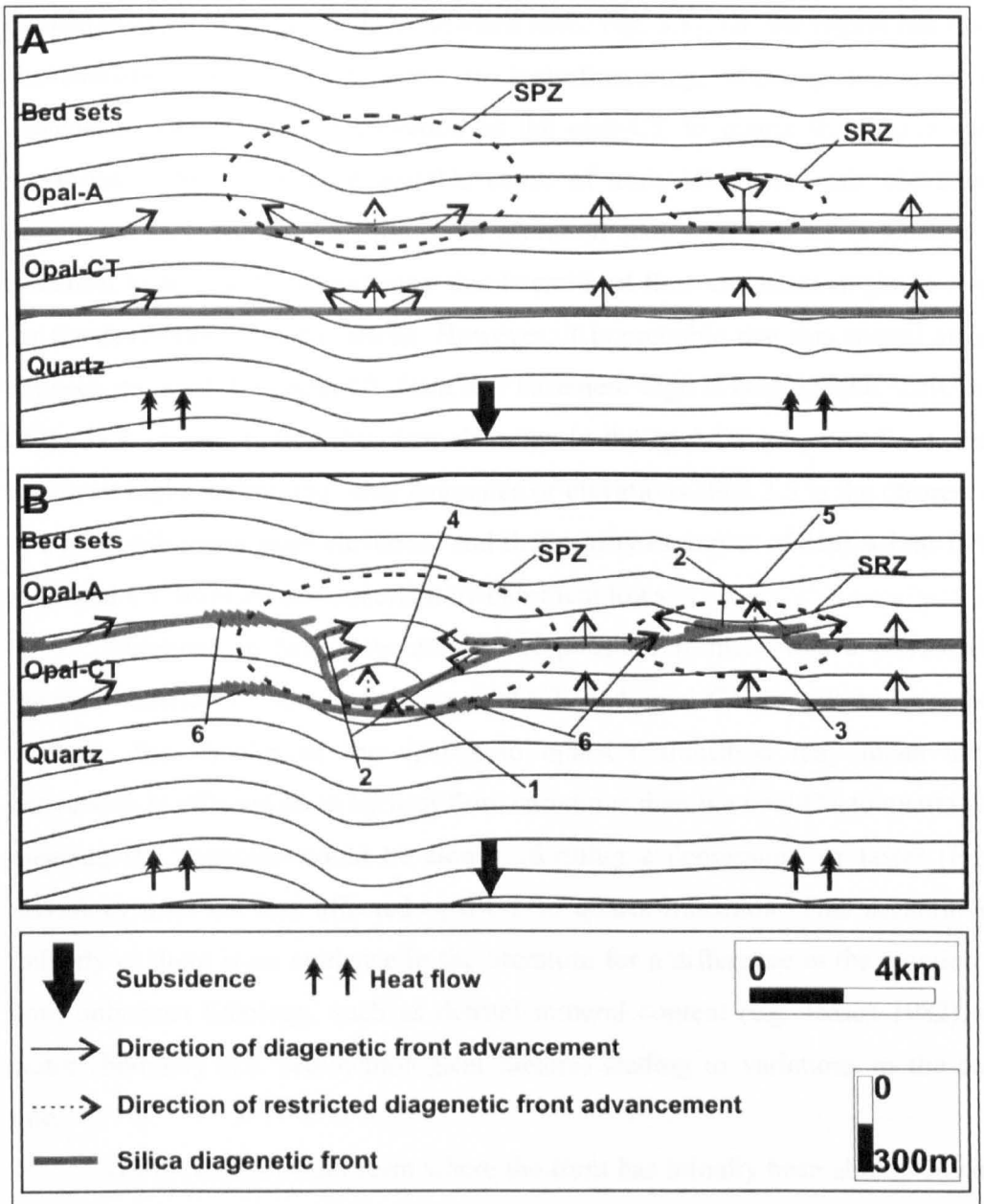

Fig. 3.8: Schematic diagram showing how depressions and elevations in the diagenetic front form. (**A**) Diagenetic fronts advance relatively upward through strata that contain zones of silica-poor (SPZ) and silica-rich (SRZ) sediment. (**B**) Formation of depressions (1) and elevations (3) in the diagenetic front. Terraces (2) form in the unconverted sediment on the margins of depressions and elevations. Differential compaction also occurs in the sediments above these features: antiformal folds (4) above the depressions and downward flexures (5) above the elevations. In inclined strata serrated patterns form (6).

In contrast to depressions, elevations in the opal-A to opal-CT diagenetic front (marked 3, Fig. 3.8) could be accounted for by the front advancing through areas that are

particularly rich in biogenic silica (marked SRZ, Fig. 3.8). Or, the region has rheological characteristics that make it prone to hydrofracturing, allowing increased rates of diagenesis. The lack of an elevation in the opal-CT to quartz front rules out lateral variations in heat flow as a possible cause of multi-kilometre scale elevations. This despite the fact that the example of an elevation shown in Fig. 3.5 is situated above a basement high, which could suggest that lateral heat flow variations might be responsible for the development of elevations. However, it is probable that this spatial arrangement between the opal-A to opal-CT front and basement high is coincidental. This is because of the lack of a spatially coincident elevation in the opal-CT to quartz front, the lack of basement highs underlying other examples of elevations (Fig. 3.5 is the clearest example of a multi-kilometre scale elevation) and that nearby examples of depressions in the opal-A to opal-CT front are not underlain by basement lows.

Variations in heat flow may be responsible if there was a difference in the reaction kinetics of the opal-A to opal-CT and opal-CT to quartz transitions. For example, the kinetics of the opal-A to opal-CT transition may mean the rate of conversion is affected more by heat flow variations than the opal-CT to quartz transition, meaning the transition could be slower (forming a depression) or faster (forming an elevation) than the less affected opal-CT to quartz transition. This scenario is highly unlikely as there is no evidence in the literature for a difference in the reaction kinetics, with only host lithology, such as detrital mineral content (e.g. Isaacs 1982), and pore water chemistry (i.e. sedimentological factors) leading to variations in the conversion rate.

The elevation would form where the front has initially been able to advance more rapidly upwards than the surrounding sections of the front forming a multi-kilometre scale arch shape. The advancement at the elevation has subsequently been restricted, by mechanical-chemical factors (such as silica content or fracture formation), causing the front to preferentially advance laterally along beds and bed sets forming terraces along the margins of the elevation (marked 2, Fig. 3.8). The lateral advancement of terraces extending from the elevation along adjacent unconverted bed sets would allow the rest of the front to advance and reach the same stratigraphic level as the elevation by converting the sediment above the main front. Once the front passes the zone of favourable lithology, forming the elevation, the front reaches equilibrium with its surrounding

conditions (i.e. host lithology, temperature and burial rate) and no longer undergoes differential advancement. Elevations and depressions are examples of where the lithological controls occur over a large area.

3.6 Front advancement processes

The above features provide a record of diagenetic front advancement within a clastic sedimentary basin. Together with outcrop analogues and siliceous sediment exposed elsewhere (e.g. Monterey Formation, California) they can provide clues as to what processes and interrelated processes are important in front advancement.

3.6.1 Bedding and lithology control

A variety of outcrop and borehole data show that diatomites are commonly laminated and interbedded at centimetre- to metre-scale (e.g. Compton 1991; Tada 1991) (Fig. 1.8). Outcrop evidence from the Monterey Formation also indicates that brecciation and microfracturing can accompany the reaction as a result of hydrofracturing and volumetric contraction (Eichhubl & Boles 1998; Eichhubl 2004). Sediments richer in silica are converted at a faster rate than those containing a greater proportion of detrital minerals (e.g. Isaacs 1981; 1982; Bohrmann *et al.* 1994). It is reasonable to propose that many patterns probably form as a result of bedding and lithology variations with conversion occurring in beds and bed sets that are richer in opal-A first, either at a slightly shallower DOC or as a result of higher ROFA, than beds that have a higher detrital mineral content. This simple mechanism has already been shown as one of the ways to account for the serrated patterns of the fronts in inclined strata.

In contrast, wings form where the diagenetic front has 'jumped' to a shallower stratigraphic level. These localised regions where the reaction has been initiated in overburden strata are termed 'seed areas' (Meadows & Davies 2007). There are several mechanisms that could account for the development of seed areas (Fig. 3.9).

The silica diagenetic transformations are dehydration reactions that can generate excess pore pressure in the strata above the diagenetic fronts (Hesse 1990). This generation of overpressure could cause hydrofracturing in the sediments overlying the fronts. Opening of fractures by hydrofracturing of materials like diatomites with very low permeabilities occurs when the fluid pressure is so high that the minimum principal

effective stress, σ'_3, has been reduced to zero and the tensile stresses exceed the cohesive strength of the sediment (Bjørlykke & Høeg 1997). Seed areas may form where the density of hydrofracture generation is particularly high (Fig. 3.9A), causing enhanced rates of diagenesis (Eichhubl & Behl 1998) leading to localised differential front advancement. Zones of denser hydrofracture generation may result from lateral variations in sediment rheology or differences in pore pressure in the overlying strata.

The concentration of opal-A in overburden sediments may vary and seed areas would preferentially develop in areas where the silica concentration is higher (Fig. 3.9B), leading to differential front advancement. It could also be that part of the bed set that the front has reached is thinner than the adjacent areas (Fig. 3.9C). Due to there being less sediment for the front to convert at the thinnest points of a bed set the front would preferentially advance to the next bed set at these areas. It is likely that all of the mechanisms that can generate seed areas play a role in the formation of wings, but without well calibration of the succession the exact mechanisms and their relative importance remain unclear.

3.6.2 Role of fracturing and brecciation

It is well known that fracturing enhances the rate of the diagenetic process (Eichhubl & Behl 1998). Microfractures can form due to the volumetric contraction as a result of the conversion of opal-CT to quartz (Eichhubl 2004). Fractures also form as a result of overpressure created due to the expulsion of fluids by the reactions (Hesse 1990), which causes hydrofractures that are beyond seismic resolution to propagate in the overlying sediment (see section 3.6.1 above). Comparisons with outcrop examples, especially the Monterey Formation, indicate that hydrofracturing varies as a function of lithology. The increase in pore fluid pressure due to the reactions would provide the conditions for brittle fracture, but as a result of the effect that detrital content has on conversion the lithologies would fracture at different times and depths (Eichhubl & Behl 1998). The rheology of the lithology would have an effect on the type and extent of fracturing (e.g. Gross 1995), for example, well cemented and competent lithologies are more susceptible to fracturing than relatively weak lithologies such as mudstones.

Hydrofractures in diatomites stimulated by water injection (Barenblatt *et al.* 2002) are predominantly parallel to bedding, which provide natural planes of weakness for

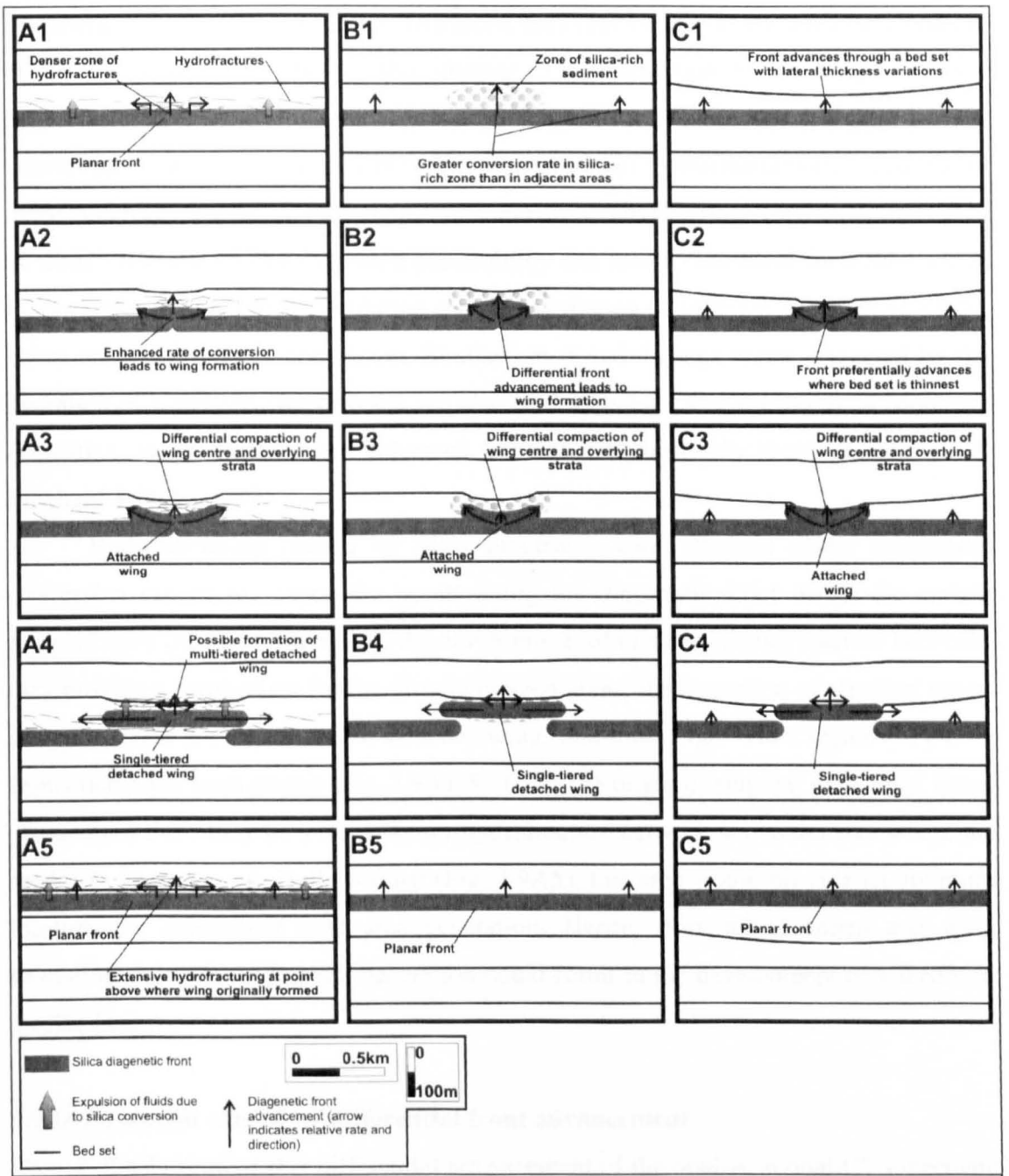

Fig. 3.9: Schematic diagram showing the mechanisms of seed area development. The diagenetic front initially tracks the stratigraphy. (**A**) Seed area generation due to increased hydrofracture generation. (**B**) Seed area generation due to a zone of silica-rich sediment. (**C**) Seed area generation due to bed set thickness variations. Sequences 1-5 show the formation of attached wings due to differential advancement at a seed area and subsequent evolution into single-tiered attached wings and then via lateral advancement, and joining with other wings at that stratal level, into planar fronts.

mechanical failure, and cause regions of significant brecciation and considerably enhanced permeability. This would also provide a mechanism for the advancement of the

diagenetic front parallel to bedding. Therefore, they may be important in the development of the geometries described in this chapter. The orientation of naturally occurring hydrofractures is generally normal to the direction of σ'_3 unless the sediment is very anisotropic (Bjørlykke & Høeg 1997). These networks of hydrofractures can occur along individual beds or at several different levels and are termed 'damage zones' (Barenblatt *et al.* 2002). It is known that increased permeability can lead to increased fluid flow which in turn can cause enhanced dissolution and reprecipitation of silica (Williams *et al.* 1985), hence enhanced rates of conversion. Similar brecciated damage zones, triggered by the liberation of water and overpressure are also seen in outcrops of the siliceous Monterey Formation, where they caused enhanced rates of diagenesis (Eichhubl & Behl 1998; Eichhubl & Boles 1998).

Hydrofracturing caused by silica diagenesis can influence where subsequent conversion can occur, hence the points along the diagenetic front where the certain morphologies can form. Therefore, the development of localised denser fracture networks may provide a mechanism for the growth of seed areas, the formation of attached wings and subsequent development into detached wings and finally into wider regions of planar fronts that track stratigraphy (Fig. 3.9A1-5). Once the original wing has developed into a planar front there may be a relict denser hydrofracture network above the area where the seed area and wing originally formed (Fig. 3.9A5), this area would provide an optimum location for subsequent seed area generation. Hence, front advancement and wing formation due to hydrofracture generation could result in the development of a feedback mechanism.

3.7 Deformation caused by differential front advancement

Davies (2005) showed that differential advancement of the opal-A to opal-CT diagenetic front can cause folding in the overburden. This is because of the significant porosity loss the reaction causes such that areas of preferential front advancement are overlain by depressions caused by differential subsidence (Fig. 3.10). However, above many of the smaller scale morphological features in the NSB this effect is not observed, probably for two reasons, either the magnitude of the porosity change could be so small that the differential compaction effect described by Davies (2005) has no observable effect (i.e. below the seismic resolution of the dataset), or, at geological time-scales, the reaction is

occurring at essentially the same time along the length of the beds and bed sets. In many places the front tracks the stratigraphy; hence the deformation of the overlying sediments can be considered to be transient deformation, which leads to temporary folding as the diagenetic fronts convert entire bed sets removing the depressions formed by areas of preferential front advancement (Fig. 3.10).

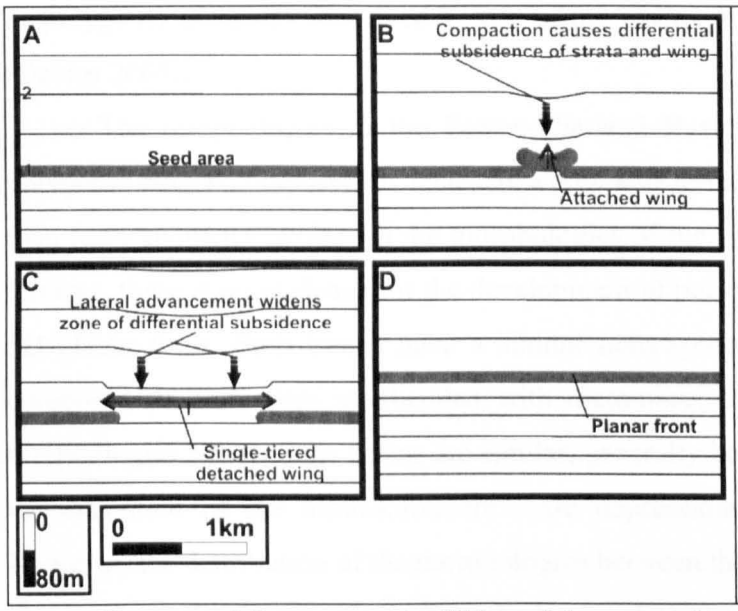

Fig. 3.10: Schematic diagram showing how differential front advancement can cause transient deformation in the overlying sediments. The diagenetic front (1) tracks the stratigraphy (2). Note that the bed sets below the diagenetic front are more compacted than those above as a result of the change in physical properties.

However, kilometre-scale differential compaction in the NSB has been observed where depressions and elevations in the opal-A to opal-CT diagenetic front develop. The subtle antiforms occurring above the depressions (marked 4, Fig. 3.4 and marked 4, Fig. 3.8) and the downward flexures above the elevations (marked 3, Fig. 3.5 and marked 5, Fig. 3.8) are both interpreted to be the result of differential front advancement and, therefore, differential compaction.

3.8 Discussion

3.8.1 3D geometry

As this chapter has mainly used 2D seismic data to describe the morphology of the boundaries a judgement has not been made on the likely plan form geometry of the features. It is likely that the terraces and serrated patterns probably form ridges in plan form that are parallel to the strike of the folds. This is based upon the occurrence of similar phenomena mapped in 3D by Davies (2005) in the Faeroe-Shetland Basin. The development of a comprehensive 2D and 3D scheme would be useful for future descriptions of silica diagenetic fronts (see Chapter 5, Fig. 5.4).

3.8.2 Controls on diagenetic front morphology and comparison with the Faeroe-Shetland Basin

The silica diagenetic boundaries in Sakhalin are amongst the largest diagenetic front patterns to be described. Many of the morphological features appear to form as a result of the interference of the front with a layered stratigraphy, rather than taking up the cell-like or polygonal geometry described before in the basins of the northeast Atlantic margin (Davies 2005).

The morphologies in the Faeroe-Shetland Basin take the form of a series of polygonal ridges composed of attached wings and terraces with polygonal or cell-like plan form geometry. Although the morphologies of the NSB include attached wings and terraces, there is no evidence for the development of polygonal ridges with the associated 3D planar form. Both basins have a similar heterogeneous stratigraphic fill, which is composed of diatomites interbedded with diatomaceous mudstones. The scale of the morphologies between the basins are similar, generally being of the order of <2 km, with the exception of the multi-kilometre scale depressions and elevations of the NSB. However, the distribution of the morphologies between the basins is different. In the NSB the morphologies develop throughout the basin wherever the silica diagenetic boundaries occur, although they are more commonly developed in the eastern part of the basin, while in the Faeroe-Shetland Basin the polygonal ridges are only developed in certain areas even though the opal-A to opal-CT transition occurs over a much larger extent of the basin. Davies (2005) noted that in the Faeroe-Shetland Basin the siliceous sediments in which the boundaries formed the cell-like geometry mantled an underlying polygonal fault system and that ridges in the diagenetic front generally formed above the fault tips, probably due to fluid flow from the faults causing enhanced rates of diagenesis. However, in the NSB there is no polygonal fault system that can influence formation of any of the morphological features; hence this specific ridge morphology did not develop.

Therefore, it is likely that the morphologies of the NSB are a more fundamental manifestation of the processes of silica diagenetic front advancement than the more specialised process derived from underlying cellular fracture patterns described by Davies (2005) in the Faeroe-Shetland Basin. Differential front advancement is more common in the Faeroe-Shetland Basin due to the regularity of morphology development associated with the extensive polygonal faulting. The irregular nature of morphology

development in the NSB means the morphologies are not as commonly developed as those in the Faeroe-Shetland Basin; hence the fronts tend to mostly follow bed sets when the strata is planar with differential front advancement only occurring where seed areas form.

It is probable that the positions of seed area formation in the NSB are controlled by a complex natural system, which is influenced by a combination of different factors. It could be one dominant factor governing the formation and position of the various morphological features or it could be a combination, but it is impossible to tell using seismic data alone.

3.8.3 Remaining questions and uncertainties

Further detailed borehole data would be required to assess whether the hypothesis that diagenetic front geometry at regional scales is controlled by a combination of lithological variation and the interference of the fronts with deformed and inclined strata. Borehole data would also help to evaluate the role fracturing plays in front advancement. Scientific drilling of some of the phenomena described would be very beneficial.

3.9 Conclusions

Silica diagenetic fronts are dynamic, time-dependent phenomena that have mostly been overlooked in terms of their importance in the evolution of sedimentary basin fills. Seismic analysis has a significant role to play in understanding how the fronts advance and how this advancement changes the properties and structure of the host sediment.

The silica diagenetic boundaries of the NSB reveal a number of morphological features that form as a result of the interference of the diagenetic front with inclined and folded stratigraphy as well as with variations in composition and rheology of the host lithology. The morphological elements can be explained in terms of variations in the relative rates of front advancement, both parallel and orthogonal to bedding, which are probably controlled by lithological variations, the inclination of the host strata and feedback between diagenesis and possible hydrofracture generation. Wings, terraces and serrated patterns are all indicative of the attempts by the fronts to advance to higher stratal levels, while multi-kilometre scale depressions and elevations in the opal-A to

opal-CT front probably result from ROFA being restricted or enhanced by localised variations in host lithology.

The fronts of the NSB lack the regular cell-like or polygonal geometry of the basins of the northeast Atlantic margin (e.g. Davies 2005), due to different controls on seed area formation and front advancement. This has lead to an irregular geometry of the diagenetic fronts. These varied front patterns between basins indicate the factors effecting front advancement and the growth of the various morphological features differ depending on the stratigraphic, sedimentological and structural architecture of a particular basin. Therefore, it can be concluded that within individual sedimentary basins there could be unique frontal geometries due to the variations in the controls on the diagenetic fronts.

The factors that influence the geometry of the fronts include the location and extent of fluid flow conduits (e.g. hydrofractures), pore water chemistry, host rock lithology and variations in heat flow. Within the NSB the interaction of all these factors, together with the lack of one dominant control, during the diagenetic transitions created the irregular frontal geometry that is observed. The precise diagenetic processes cannot be accurately determined using seismic data alone. However, the visualisation of diagenetic fronts within a basin using seismic reflection data has the potential to be very useful at this scale.

Chapter 4: Estimating Porosity Reduction due to Silica Diagenesis using Seismic Reflection Data

4.1 Introduction

It has long been known that compaction is an important process in sedimentary rocks that usually causes an exponential reduction in sediment porosity during burial (e.g. Dzevanshir *et al.* 1986; Wilson & McBride 1988). Determining the rate of porosity reduction with depth is an important aspect of sedimentary basin analysis that has profound implications for many aspects of sedimentary and structural geology. It also has commercial relevance in terms of the capacity of sediment to host fluids and gases such as oil, CO_2 and thermogenic gas.

In sedimentary rocks, information inferred from seismic reflection data have often been used to make a host of predictions, including the environment of deposition (e.g. Diaz *et al.* 1990; Posamentier & Kolla 2003; Braaksma *et al.* 2006), the lithology (e.g. Fournier *et al.* 2002; Davies *et al.* 2003; Posamentier & Kolla 2003), fluid content (e.g. Davies *et al.* 2003), and in the absence of borehole calibration to make estimations of porosity, based upon general knowledge of the depositional system (e.g. Brown *et al.* 1996). Brown *et al.* (1996) used differential compaction in the strata above a rim in a rimmed reef to estimate the relative porosity, i.e. whether it is high or low, to deduce the effect of post-depositional changes. Changes in the geometry of seismic reflections with depth have not been used to directly and quantifiably estimate porosity loss during burial. This is probably because the magnitude of these changes is usually so small, therefore making accurate measurements difficult.

Compaction of sediment during burial is usually such a gradual process that its effects on seismic reflections are very difficult to identify. The effect of compaction is also difficult to isolate from other burial related processes using seismic data, such as the general increase in seismic velocity that occurs with lithification during burial. Usually the amount of compaction is calculated using the following equation:

$$T_f = (1-\Phi_i)T_i / (1-\Phi_f) \qquad (1)$$

Where: T_i is the initial thickness, T_f is the final thickness, Φ_i is the initial porosity and Φ_f is the final porosity. Lateral variations in the magnitude of compaction, both mechanical and chemical, can cause differential subsidence in sedimentary basins

during burial and this effect can be significant enough to cause folds to form (e.g. Davies 2005). Recently, this effect has been identified within biosiliceous successions, where distinct reflections can be mapped that represent boundaries across which significant compaction is taking place due to the conversion of opal-A to opal-CT (Davies 2005). Davies (2005) proposed that differential compaction occurs at some of these boundaries as a result of variations in the depth of the diagenetic boundary; hence the point at which porosity reduction occurs. The differential compaction causes kilometre-scale folding of the overburden above the boundary (Fig. 4.1). In this chapter the hypothesis put forward by Davies (2005) is tested by modelling the opal-A to opal-CT boundary, together with the associated deformation of the overburden, and describe a method for estimating the amount of porosity change that occurs at this boundary.

The method described here is an example of forward modelling where magnitude of the porosity drop is calculated from a model of how the opal-A to opal-CT transformation influences the seismic expression of the strata. This method requires seismic imaging of the opal-A to opal-CT boundary and of the reflections above it. The cost of drilling to establish the amount of compaction is significant; therefore this method represents a new technique for porosity estimation that could be applied where no borehole data exists.

4.2 Diagenetic boundaries and deformation

As a result of the physical property changes associated with the reactions (see Chapter 1.3) silica diagenetic boundaries are frequently imaged as moderate- to high-amplitude normal polarity reflections on seismic data, which can cross-cut stratigraphy (Fig. 3.1). These seismic diagenetic boundaries can be mapped over areas of up 10^5 km^2 (e.g. Davies & Cartwright 2002; Meadows & Davies 2007).

They sometimes develop regular wavelength morphological forms that have yet to be recognised in the field but have been identified on several seismic data sets, from three different basins (see Davies *et al.* 1999; Davies 2005; Davies & Cartwright 2007; Meadows & Davies 2007). Some of these morphologies can take the cross-sectional form of ridges and troughs that have a polygonal plan form geometry (e.g. Davies 2005). They can also vary considerably in size (Fig. 3.2), from multi-kilometre scale features to wings that are <1 km in length, which are elongate to concave-upwards features that form just above the diagenetic boundary (Meadows & Davies

2007). These different morphologies are probably the result of a combination of factors such as the interference of the diagenetic boundaries with inclined and folded stratigraphy together with lateral changes in the properties and therefore, depth of transformation of the sediment (Meadows & Davies 2007). Many of the morphologies are the result of differential advancement of the diagenetic boundaries, i.e. there is variation in depth of conversion (DOC), and hence conversion will occur earlier at some points laterally leading to differential compaction as a result of porosity reduction (Fig. 4.1) (Davies 2005). It is this earlier hypothesis that this chapter aims to test by modelling the effect of differential advancement at the opal-A to opal-CT boundary and through the porosity estimating method that is developed in this chapter.

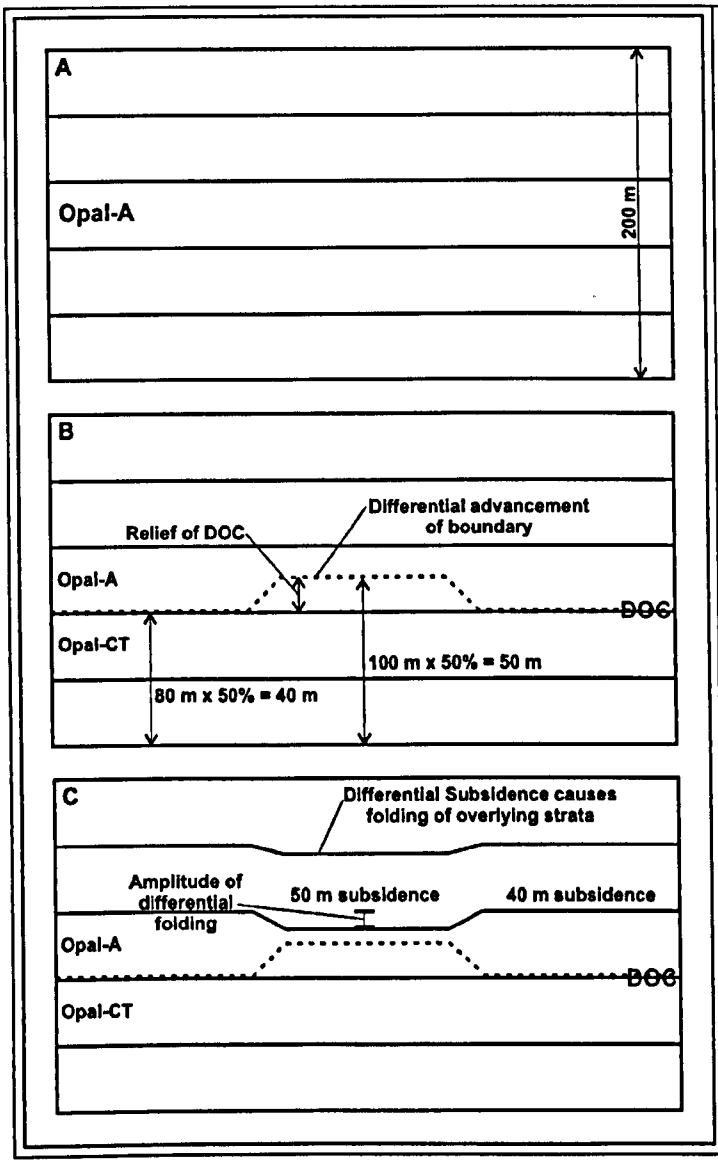

Fig. 4.1: Diagram illustrating the effects of differential advancement of the diagenetic front on the overlying sediment. The diagram also summarises the following terms: differential advancement, relief of the DOC and amplitude of the folding caused by differential compaction, which are used throughout the chapter. **(A)** Strata, 200 m thick, prior to conversion. **(B)** The sediment converts from opal-A to opal-CT at a diagenetic boundary. However, part of the boundary converts sediment at a shallower depth than another part. **(C)** This leads to differential front advancement, hence to differential compaction of the overlying strata, as a result of porosity reduction (50% in this example), causing folding to occur.

4.3 Modelling

The compaction equation (equation 1) is used to replicate the geometry, using a forward modelling methodology, of the reflections identified above the diagenetic boundary across which the porosity is expected to have changed (Fig. 4.2). It became apparent that there were several different methods for modelling the differential compaction and the porosity loss associated with the opal-A to opal-CT transition depending on what initial parameters were used in equation 1 (see section 4.5).

These models have their parameters adjusted to match the observations made from several different seismic datasets. These parameters include the porosity, both initial and final, and the relief of DOC. They are derived using realistic values from seismic datasets and other sources of information for the relevant seismic case studies. Once the models are adjusted to match the parameters from the case studies the model can then be used to calculate an estimate of the porosity drop or the amplitude of the differential compactional folding, depending on the known parameters (see section 4.5), associated with the opal-A to opal-CT transition in specific examples. From this method a form of 'porosity profile' can be determined from the seismic data, hence giving some idea of how the porosity changes across the diagenetic boundary through the use of seismic data.

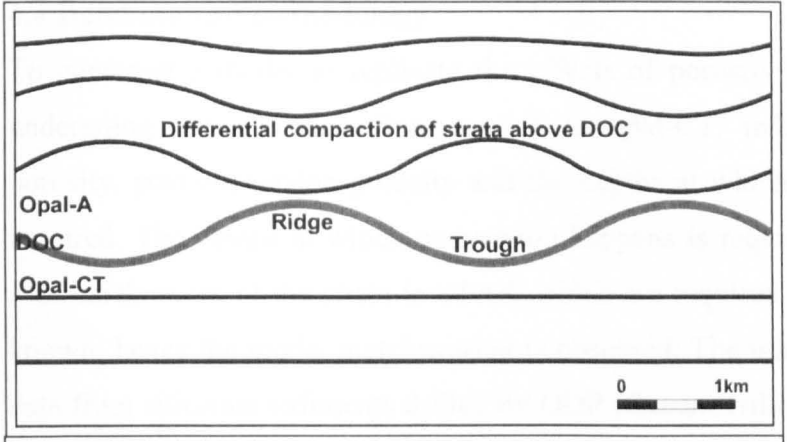

Fig. 4.2: Schematic diagram summarising the ridge-trough morphology of the opal-A to opal-CT boundary described by Davies (2005). This form of frontal morphology initially developed due to differential advancement of the diagenetic boundary. Ridge relief and width are then progressively increased due to earlier opal-A to opal-CT conversion above ridges as well as conversion laterally along bed sets (Davies 2005). This caused compaction and subsidence in the overlying strata and to the development of a series of downward flexures aligned with the ridges in the DOC.

Previous work on estimating rock properties from seismic data has mainly used deterministic methods to achieve this aim. A deterministic method involves relating one property to another. For example, Spikes & Dvorkin (2003) used

deterministic relations to interpret rock properties (pore fluids, porosity and lithology) from seismic velocity (P- and S-wave data). All deterministic equations are calibrated at a well. The equations are then applied to upscaled well log data to confirm their validity at the seismic scale (Spikes & Dvorkin 2003). The basis of every deterministic model is a series of controlled experiments where the physical properties are measured under the same environmental conditions, such as in well log measurements (Spikes & Dvorkin 2003). These data are then statistically analysed to reveal any trends between the physical properties, which can then be used to estimate unknown properties from the properties that are known.

4.4 Database and methodology

To construct a model to replicate the effects of porosity change on the sediments undergoing the transition from opal-A to opal-CT, information on the starting porosity, post-conversion porosity and the depths at which the transition occurs are required. The depths at which conversion happens is required so that the initial and final thicknesses of the strata involved, which are required for use in equation 1, are known; hence the model matches what is observed. The initial models were based on data from siliceous sediments drilled by ODP (Ocean Drilling Program) Leg 127/128 in the Sea of Japan, which is one of the best documented examples of a silica diagenetic boundary in terms of sediment properties and where there are also some poor quality 2D seismic data that image the opal-A to opal-CT boundary. There is a lack of data, especially relating to sediment properties, for most areas where silica diagenesis occurs. In the Sea of Japan the sediments typically undergo a ~30% drop in porosity at a DOC located at 300 to 400 mbsf (metres below seafloor) (Fig. 4.3), with an initial porosity of ~80% and a post-conversion porosity of ~50% (Tamaki *et al.* 1990). Hence, for the initial models the porosity values were based upon the data from the Sea of Japan. In this chapter the term relief is defined as the depth between the shallowest and deepest DOC located along the opal-A to opal-CT boundary (Fig. 4.1). However, the depth of the diagenetic boundaries in basins worldwide can vary considerably, from less than 300 mbsf to more than 1000 mbsf, this variation can also occur within the same basin (Meadows & Davies 2007 and references therein).

It is also essential to replicate the effects the transition has on the strata that can be identified on seismic data (Figs. 4.1 and 4.2). Davies (2005) and Meadows & Davies (2007) described unusual deformational patterns related to the variations in the depth of the diagenetic boundary. This has caused differential compaction of the overlying sediment (Figs. 4.1 and 4.2). The effect of differential compaction manifests itself as folding in the strata overlying the diagenetic boundary. Antiforms develop above regions of the boundary where upward advancement has been suppressed (deeper DOC) and synforms form above the boundary where upward advancement has occurred more rapidly (shallower DOC) - figures 4.1 and 4.2. Figure 4.1 summarises some of the key terms which will be used repeatedly throughout this chapter. The hypothesis developed by Davies (2005) and Meadows & Davies (2007) is that the amplitude of the folding created by differential compaction is related to the size of the porosity drop and to the differential relief of the diagenetic boundary. It is this hypothesis that is tested in this chapter through modelling. The amplitude of the folding caused by differential compaction is known from seismic data. Hence by using the value for the amplitude of the folding and combining with the other known parameters, such as initial porosity and relief of the DOC, these values can be entered into a rearranged equation 1 (see section 4.4.1 and 4.5). This would enable the magnitude of the porosity drop that occurs to be calculated.

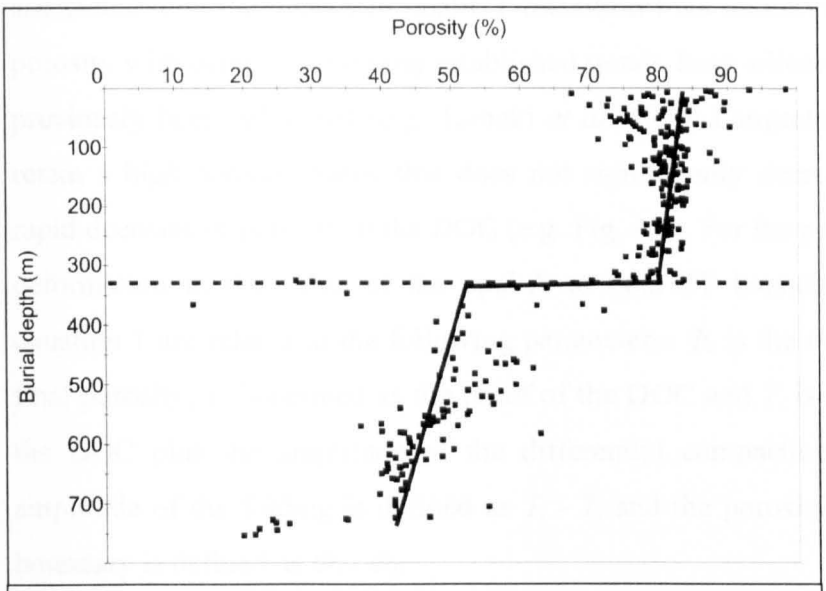

Fig. 4.3: Porosity-depth graph for siliceous sediments from ODP Leg 127/128, Site 795, Sea of Japan. Dashed line indicates the approximate position of the opal-A to opal-CT transition and the solid line indicates the porosity trend with depth.

4.4.1 Modelling process

When using the compaction equation to model the magnitude of the porosity drop associated with the opal-A to opal-CT transition I am assuming that the reduction in porosity with depth is following established trends from siliceous sediments that have previously been calibrated (e.g. Tamaki *et al.* 1990; Langseth & Tamaki 1992), i.e. retain a high porosity value that does not significantly decrease with depth until a rapid decrease in porosity at the DOC (e.g. Fig. 4.3). For the purpose of modelling the deformation in the strata at the opal-A to opal-CT boundary the components of equation 1 are related to the following parameters: Φ_i is the initial porosity, Φ_f is the final porosity, T_f is defined as the relief of the DOC and T_i is defined as the relief of the DOC plus the amplitude of the differential compactional folding. Hence the amplitude of the folding is defined as T_i - T_f and the porosity drop at the diagenetic boundary is defined as Φ_i - Φ_f.

4.5 Replicating opal-A to opal-CT boundary relief

It was found that two mechanisms could be used to replicate the deformation in the strata above the opal-A to opal-CT boundary. One mechanism involves introducing variations in the relief of the DOC during each run of the model. These are termed the 'relief models'. The second involves calculating the final porosity during each run of the model. These are termed the 'porosity models'. In the following sections the basis for these models are outlined.

4.5.1 The relief model

One method of generating differential advancement of the diagenetic front, hence differential compaction, is to vary the relief of the DOC while keeping the magnitude of the porosity drop constant between each run of the model. By changing the amount of differential advancement, i.e. the relief of the DOC, you can change the amplitude of the folds above the diagenetic boundary. This method is termed the relief model (Table 4.1). In the relief model equation 1 is rearranged in order to find T_i:

$$T_i = (1-\Phi_f)T_f / (1-\Phi_i) \qquad (2)$$

The value of T_f is then subtracted from T_i in order to calculate the amplitude of the differential compactional folding. This model assumes that initial and final porosities are known, while the relief of the DOC is varied in order to produce changes in the

amplitude of the folding. In this model the larger the relief of the DOC the greater the amplitude of the differential compactional folding will be (Table 4.1).

Relief of DOC (m)	Porosity Drop (%)	Initial Porosity (%)	Final Porosity (%)	Relief + Amplitude of Folding (m)	Amplitude of Folding (m)
25	30%	80%	50%	62.5	37.5
50	30%	80%	50%	125	75
75	30%	80%	50%	187.5	112.5
100	30%	80%	50%	250	150
125	30%	80%	50%	312.5	187.5
150	30%	80%	50%	375	225
175	30%	80%	50%	437.5	262.5
200	30%	80%	50%	500	300
225	30%	80%	50%	562.5	337.5
250	30%	80%	50%	625	375
25	15%	80%	65%	43.75	18.75
50	15%	80%	65%	87.5	37.5
75	15%	80%	65%	131.25	56.25
100	15%	80%	65%	175	75
125	15%	80%	65%	218.75	93.75
150	15%	80%	65%	262.5	112.5
175	15%	80%	65%	306.25	131.25
200	15%	80%	65%	350	150
225	15%	80%	65%	393.75	168.75
250	15%	80%	65%	437.5	187.5
25	15%	50%	35%	32.5	7.5
50	15%	50%	35%	65	15
75	15%	50%	35%	97.5	22.5
100	15%	50%	35%	130	30
125	15%	50%	35%	162.5	37.5
150	15%	50%	35%	195	45
175	15%	50%	35%	227.5	52.5
200	15%	50%	35%	260	60
225	15%	50%	35%	292.5	67.5
250	15%	50%	35%	325	75

Table 4.1: Table showing the variables input into the relief model and the values for the amplitude of the differential compactional folding that were calculated using equation 2.

4.5.2 The porosity model

Another method of generating differential advancement of the diagenetic front, hence differential compaction, is to vary the magnitude of the porosity drop at the boundary, while keeping the relief of the DOC constant during each run of the model (Table

4.2). In this model the initial porosity is kept constant while the final porosity needs to be calculated (Table 4.2). This method is termed the porosity model (Table 4.2). In the porosity model equation 1 is rearranged in order to find Φ_f:

$$\Phi_f = 1 - ((1 - \Phi_i)\, T_i / T_f) \qquad (3)$$

This model assumes that the initial porosity, relief of the DOC and the amplitude of the folding are known, once Φ_f is known the magnitude of the porosity drop can be calculated by subtracting the initial porosity from the final porosity (see section 4.4.1). The greater the amplitude of the differential compactional folding in the model is the larger the porosity drop will be (Table 4.2).

Relief of DOC (m)	Relief + Amplitude of Folding (m)	Amplitude of Folding (m)	Initial Porosity (%)	Final Porosity (%)	Porosity Drop (%)
100	105	5	80%	79.0%	1.0%
100	110	10	80%	78.0%	2.0%
100	115	15	80%	77.0%	3.0%
100	120	20	80%	76.0%	4.0%
100	125	25	80%	75.0%	5.0%
100	130	30	80%	74.0%	6.0%
100	135	35	80%	73.0%	7.0%
100	140	40	80%	72.0%	8.0%
100	145	45	80%	71.0%	9.0%
100	150	50	80%	70.0%	10.0%
100	155	55	80%	69.0%	11.0%
100	160	60	80%	68.0%	12.0%
100	165	65	80%	67.0%	13.0%
100	170	70	80%	66.0%	14.0%
100	175	75	80%	65.0%	15.0%
200	205	5	80%	79.5%	0.5%
200	210	10	80%	79.0%	1.0%
200	215	15	80%	78.5%	1.5%
200	220	20	80%	78.0%	2.0%
200	225	25	80%	77.5%	2.5%
200	230	30	80%	77.0%	3.0%
200	235	35	80%	76.5%	3.5%
200	240	40	80%	76.0%	4.0%
200	245	45	80%	75.5%	4.5%
200	250	50	80%	75.0%	5.0%
200	255	55	80%	74.5%	5.5%
200	260	60	80%	74.0%	6.0%
200	265	65	80%	73.5%	6.5%
200	270	70	80%	73.0%	7.0%
200	275	75	80%	72.5%	7.5%
100	105	5	40%	37.0%	3.0%
100	110	10	40%	34.0%	6.0%

100	115	15	40%	31.0%	9.0%
100	120	20	40%	28.0%	12.0%
100	125	25	40%	25.0%	15.0%
100	130	30	40%	22.0%	18.0%
100	135	35	40%	19.0%	21.0%
100	140	40	40%	16.0%	24.0%
100	145	45	40%	13.0%	27.0%
100	150	50	40%	10.0%	30.0%
100	155	55	40%	7.0%	33.0%
100	160	60	40%	4.0%	36.0%
100	165	65	40%	1.0%	39.0%
200	205	5	40%	38.5%	1.5%
200	210	10	40%	37.0%	3.0%
200	215	15	40%	35.5%	4.5%
200	220	20	40%	34.0%	6.0%
200	225	25	40%	32.5%	7.5%
200	230	30	40%	31.0%	9.0%
200	235	35	40%	29.5%	10.5%
200	240	40	40%	28.0%	12.0%
200	245	45	40%	26.5%	13.5%
200	250	50	40%	25.0%	15.0%
200	255	55	40%	23.5%	16.5%
200	260	60	40%	22.0%	18.0%
200	265	65	40%	20.5%	19.5%
200	270	70	40%	19.0%	21.0%
200	275	75	40%	17.5%	22.5%

Table 4.2: Table showing the variables input into the porosity model and the values for the porosity drop that were calculated using equation 3.

4.6 Case studies

Four examples of differential diagenetic front advancement from different basins worldwide were chosen in order to replicate the patterns seen on seismic data and estimate the magnitude of the porosity drop across the opal-A to opal-CT boundary. In these case studies the relief of the DOC is already defined from seismic data, hence the relief model cannot be used (i.e. this value is known and is used in the porosity model equation instead). Hence, the porosity model is used to try and estimate the magnitude of the porosity drop associated with the conversion.

In the case studies I defined the initial thickness (T_i) as the final thickness (T_f) (i.e. the relief of the DOC) plus the amplitude of the differential compactional folding (see section 4.4.1), which is defined from the seismic data. In order for the porosity drop to be estimated the initial porosity must also be known. This information is most easily obtained from well data. This chapter has only got specific porosity data for the

North Sakhalin Basin. There is no porosity data available for the Faeroe-Shetland Basin. There is some well data available for the Vøring and Møre Basins. However, these are exploration wells and are of low data quality, especially at shallow depths where the opal-A to opal-CT boundary is most likely to be identified. At shallow depths the log quality is not very good because these depths are generally not of interest to hydrocarbon exploration. However, the scientific wells of ODP Leg 104 (Norwegian Sea) can provide a good proxy for the initial porosity for the nearby Vøring and Møre Basins. The porosity data from ODP Leg 104 relates to unconverted diatomaceous sediments and ranges from 63 to 81% with an average value, which is used in the examples below, of 73%.

4.6.1 North Sakhalin Basin (NSB)

The morphologies associated with the diagenetic boundaries in the NSB were described in detail by Meadows & Davies (2007). Unreleased BP well data suggest that the bulk sediment in the NSB has a maximum initial porosity of 52%. For the purposes of modelling an example of a multi-kilometre scale depression and multi-kilometre scale elevation (see Meadows & Davies 2007) were selected in order to estimate the magnitude of the porosity drop (Fig. 4.4).

Seismic data defined the relief on the multi-kilometre scale depression as 250 m and the amplitude of the differential compactional folding as 60 m (Fig. 4.4A), which will give an initial thickness of 310 m. The porosity model suggested that the magnitude of the porosity drop is 11% from 52% to 41% across the boundary (Fig. 4.4B).

Seismic reflection data defined the relief on the multi-kilometre scale elevation as 150 m and the amplitude of the differential compactional folding as 45 m (Fig. 4.4C), which will give an initial thickness of 195 m. The porosity model suggested that magnitude of the porosity drop is 14% from 52% to 38% across the boundary (Fig. 4.4D).

4.6.2 Faeroe-Shetland Basin

The ridge and trough morphology associated with the opal-A to opal-CT boundary in the Faeroe-Shetland Basin (FSB) was initially described by Davies *et al.* (1999) and Davies & Cartwright (2002) and with significant revised interpretation by Davies (2005). There is no available porosity data with which to define an initial porosity

value for the model so a value of 80% was used based on ODP data of other silica diagenetic boundaries (see Fig. 4.3). Seismic data defined the relief of the DOC as 75 m and the amplitude of the differential compactional folding as 45 m (Fig. 4.5A), which will give an initial thickness of 120 m. The porosity model suggests that the

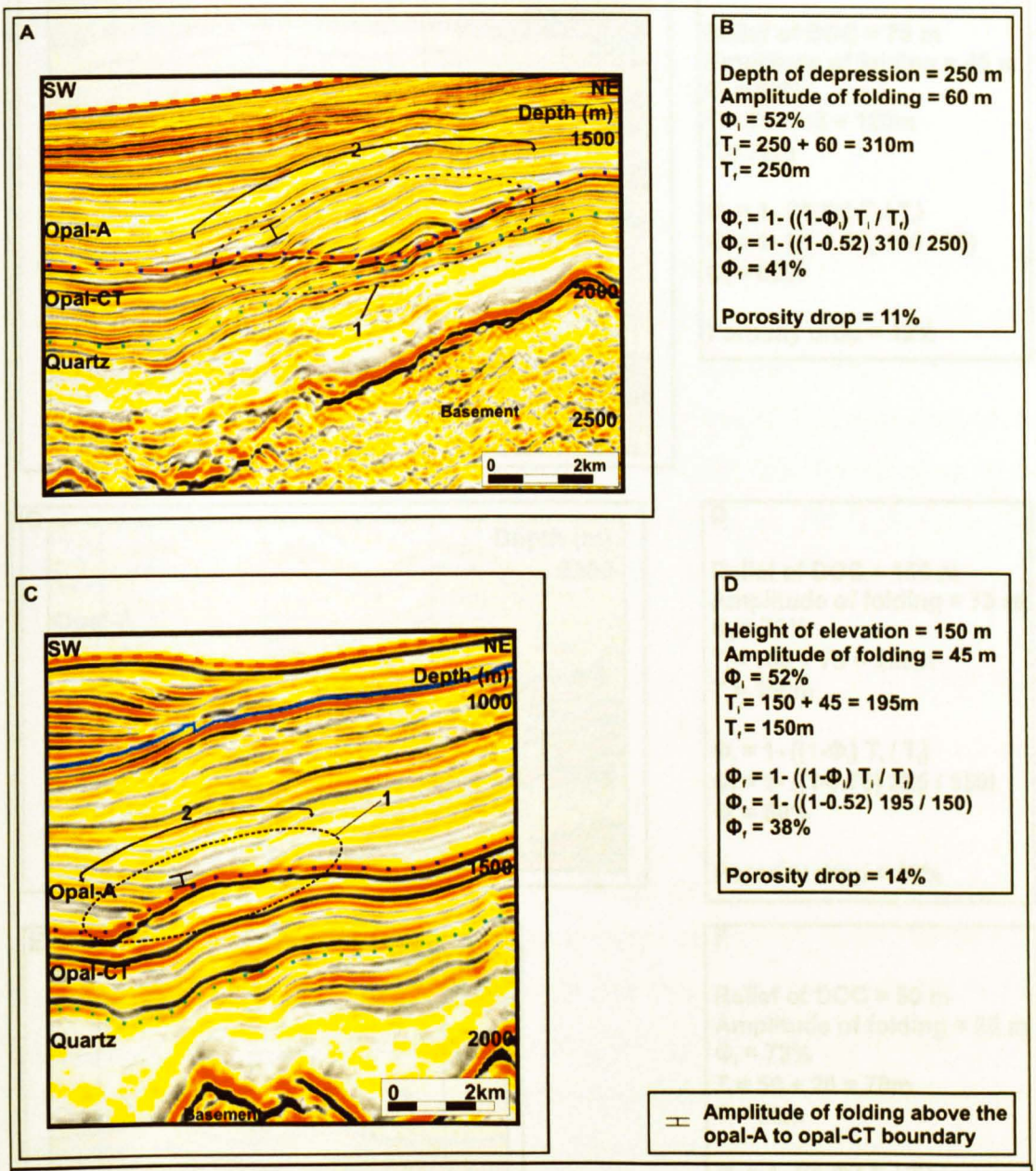

Fig. 4.4: Estimated porosity values required to produce the differential compaction in the strata above the multi-kilometre scale depressions and elevations identified in the NSB. **(A)** Example of a depression (1) from seismic data from the NSB. Note the antiformal folding in the strata overlying the depression (2). **(B)** Calculation of the porosity drop, associated with the depression, using the porosity model. **(C)** Example of an elevation (1) from seismic data from the NSB. Note the downward flexure of the overlying strata (2). **(D)** Calculation of the porosity drop, associated with the elevation, using the porosity model. The purple dotted line on seismic data marks the position of the opal-A to opal-CT boundary, while the pale blue dotted line marks the opal-CT to quartz boundary.

magnitude of the porosity drop could have been 12% from 80% to 68% across the boundary (Fig. 4.5B).

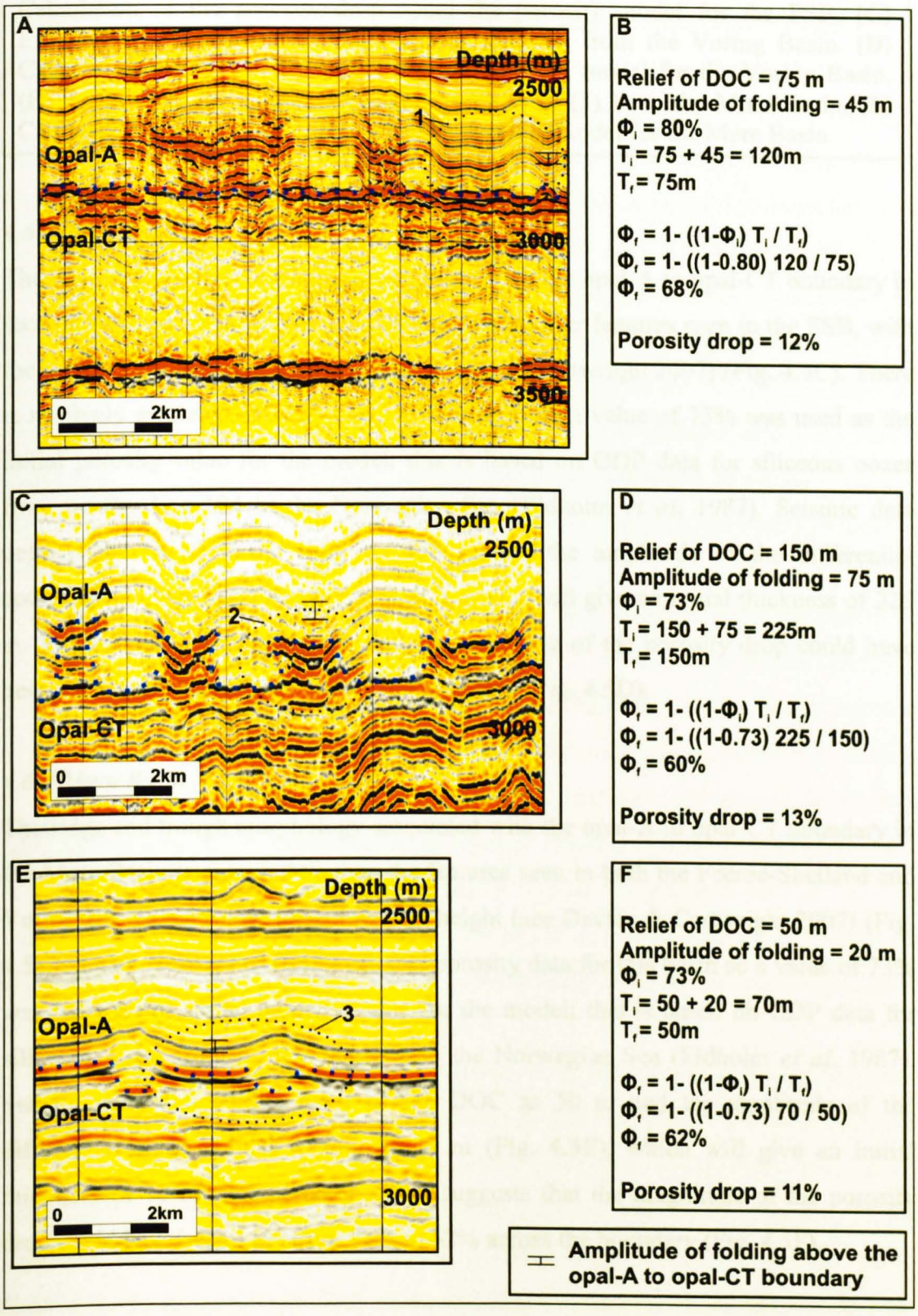

Fig. 4.5 (previous page): Estimated porosity values required to produce the ridge and trough morphologies identified in the basin of the Northeast Atlantic margin. **(A)** Example of the ridge and trough morphology (1) from the FSB. The high-amplitude reflections above the opal-A to opal-CT boundary are a gas cloud. **(B)** Calculation of the porosity drop using the porosity model for the FSB. **(C)** Example of the ridge and trough morphology (2) from the Vøring Basin. **(D)** Calculation of the porosity drop using the porosity model for the Vøring Basin. **(E)** Example of the ridge and trough morphology (3) from the Møre Basin, **(F)** Calculation of the porosity drop using the porosity model for the Møre Basin.

4.6.3 Vøring Basin

The ridge and trough morphology associated with the opal-A to opal-CT boundary in the Vøring Basin is more pronounced than the smaller features seen in the FSB, with the ridges more columnar in shape (see Davies & Cartwright 2007) (Fig. 4.5C). There is no freely available porosity data for this basin so a value of 73% was used as the initial porosity value for the model; this is based on ODP data for siliceous oozes from nearby Leg 104 in the Norwegian Sea (Eldholm *et al.* 1987). Seismic data defined the relief of the DOC as 150 m and the amplitude of the differential compactional folding as 75 m (Fig. 4.5C), which will give an initial thickness of 225 m. The porosity model suggests that the magnitude of the porosity drop could have been 13% from 73% to 60% across the boundary (Fig. 4.5D).

4.6.4 Møre Basin

The ridge and trough morphology associated with the opal-A to opal-CT boundary in the Møre Basin is more subtle than the features seen in both the Faeroe-Shetland and Vøring Basins, with the ridges lower in height (see Davies & Cartwright 2007) (Fig. 4.5E). Again there is no freely available porosity data for this basin so a value of 73% was used as the initial porosity value for the model; this is based on ODP data for siliceous oozes from nearby Leg 104 in the Norwegian Sea (Eldholm *et al.* 1987). Seismic data defined the relief of the DOC as 50 m and the amplitude of the differential compactional folding as 20 m (Fig. 4.5E), which will give an initial thickness of 70 m. The porosity model suggests that the magnitude of the porosity drop could have been 11% from 73% to 62% across the boundary (Fig. 4.5F).

4.7 Effect of seismic velocity and other uncertainties

It is possible that some of the diagenetic patterns replicated in this study might be a consequence of the substantial increase in seismic velocity associated with the transition of opal-A to opal-CT. Typically, the velocity in unconverted sediments is ~ 1700 m s^{-1} while it is ~ 2000 m s^{-1} in converted sediments (e.g. Guerin & Goldberg 1996). For example, 120 m thick bed sets in unconverted sediment with a seismic velocity of 1700 m s^{-1} would have a thickness of 141 ms on a seismic line (Fig. 4.6A). If the velocity increases abruptly at the DOC, without an associated porosity drop, to 2000 m s^{-1} then a thickness of 120 m would only represent 120 ms on a seismic line. This would produce a 'pull-up' effect leading to an apparent decrease in inclination of bed sets beneath the DOC (Fig. 4.6B). However, if the velocity remains constant above and below the DOC at 1700 m s^{-1} and a porosity reduction of 35%, from an initial porosity of 80% to a final porosity of 45%, then a thickness of 120 m would compact to 43.6 m, using equation 1, which would only represent 51 ms on a seismic line. The effect of the porosity drop associated with the conversion would produce a significant decrease in the inclination of the bed sets, due to the compaction, below the DOC (Fig. 4.6C). In reality there would be a combined effect on the inclination of the bed sets below the DOC resulting from both the velocity increase and porosity reduction (Fig. 4.6D). However, the combined effect only results in a slight decrease in the inclination of the strata when compared to the effect of the porosity reduction on its own, even at smaller reductions in porosity. Therefore, the change in porosity has more of an effect than the change in seismic velocity in affecting the strata as a result of the conversion of opal-A to opal-CT. Hence, the patterns seen on seismic data that result from differential advancement of the opal-A to opal-CT boundary are most likely to be a consequence of the porosity reduction, which has a significant effect on the seismic expression of the strata.

An important uncertainty in the estimation of the porosity drop directly from seismic data is the value for the initial porosity that is selected for the model. This is because the amplitude of the folding caused by differential compaction, for a given value of porosity reduction, will vary depending on the initial porosity of the sediment. For example, using equation 1, a 25% porosity drop in a bed set 100 m thick undergoing conversion will result in a bed set 28.57 m thick for a drop from 90% to 65%, while a reduction from 40% to 15% will result in a bed set 70.59 m thick (see Table 4.3). Hence, these differences in the amount of compaction due to differing

initial porosities will cause variation in the amplitudes of the differential compactional folding in the strata above the DOC even though the magnitude of the porosity drop is identical. This means that without knowing the initial porosity of the sediment porosity drop cannot be accurately estimated. Although through the use of known porosities from sources such as the ODP the magnitude of the porosity drop can be

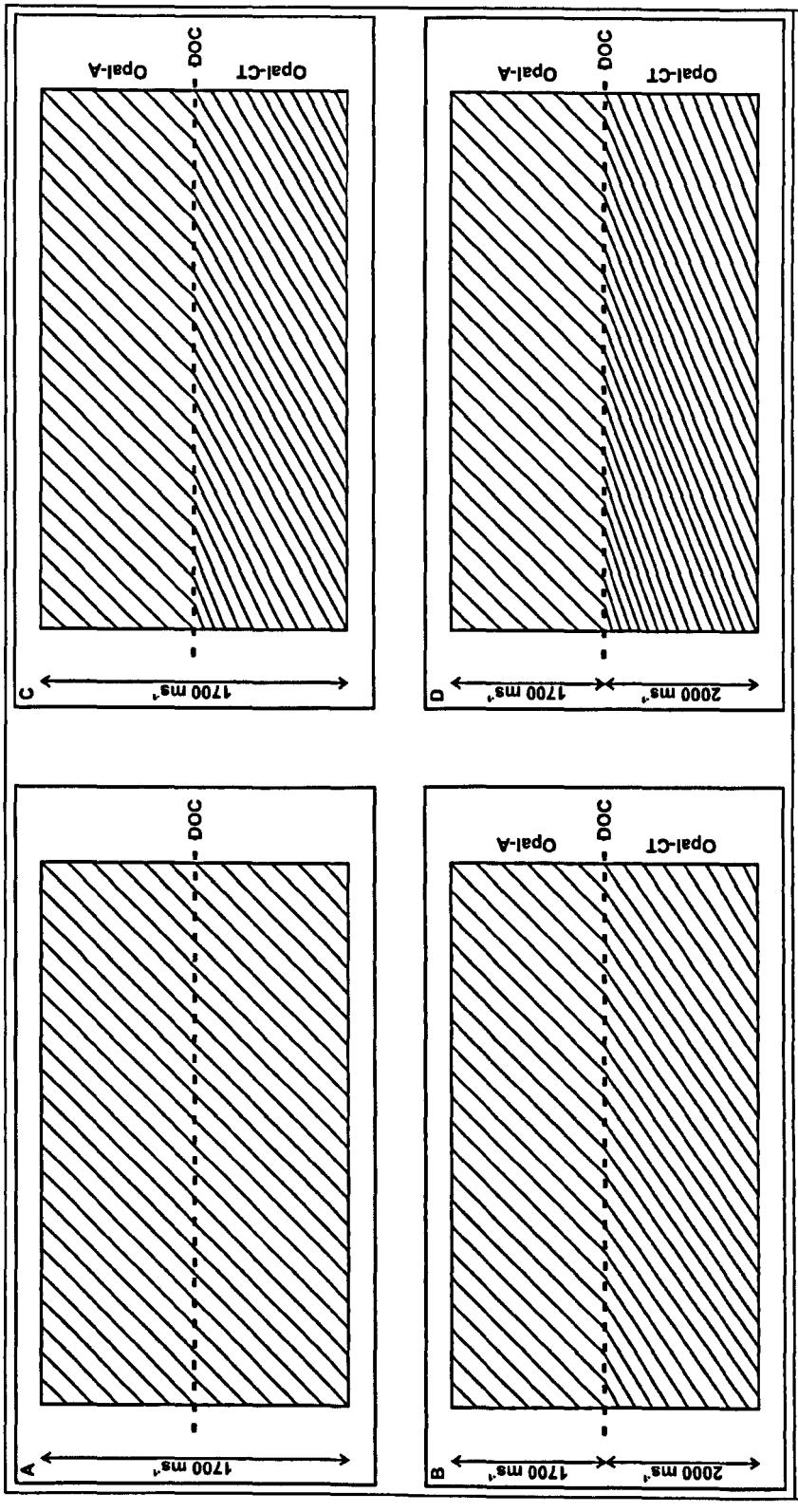

Fig. 4.6: Schematic diagram showing the relative effects of velocity change and porosity reduction on the seismic expression of sediment undergoing conversion. **(A)** Unconverted sediment with a uniform velocity. **(B)** Velocity increase at the DOC with no porosity change. **(C)** Porosity reduction (~35%) at the DOC with no change in velocity. **(D)** Combination of velocity increase and porosity reduction at the DOC. See text for further explanation.

estimated to some degree of accuracy from seismic data (e.g. Fig. 4.5). Most ODP porosity data is calculated from cores, these maybe prone to expansion after the overburden pressure is released, therefore they might have an exaggerated value for porosity. However, biogenic siliceous sediments are primarily composed of diatom and radiolarian tests, which are resistant to mechanical compaction (Hesse 1990; Tada 1991) even at depth; hence any exaggeration of porosity from core data is unlikely to be significant.

Initial Porosity (%)	Final Porosity (%)	Porosity Drop (%)	Initial Thickness (m)	Final Thickness (m)	Change in Thickness (m)
90	65	25	100	28.57	71.43
80	55	25	100	44.44	55.56
70	45	25	100	54.55	45.45
60	35	25	100	61.54	38.46
50	25	25	100	66.67	33.33
40	15	25	100	70.59	29.41

Table 4.3: Table showing how the change in thickness, for a given porosity reduction, will vary depending on the initial porosity of the sediment.

4.8 Discussion

4.8.1 Usefulness of the models

Of the two models used to try to estimate the porosity drop at the DOC in this chapter the most useful was the porosity model. This is because it fitted all the parameters known from the seismically imaged examples, such as the relief of the DOC and the amplitude of the differential compactional folding. The relief model is also useful, but generally the relief of the DOC and the amplitude of the folding will be known from seismic data and it will be the final porosity that will need to be calculated, hence the porosity model will be used instead. These models can applied to other examples where differential compaction occurs, such as carbonate mounds, which are generally resistant to compaction when compared to surrounding facies, in order to estimate the relative porosity drop. This process may only be applicable to examples where the differential compaction is of a high enough magnitude to be detected.

4.8.2 Graphical trends

Graphs plotted for the two models show that as the relief or porosity drop increase the amplitude of the folding increases as well with a linear relationship (Figs. 4.7 and 4.8). The graph for the relief model (Fig. 4.7) shows that higher values for the

amplitude of the folding are associated with models that use a high initial porosity with a large porosity drop, while models with lower initial porosities and smaller porosity drops produce folding with lower amplitudes for the same values of DOC relief. The graph for the porosity model (Fig. 4.8) shows larger porosity drops are associated with models that use a high initial porosity with a large value for the relief of the DOC, while models with lower initial porosities and a lower value for the relief produce smaller porosity drops for the same values for the amplitude of the folding. The graph in figure 4.9 plotted from the values in table 4.3 shows how initial porosity affects the thickness of the strata. It has already been pointed out that a 25% drop from 90% will not produce the same effect, in terms of the change in thickness, as a 25% drop from 80% initial porosity (Fig. 4.9). The post-conversion thickness and the change in thickness are related to the initial porosity with an exponential relationship (Fig. 4.9).

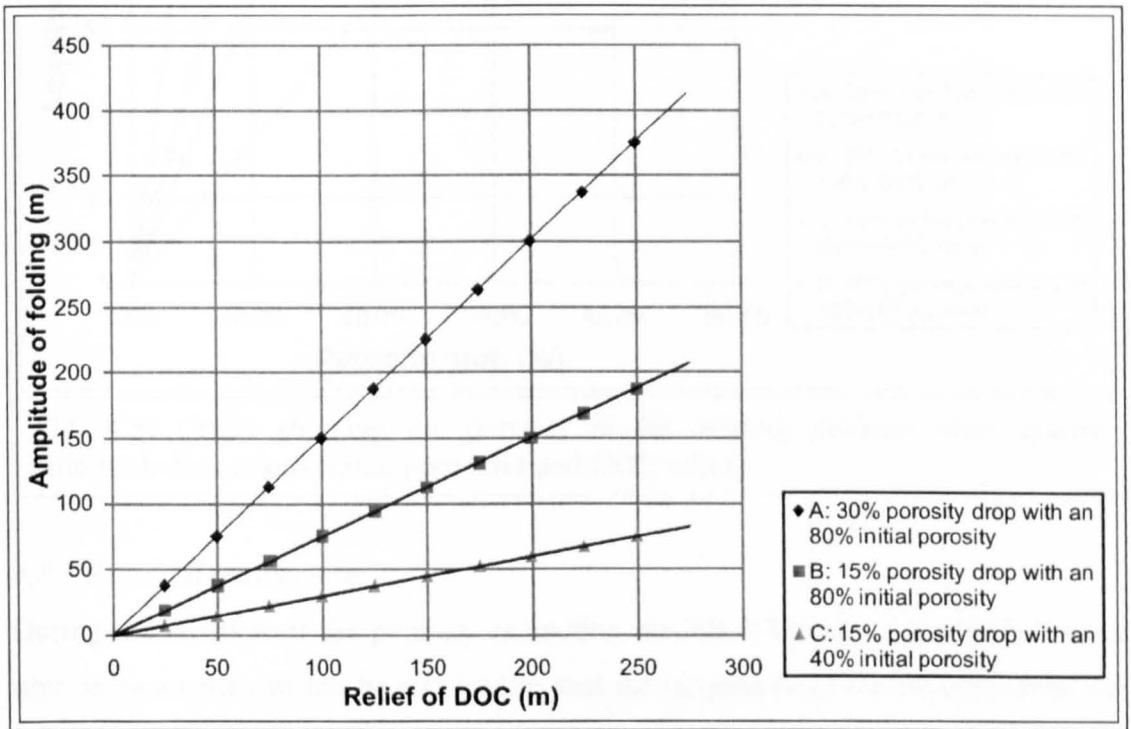

Fig. 4.7: Graph showing the relief model relating relief of the DOC against amplitude for various initial and final porosities.

The fact that the porosity drop for the two NSB examples (Fig. 4.4) were similar, together with a specific initial porosity value, would seem to indicate that there is a porosity reduction of 11-14% from 52% to 41-38% associated with the opal-A to opal-CT conversion in that basin. The fact that the porosity drops are also very similar (between 11 and 13%) for the three basins of the Northeast Atlantic margin (Fig. 4.5) might indicate that the siliceous sediment is behaving in the same way. This

could indicate that the sediment has a similar composition, which in turn will produce similar changes in porosity (e.g. Isaacs 1981). However, the lack of an accurate value for the initial porosity in these basins could mean that this might not be the case and a different value for initial porosity might produce a similar range of results for the porosity drops.

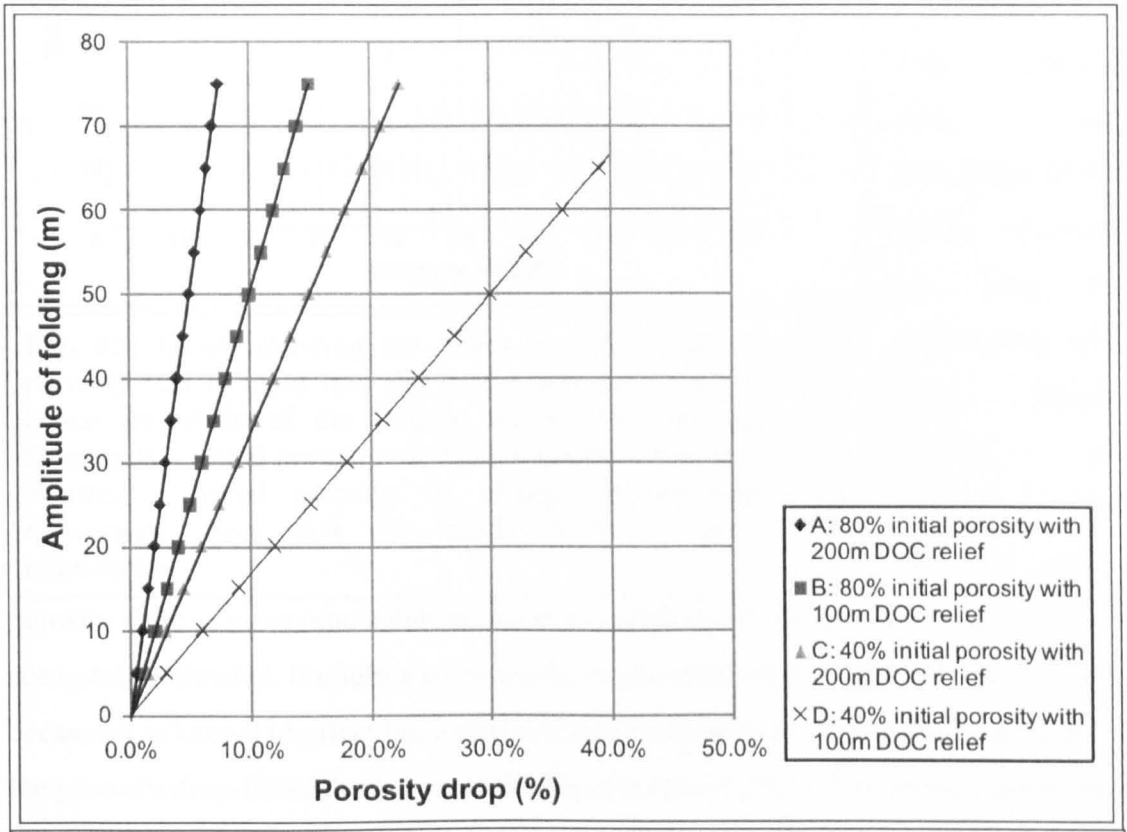

Fig. 4.8: Graph showing the porosity model relating porosity drop against amplitude for various initial porosities and DOC reliefs.

4.8.3 Required parameters

During the creation of the porosity estimation models it became apparent that more precise parameters would be required so that the magnitude of the porosity drop can be accurately estimated. There are three parameters that need to be accurately known in order to use the porosity model. The first parameter is an accurate value for the relief of the DOC, which can be used in the models as final thickness (T_f). The second parameter is an accurate value for the amplitude of the differential compactional folding, which can be added to the relief to provide a value for the initial thickness (T_i). The final parameter is a value for the initial porosity (Φ_i), which defines the magnitude of the compaction. By knowing the initial porosity the model will be able to use the porosity model to calculate the exact value of the final porosity, hence

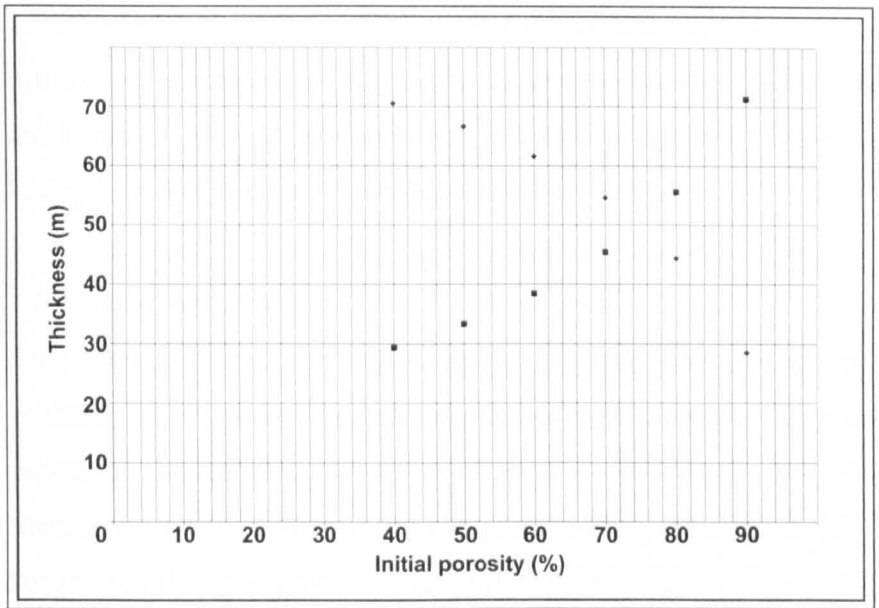

Fig. 4.9: Graph showing the effect that the value of initial porosity that is input into the model will have on thickness, hence amplitude of the folding for a 25% porosity drop. Diamonds = initial porosity vs. final thickness after conversion. Squares = initial porosity vs. change in thickness after conversion. Note that the trends show an exponential relationship.

giving the magnitude of the porosity drop. The first two parameters can be worked out from seismic data, but knowledge of the initial porosity can only be gained from well data. Hence, without an accurate value for the initial porosity there is no unique solution and the magnitude of the porosity drop cannot be accurately estimated. It might also be useful to know the silica content of the sediment because it is known to affect the initial and final porosities as well as the magnitude of the porosity drop for each of the transitions (see Isaacs 1981). The silica content also controls the position of the DOC; sediment with a high silica content has an earlier opal-A to opal-CT transition but a later opal-CT to quartz transition (e.g. Williams *et al.* 1985).

4.8.4 Causes of differential advancement

Many of the morphological features are a result of differential advancement and the associated differential compaction through porosity reduction. However, there are many processes that can cause differential advancement to occur. Davies (2005), Davies & Cartwright (2007) and Meadows & Davies (2007) have suggested several mechanisms: (1) a zone of denser hydrofracturing caused by fluid expulsion during the reaction could lead to enhanced fluid flow hence enhanced conversion; (2) lateral variation in the silica content of the sediment would lead to earlier conversion where the sediment was more silica-rich; (3) lateral variation in the thickness of the strata would lead to preferential advancement where the strata is thinnest; (4) in the case of

the Faeroe-Shetland Basin, fluid flow from underlying polygonal faults could result in differential advancement due to enhanced conversion in the strata above the fault tips and lastly (5) mass transfer of silica. The causes of these phenomena are not discussed in depth in this chapter – see Chapter 3.

4.8.5 Remaining issues

The main drawback in modelling the porosity drop using seismic data is that it probably only works for extreme and abrupt changes in porosity associated with diagenetic boundaries that are well imaged on seismic data. In other words where there is evidence of differential compaction from the seismic data, from which values for the relief of the DOC and amplitude of the differential compactional folding can be worked out.

Throughout this chapter there has been the assumption that there is no mass transport of the mineral concerned, in this case silica, within the model. In the models the assumption was made that all of the compaction above the opal-A to opal-CT boundary was due to sudden reduction in porosity of the sediment as a result of the conversion. However, if mass transport occurred it would contribute to the amount of compaction that the sediment undergoes. This means any effort to estimate the magnitude of the porosity change from the amount of differential compaction measured from seismic data would be flawed as the models have not taken into account the possible effects of mass transport. There is little evidence for the mass transport of silica due to the conversion of opal-A to opal-CT and the minor redistribution that occurs happens on a localised bed-by-bed scale (e.g. Tada 1991).

4.9 Conclusions

Using the geometry of reflections to try to estimate the magnitude of the porosity drop from the differential compactional folding above the opal-A to opal-CT boundary on seismic reflection data is a viable method. However, it probably can only be used in specific circumstances where porosity reduction is significant. Therefore, this method should be acceptable for many uses, such as decompaction and basin modelling in extreme latitudes, where siliceous sediments predominate, where there is a need for porosity-depth trends.

Three parameters are required in order for the value of the porosity drop to be estimated using the models: (1) relief of the DOC; (2) the amplitude of the differential

compactional folding of the strata above the diagenetic boundary; and (3) the value of the initial porosity. The first two are easily worked out from the seismic data. However, the last parameter requires access to porosity data from well logs, etc. without this value an accurate value for the final porosity cannot be given, only a range of possible porosity drops, with varying initial and final porosities, can be deduced from the models. Of these ranges only a few may be close to the true value of the porosity drop.

The two models developed for the purpose of estimating the porosity drop show that there are several ways in which to replicate the patterns seen in the various seismic examples of silica diagenetic boundaries. However, it is the porosity model that is the closest to real-life as it matches the parameters that can be worked out from the various seismic case studies. Hence, the diagenetic frontal morphologies modelled in this chapter can be replicated using porosity variations in the sediment and differential advancement of the opal-A to opal-CT boundary. This validates the earlier hypotheses of Davies (2005) and Meadows & Davies (2007), which stated that many of the morphologies were the result differential advancement and lateral variations in the host strata that affected the position of the DOC and caused folding in the overburden strata. The differential compaction due to silica diagenesis is a fundamental process previously unrecognised with respect to sedimentary basin analysis and porosity estimation.

In siliceous sedimentary successions, applying an exponential porosity trend may be inaccurate. This technique could be applied to some siliceous successions in extreme latitudes where the sediment is rich in biogenic silica, where the lack of commercial or scientific drilling means that no other prior information on porosity-depth functions is available.

Chapter 5: Discussion

5.1 Implications for the analysis of silica diagenetic boundaries worldwide

5.1.1 Stratigraphic position of the boundaries in relation to the present day seabed

Many of the first silica diagenetic boundaries to be identified were found to be parallel to the present day seabed (e.g. Hein *et al.* 1978). This observation, combined with the knowledge that the reactions are primarily controlled by temperature, led to the idea that diagenetic boundaries, specifically the opal-A to opal-CT transition, could be used as isothermal markers which would represent the temperature at which conversion occurred (e.g. Kuramoto *et al.* 1992). However, this use of the diagenetic boundaries as isothermal markers has been based on the observation that some boundaries are parallel to the present day seabed, and the assumptions that the basin has a uniform geothermal gradient and that the reaction occurs at a single temperature. It needs to be taken into account that even if the boundary can be used as an isothermal marker, the temperature of conversion needs to be known as this temperature can be highly variable, ranging from 2 to 56 °C (Hein *et al.* 1978; Keller & Isaacs 1985; Nobes *et al.* 1992a; Bohrmann *et al.* 1994) for the opal-A to opal-CT reaction. To do this accurate temperature data would be required from well data to produce a geothermal gradient that could be used to calculate the temperature of conversion. As has been observed in Chapter 2 in the NSB, as well as in several other basins, the diagenetic boundaries do not have to be parallel to the present day seabed but can be parallel to other prominent stratigraphic boundaries. In the case of the NSB the boundaries mostly show a high degree of parallelism to an unconformity that is Late Miocene in age. When the boundaries are not parallel to the present day seabed they are not present day isothermal markers, but are probably palaeo-isotherms parallel to a palaeo-seabed. This has implications for the identification of diagenetic boundaries worldwide in terms of whether they are parallel to the seabed or not; unless the diagenetic boundaries are parallel to the seabed they are unlikely to be present day isothermal markers.

5.1.2 Boundary geometries

The silica diagenetic boundaries from the NSB, which are described in Chapters 2 and 3, are amongst the largest diagenetic front patterns to have been studied so far, covering an area of 107000 km^2. Silica diagenetic boundaries, exhibiting various morphological features, have been identified in several basins worldwide, but mainly in the basins of the northeast Atlantic

margin (Davies & Cartwright 2002; Davies 2005; Davies & Cartwright 2007). In the basins of the northeast Atlantic margin (Faeroe-Shetland, Vøring and Møre Basins) the morphologies of the diagenetic boundaries mostly adopt a cell-like or polygonal geometry as opposed to the geometries seen in the NSB that appear to be the result of the interference of the diagenetic boundaries with a layered stratigraphy. This cell-like geometry seen in the northeast Atlantic margin appears to mainly be the result of a combination of an underlying polygonal fault system and fluid flow along these faults enhancing the rate of conversion (Davies 2005). In the NSB there is no polygonal fault system that can influence morphology development; hence this specific polygonal geometry did not develop.

It is possible that the morphologies of the NSB are a more fundamental manifestation of the processes of silica diagenetic front advancement than the more specialised process, resulting from underlying polygonal faulting, seen in the northeast Atlantic margin (Meadows & Davies 2007). It is likely that morphology development in the NSB is controlled by a complex natural system, which is influenced by a combination of different factors. The variety of morphological features so far identified from only a small number of basins could indicate that with the increasing coverage of 2D and 3D seismic surveys further geometries associated with silica diagenetic boundaries could be described. This in turn could lead to integrated 2D and 3D seismic recognition criteria, similar to figure 3.2, which could aid seismic interpreters in identifying and describing silica diagenetic boundaries wherever they are recognised. Also increased identification of silica diagenetic boundaries and their associated geometries will lead to a greater understanding of the various processes, such as fluid flow, that govern silica diagenesis.

5.1.3 Porosity estimation

The ability to use differential compaction of the overlying strata associated with some of the diagenetic boundary morphologies could prove to be very useful. Using information derived from seismic data together with knowledge of initial porosity, the porosity drop associated with the opal-A to opal-CT reaction can be calculated. This method can be applied to any silica diagenetic boundary identified on seismic data, as long as there are some other data that can be used to estimate initial porosity. This method could also be used to compare the responses of different sediments in different basins, which will have different compositions, to the conversion of opal-A to opal-CT. For example, sediment with a higher biogenic silica content will have a different magnitude of porosity reduction than a sediment with a higher

detrital content (e.g. the sediment has a higher proportion of clay with respect to biogenic silica). With further work and data the porosity drop associated with the opal-CT to quartz boundary can be factored into the model to give a more complete porosity-depth trend for basins that contain siliceous sediments.

5.2 Use of diagenetic boundaries in basin analysis

Silica diagenetic boundaries can have several uses in basin analysis. The boundaries, especially the more easily identifiable opal-A to opal-CT boundary, can be used in conjunction with knowledge of the geothermal gradient and stratigraphic position as a potential isothermal marker. Due to the large areal extent of silica diagenetic boundaries its use as an isotherm can be applied across a basin wherever the boundaries are identified and where they are parallel to the seabed, hence are present day isothermal markers. If the boundaries are palaeo-isotherms parallel to a palaeo-seabed then they cannot be used as a present day temperature marker in the basin, but can be used to give an indication that the prevailing conditions in the basin have changed since the boundaries originally formed, which has caused the rate of conversion at the boundary to slow and therefore can no longer maintain parallelism with the present day seabed (see Chapter 2.9 and 2.10). The diagenetic boundaries can hypothetically be used to estimate the general heat flow within the basin. For example, a stratigraphic high in the boundary compared to adjacent parts of the boundary might indicate that there is higher heat flow at that point of the basin compared to those adjacent parts (see Chapter 3.5).

The differential compaction associated with the silica diagenetic boundaries, together with knowledge of initial porosity, can be used to give an indication of the porosity drop associated with the transitions (see Chapter 4). This in turn can be used to create a porosity-depth trend across the diagenetic boundaries for a basin containing siliceous sediments, which would be useful if little or no other data existed for that particular basin. This method to estimate the porosity reduction would only be able to be used if the magnitude of the differential compaction in the overlying strata was large enough to be detected on seismic reflection data.

5.3 Implications for hydrocarbon exploration

The high-amplitude, positive polarity, cross-cutting nature of the silica diagenetic boundaries mean that they have the potential to be mistaken for hydrocarbon flat spots, which exhibit

very similar attributes when seen on seismic reflection data (Fig. 5.1). There are several ways in which diagenetic boundaries and flat spots can be differentiated: (1) diagenetic boundaries are generally more laterally extensive and cover a greater area of a basin; (2) with increased quality of seismic reflection data diagenetic boundaries have been observed to be associated with various frontal/boundary morphologies (see Chapter 3, Fig. 3.2), which readily distinguish them from hydrocarbon flat spots; (3) flat spots are generally limited to structural traps, such as anticlines, while diagenetic boundaries are not; and (4) silica diagenetic boundaries will only occur in siliceous sediments, hence analysis of available well data will either indicate that diagenetic boundaries are present (by drilling through them) or if caution should be used in identifying cross-cutting, positive polarity, high-amplitude seismic reflections (if the wells show a high biogenic silica content of the sediment).

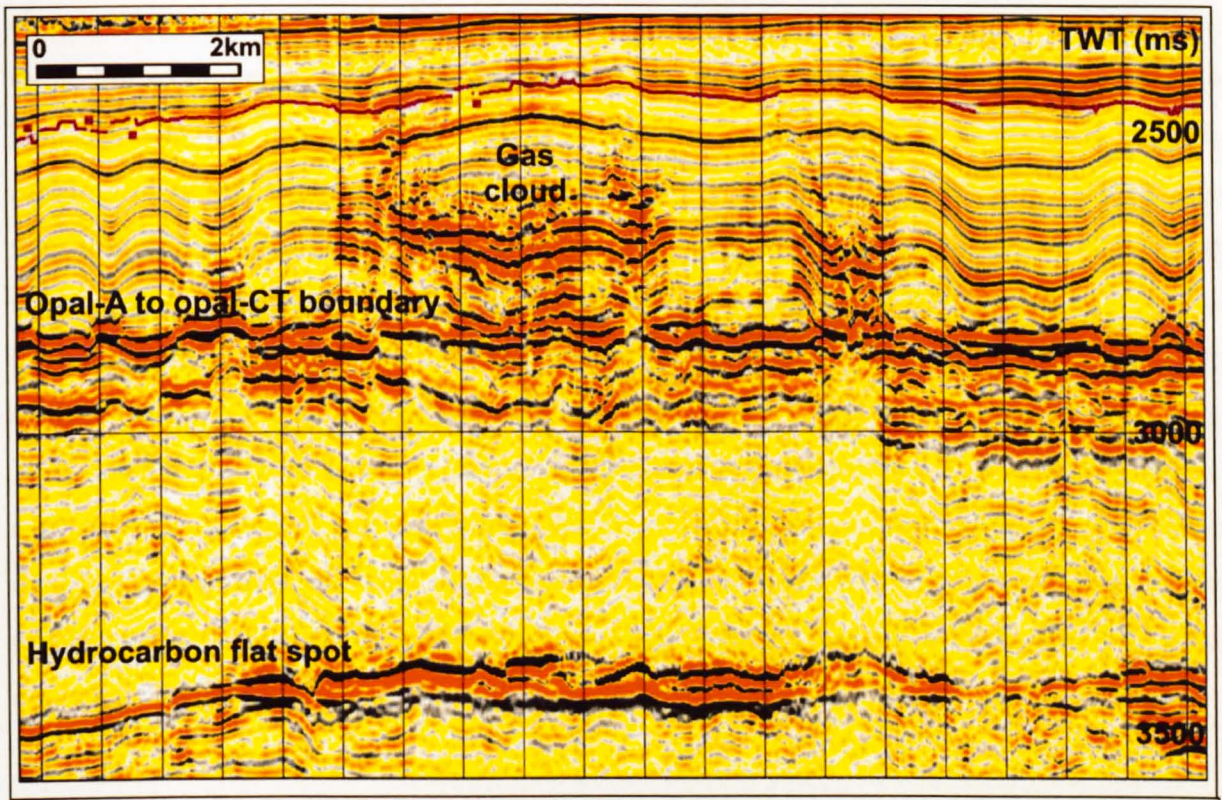

Fig. 5.1: Seismic line from the FSB illustrating the similarities between the reflections that represent silica diagenetic boundaries and hydrocarbon flat spots.

Any attempt to determine the thermal maturity of a basin using silica diagenetic boundaries as a present day isothermal marker, if they are not parallel to the present day seabed, could lead to significant errors and might result in potential source rocks being categorised as under or overmature and entire basins being written off as potential hydrocarbon reserves. Diagenetic boundaries could be useful in determining basin thermal maturity, especially in Arctic exploration, if enough time (thousands to millions of years –

e.g. Tada 1991) passes for the boundaries to acquire equilibrium with the prevailing conditions in a basin. However, they are easily disrupted by changing conditions and could display palaeo-isothermal behaviour as shown by some boundaries that develop parallel relationships to prominent stratigraphic horizons.

5.4 The need for well data

One of the prevailing issues concerning this thesis is the lack of well data to support the research. It is unfortunate there was limited access to well data for the various themes addressed in this thesis. However, the limited data available (see Chapter 1.6 and Appendix II) was sufficient to support the observations and interpretations derived from seismic data. Access to additional non-seismic data would have been useful as it would have provided more evidence to support the interpretations and would have provided additional analytical tools. For example, porosity data, both initial and final porosities, could have been used to help validate the method of estimating the porosity reduction; while detailed thermal, lithological and biostratigraphical data could have been useful to help understand the reasons why some silica diagenetic boundaries are parallel to prominent stratigraphic boundaries and are no longer isothermal markers parallel to the present day seabed. Such data would also have been useful to help understand the processes that cause the various frontal morphologies to develop along the diagenetic boundary. Finally a full set of geophysical attributes for the NSB, including P- and S-wave velocities and bulk density, could have been used to generate a synthetic seismogram for that basin. Then it would have been possible to tie the seismic data to the well data, showing conclusively that the high-amplitude, cross-cutting, positive polarity reflections were the result of physical property changes associated with the silica diagenetic boundaries.

5.4.1 IODP wells

Throughout the thesis available ODP wells have been used as a guide to understanding the physical property changes associated with the silica diagenetic reactions (see Chapter 1) and as a source of data to use as an estimate for initial porosity for nearby examples (see Chapter 4). However, the lack of IODP (formerly known as the ODP) wells specifically targeted to study a basin-scale occurrence of silica diagenesis has limited our understanding of the various aspects of this complicated phenomenon. It would be beneficial to have a dedicated IODP leg to study basin-scale silica diagenetic boundaries, such as those identified in the

FSB or NSB, with some of the wells located so that they drill some of the interesting boundary morphologies described by Davies (2005) and Meadows & Davies (2007). These wells would provide a full set of physical and chemical data that could be used in conjunction with seismic reflection data to analyse silica diagenetic boundaries.

5.4.2 What would be required for an ideal dataset?

Based upon what is written in sections 5.1 and 5.4 the following would be required for the ideal dataset:

- Extensive coverage of both 2D and 3D seismic reflection data over a particular basin in which silica diagenetic boundaries occur, to allow for detailed analysis of the morphologies and of the stratigraphic position of the boundaries.
- Wells drilled through both the opal-A to opal-CT and opal-CT to quartz boundaries to provide lithological, chemical and physical data above and below each of the boundaries.
- The physical data would ideally include: seismic velocities (both P- and S-wave), density and porosity, which would be useful in producing synthetic seismograms and calibrating porosity estimation using differential compaction.
- Additional data would also include information on sedimentation/burial rates both past and present, as well as geothermal data and any data that might indicate differences between the present day temperature and palaeo-temperature of a basin, such as vitrinite reflectance.

5.5 Geological phenomena associated with silica diagenesis

The silica diagenetic reactions are increasingly being linked to other geological phenomena which have been identified on seismic reflection data. These phenomena appear to originate from or have their bases at the silica diagenetic boundaries, particularly the opal-A to opal-CT boundary. This has led some to speculate (e.g. Volpi *et al.* 2003) that the reactions are initiating these features primarily through fluid expulsion caused by the dissolution-reprecipitation phase changes and porosity reduction, which in turn can lead to the generation of overpressure in the overlying strata.

5.5.1 Fluid flow due to silica diagenesis

The seismic reflection data from the NSB provides evidence for focussed fluid flow- and overpressure-features that have formed directly above the opal-A to opal-CT boundary. These features are probably related to the transition of opal-A to opal-CT causing porosity reduction and fluid expulsion (Davies *et al.* 2008). These features include normal faulting and fluid escape structures. Pairs of near-vertical normal faults occur in the sediment above the opal-A to opal-CT boundary, forming a 'horst and graben-style' pattern (red dashed lines and marked Z, Fig. 5.2). The faults generally begin at the opal-A to opal-CT boundary and tip out in the sediment ~500 m above the boundary. The faults show ~10-20 m of displacement and the distance between each fault pair is 0.5-1 km. Fluid escape structures occur as a column of downwarped and disrupted reflectors (marked X, Fig. 5.2) that originate at the opal-A to opal-CT boundary, which have pockmarks on the seabed (marked Y, Fig. 5.2) directly above the point of origin. Not all these structures reach the seabed. The columns are generally thinner at the base than they are at the top. The heights of the columns depend on the thickness of the sediment above the opal-A to opal-CT boundary, but are ~1 km wide.

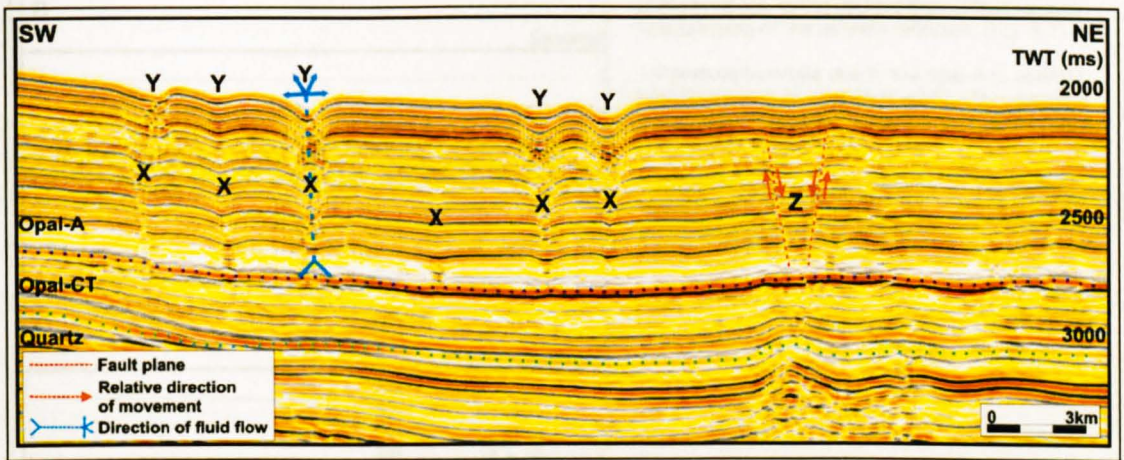

Fig. 5.2: Seismic line showing an example of structures resulting from overpressure release and fluid flow caused by the opal-A to opal-CT transition. Note the disrupted and downwarped reflectors (X) that originate from the opal-A to opal-CT boundary, which have pockmarks (Y) directly above them. These possibly result from the compaction of the strata due to fluid flow. A combination of pressure increase and fluid expulsion due to the transition can lead to expansion in the strata above the boundary resulting in normal faulting (Z).

Figure 5.3 shows how overpressure- and fluid flow-related features associated with the opal-A to opal-CT transition evolved. The transition of opal-A to opal-CT results in the expulsion of fluids (marked 3, Fig. 5.3B) into the porous sediments above the front due to the porosity reduction associated with the phase change. This can cause a zone of overpressure to form above the boundary (marked 4, Fig. 5.3B) if the overlying sediment has a low

permeability. The release of the overpressure (marked 5, Fig. 5.3C), possibly due to removal of overburden as a result of erosion (marked 8, Fig. 5.3C), causes a variety of features to form. Fluid escape structures (marked X, Fig. 5.2 and marked 6, Fig. 5.3C) form as a column that is sometimes topped by a pockmark if it reaches the seabed. Compaction in the bed sets above this part of the front due to the upward flow of fluids causes the downwarping of the seismic reflectors. Normal faulting (marked Z, Fig. 5.2 and marked 7, Fig. 5.3C) is caused by a combination of pressure increase due to the opal-A to opal-CT transition and fluid expulsion leading to expansion in the sediments above the front, which is accommodated by the generation of a series of normal faults.

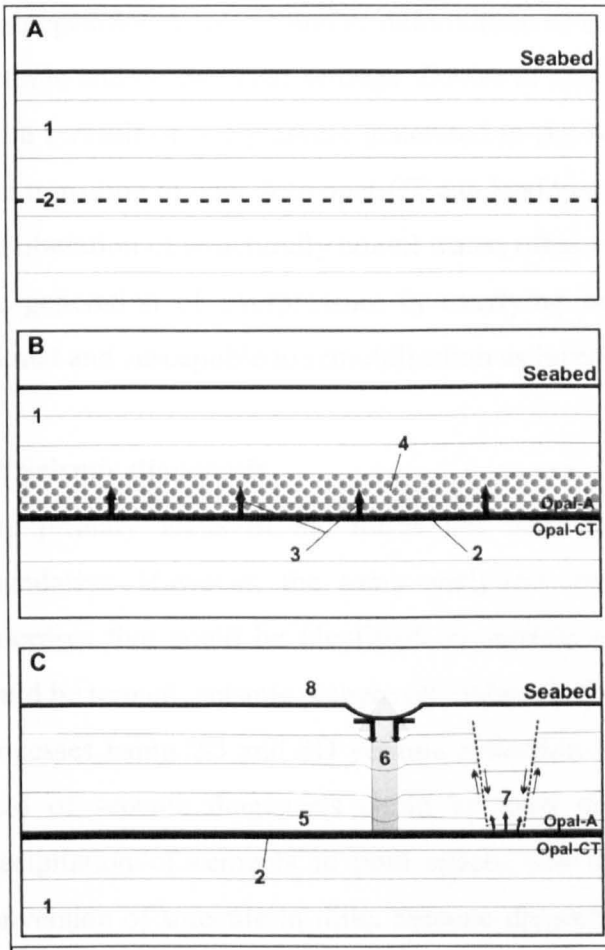

Fig. 5.3: A 3-stage schematic model showing the evolution of overpressure- and fluid flow-related features associated with the opal-A to opal-CT transition. **(A)** Deposition of the diatomaceous sediments and burial to the depth of conversion (DOC) where the opal-A to opal-CT diagenetic front forms. **(B)** The transition of opal-A to opal-CT leads to the expulsion of fluids (3) due to the porosity reduction causing a zone of overpressure (4) to form above the front. **(C)** The release of the overpressure (5), possibly due to the erosion of the overburden (8), causes a variety of features to form (6 and 7). See text for further explanation.

5.5.2 Submarine slope failure triggered by silica diagenesis

Davies & Clark (2006) suggested that some submarine slope failures along the northeast Atlantic margin could be attributed to silica diagenesis. The rapid compaction and fluid expulsion associated with the transition of opal-A to opal-CT could lead to the overpressure of the overlying sediment. Overpressure reduces the shear strength of the sediment making it more susceptible to failure (Davies & Clark 2006).

5.5.3 Giant clastic injectites

Postdepositional soft sediment deformation is a common phenomenon that occurs in many tectonic and depositional settings. Davies *et al.* (2006) attributed large-scale clastic injectites to be a result of overpressure generated in the sediment by transition of opal-A to opal-CT. The transition of opal-A to opal-CT can lead to a sudden, marked reduction in porosity and to the liberation of structurally bound water, often at shallow depths (<0.5 km). This can lead to the generation of overpressure in overlying sediments, hence rendering these sediments primed and susceptible to remobilisation as injectites (Davies *et al.* 2006).

5.6 Seismic diagenesis

The primary focus of the thesis has been the seismic expression of silica diagenetic boundaries. However, the same analytical methods can be applied to other diagenetic processes that could be identified on seismic reflection data. This investigative technique could be termed 'seismic diagenesis', which is defined in this thesis as the study of diagenetic processes using 2D and 3D seismic reflection data as the principal analytical method. The field of seismic diagenesis could be used on other diagenetic processes including the precipitation of cements in pore spaces and the transition of clay minerals, such as the conversion of smectite to illite. Seismic diagenesis can be applied to any diagenetic process that causes changes in the physical properties of the host sediment which in turn can be detected on seismic data. Seismic diagenesis provides an additional and useful investigative tool for use in the fields of basin analysis and hydrocarbon exploration.

5.7 Remaining questions and uncertainties

Most of the mechanisms for the development of regional-scale diagenetic front morphologies, palaeo-isothermal behaviour of the diagenetic boundaries and for the parallel relationships

with specific stratigraphic horizons other than the seabed remain speculative in the absence of additional detailed borehole data. Hence, with respect to the NSB and many other basins where silica diagenetic boundaries have been observed, multiple scientific drilling, sampling and examination of such phenomena would be required. The main drawback in using differential compaction to model the magnitude of the porosity drop is that it probably only works for extreme and abrupt changes in porosity associated with silica diagenetic boundaries that are well imaged on seismic data. In other words, these extreme and abrupt changes in porosity produce differential compaction of the overburden above the opal-A to opal-CT boundary, which is large enough to be identified and measured on seismic data.

5.8 Implications of this thesis

The research presented in this thesis illustrates the potential of the use of seismic diagenesis as an investigative tool within the field of basin analysis. The analytical methods used in this thesis can be applied to other diagenetic processes that could potentially be identified on seismic reflection data. As a whole this thesis has contributed to our knowledge and understanding regarding the recognition and description of silica diagenetic boundaries on seismic data. Chapter 2 implies that when the silica diagenetic boundaries are not parallel to the present day seabed, but are parallel to other prominent stratigraphic horizons, such as unconformities, the boundaries probably cannot be used as present day isotherms with which to work out the thermal structure of a particular basin. This aspect of the thesis can be applied to analysis of the thermal structure of other basins where diagenetic boundaries are parallel to stratigraphic horizons other than the present day seabed. The boundary morphologies described in Chapter 3 increases the number of known morphologies associated with the silica diagenetic boundaries. This provides the basis of a standardised categorisation system (Fig. 5.4) for the recognition of these boundary geometries on seismic data from different basins worldwide. This thesis also provides a tentative explanation for the cause of these morphologies based upon fluid flow, fracturing and variations in lithology in addition to interaction with an inclined and deformed host strata. Chapter 4 provides a method of estimating the change in porosity across the opal-A to opal-CT boundary based upon the amount of differential compaction observed in the strata above the boundary and limited knowledge of initial porosity. This methodology can be applied to silica diagenetic boundaries or to any other process that causes significant amounts of differential compaction that can be identified on seismic data. This method would be very useful in basins where

there is extensive seismic data but limited well data. Hence the findings of the research presented in this thesis will prove applicable to many aspects of basin analysis.

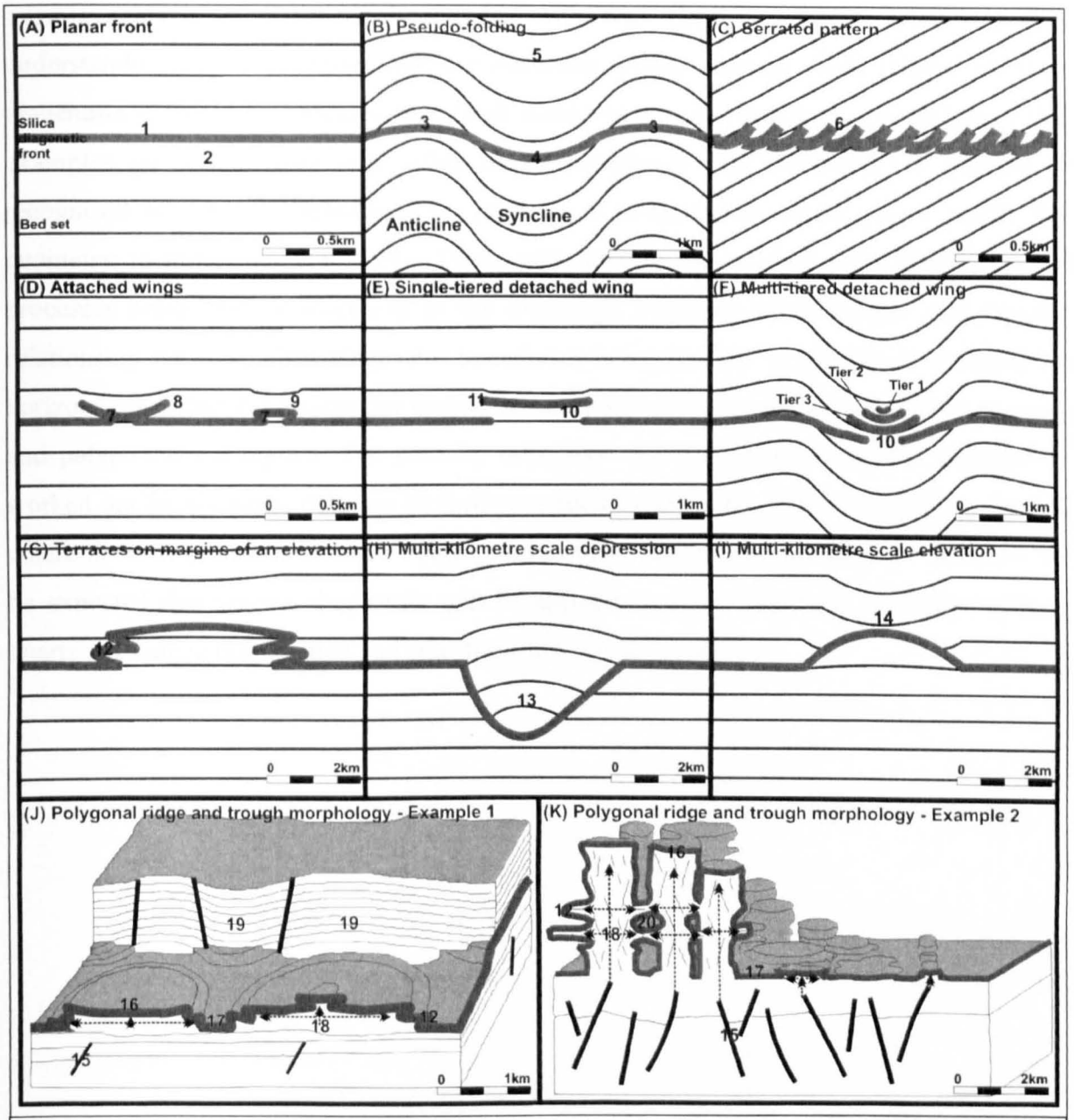

Fig. 5.4: Integrated schematic diagram summarising the key seismic attributes of various 2D (**A-I** – from figure 3.2) and 3D morphological features (**J** – modified from: Davies 2005; and **K** – modified from: Davies & Cartwright 2007). (1) Lack of frontal relief; (2) Track stratigraphy; (3) Pseudo-antiform; (4) Pseudo-synform; (5) Front is parallel to a higher stratal reflection; (6) Up-dip 'saw-tooth' pattern of front as it cross-cuts inclined stratigraphy; (7) Base attached to main diagenetic front; (8) Concave-upward shape with tapering margins; (9) Flat to dome shape; (10) Base detached from main diagenetic front; (11) Slight concave-upward to elongate shape; (12) Terrace; (13) Gentle antiformal folding; (14) Downward flexure of overlying sediment; (15) Polygonal faulting; (16) Ridge; (17) Trough; (18) Direction of diagenetic front advancement/fluid flow; (19) Differential compaction; (20) Merging of adjacent ridges as a result of lateral front advancement to eventually produce a planar front.

5.9 Future directions of research into seismic diagenesis

Much of the future research into seismic diagenesis will probably concentrate on integrating seismic analysis of diagenetic boundaries with well data to create a more complete understanding of the processes that are occurring within a basin. With respect to silica diagenesis it would be expected that there would be more research into identifying other examples on seismic data from other basins worldwide and expanding the amount of recognised boundary morphologies to produce a standardised categorisation system for geometry identification (Fig. 5.4). There will also be more work into identifying the processes behind the development of the diagenetic boundary morphologies and into the relationship between silica diagenetic boundaries being parallel to prominent stratigraphic horizons other than the present day seabed and how that probably relates to a basin's present- and palaeo-thermal regime. The porosity estimation method using differential compaction worked out from seismic data can be further applied by using the method on other examples where porosity reduction across a diagenetic boundary needs to be calculated. Finally, it can be expected that seismic diagenesis will be applied to other diagenetic processes such as quartz and calcite cementation and smectite-illite clay diagenesis.

Chapter 6: Conclusion

6.1 Reminder of aims and objectives

- To use 2D and 3D seismic reflection data to identify the diagenetic fronts and work out their morphology and areal extent.
- To understand the possible mechanisms and processes behind the development of the diagenetic boundaries.
- To understand the role that these diagenetic processes can potentially play within sedimentary basins, in terms of differential compaction and hydrocarbon exploration.

6.2 Summary of main findings (Fig. 6.1)

- Silica diagenetic boundaries are probably not present day isotherms where they have parallel relationships with prominent stratigraphic horizons other than the seabed (see Chapter 2, sections 2.8, 2.9, 2.10 and 2.12).
- Silica diagenetic boundaries of the NSB reveal a number of morphological features that form as a result of the interference of the diagenetic boundary with inclined and folded stratigraphy as well as with variations in fluid flow, lithology and fracturing of the host strata (see Chapter 3, sections 3.5, 3.6, 3.8 and 3.9).
- The differential compaction of the strata above the opal-A to opal-CT boundary on seismic reflection data can be used to try to estimate the magnitude of the porosity drop associated with the reaction (see Chapter 4, sections 4.4, 4.5, 4.6, 4.8 and 4.9).

6.3 Overall conclusions

Silica diagenetic boundaries are dynamic, time-dependent phenomena that have been overlooked in terms of their importance in the evolution of sedimentary basins. Seismic analysis has a significant role to play in understanding how the boundaries develop and how their formation changes the properties and structure of the host sediment. Analysis of seismic reflection data from basins where siliceous sediments predominate reveal a variety of morphological features associated with both the opal-A to opal-CT and opal-CT to quartz boundaries. These frontal geometries associated with silica diagenetic boundaries form as a result of the interference of the diagenetic front with inclined and folded stratigraphy as well as with variations in composition and rheology of the host lithology. The boundaries can be identified and correlated over regional scales, often covering areas of up to 10^5 km^2.

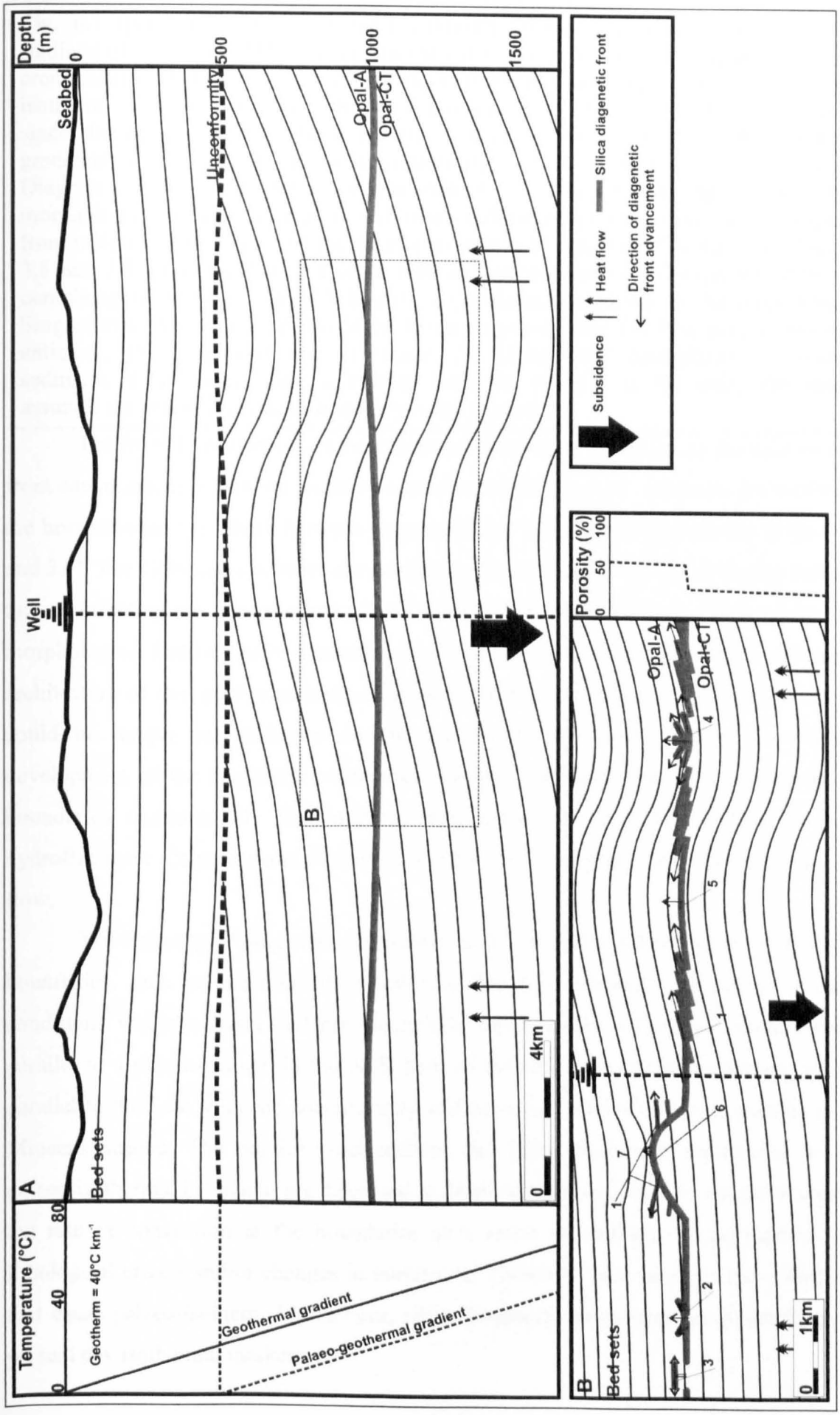
Temperature (°C)
0
40
80
A
Depth (m)
Seabed
0
Well
Unconformity
500
Opal-A
1000
Opal-CT
1500
Bed sets
Geotherm = 40°C km⁻¹
Geothermal gradient
Palaeo-geothermal gradient
B
4km
0
Subsidence
Heat flow
Silica diagenetic front
Direction of diagenetic front advancement
Porosity (%)
0
50
100
Opal-A
Opal-CT
1
2
3
4
5
6
7
1km

Fig. 6.1 (previous page): Schematic summary diagram showing some of the main findings of this thesis. **(A)** Diagram showing the opal-A to opal-CT diagenetic boundary, cross-cutting the host strata, parallel to an unconformity meaning it can be used a palaeo-isotherm. Assuming that the geothermal gradient is 40 °C km^{-1}, which has not altered since the development of the diagenetic boundary, the graph shows the geothermal gradients for the past (when the unconformity was the seabed) and present day. **(B)** Diagram showing the detail of the opal-A to opal-CT boundary. The various morphological features form as a result of a combination of interference of the diagenetic front with the stratigraphy and the development of seed areas (see Chapter 3 and Figs. 3.7, 3.8 and 3.9). The graph illustrates a typical porosity-depth trend expected from strata containing an opal-A to opal-CT boundary. (1) Serrated patterns; (2) Attached wing; (3) Single-tiered detached wing; (4) Multi-tiered detached wing; (5) Boundary cross-cuts an anticline; (6) Multi-kilometre elevation; (7) Differential compaction in overlying sediment. Both graphs were calculated from the position of the well. The diagram assumes the opal-CT to quartz boundary is not present.

The frontal geometries can be explained in terms of variations in the relative rates of front advancement, which are probably controlled by lithological variations, the inclination of the host strata and feedback between diagenesis and hydrofracture generation (Figs. 3.7, 3.8 and 3.9). The differences between the morphologies developed in different basins indicate the factors affecting the rate of advancement of the boundaries and the growth of the various morphological features differ depending on the stratigraphic, sedimentological and structural architecture of that particular basin. Therefore, within individual sedimentary basins there could be unique morphologies due to the differences in the factors controlling the development of the diagenetic boundaries. The factors that influence the geometry of the boundaries includes: (1) the location and extent of fluid flow conduits, such as hydrofractures; (2) pore water chemistry; (3) host rock lithology: and (4) variations in heat flow.

The tendency of diagenetic boundaries to be parallel to other prominent stratigraphic boundaries, such as unconformities, indicates that they are easily disrupted by changing conditions within a basin and can potentially develop into palaeo-isothermal boundaries parallel to a palaeo-seabed. In the NSB both of the silica diagenetic boundaries are mostly parallel to the Late Miocene unconformity and represent palaeo-isotherms parallel to a Late Miocene seabed. The possible mechanisms that cause diagenetic boundaries to exhibit palaeo-isothermal behaviour are discussed in detail in Chapter 2, but are related to changes in the rate of conversion at the boundaries as a result of changes in the thermal regime, lithological effects and/or changes in burial rate. Therefore, as a result of those mechanisms that cause palaeo-isothermal behaviour, silica diagenetic boundaries are probably not good present day isothermal markers.

The silica transitions are dehydration reactions that lead to the expulsion of water at the diagenetic boundaries which in turn leads to the generation of overpressure and fluid flow-related features in the sediments overlying the boundaries (Figs. 5.2 and 5.3). In this thesis it has been observed that differential advancement of the diagenetic boundaries, especially the opal-A to opal-CT boundary, can cause folding in the overburden. This differential compaction is the result of the significant porosity reduction associated with the reaction, which causes deformation in the overlying sediments. Where differential compaction takes place, areas of preferential front advancement are overlain by depressions caused by differential subsidence (Fig. 3.10 and 4.1). Using the amplitude of the folding due to differential compaction to try to estimate the magnitude of the porosity drop associated with the opal-A to opal-CT transition on seismic reflection data can be a viable method. However, it probably can only be used in specific circumstances where porosity reduction is significant. Therefore, this method should be acceptable for many uses, such as decompaction and basin modelling in extreme latitudes, where siliceous sediments predominate and there is a need for porosity-depth trends. This technique could be applied to some siliceous rich successions in extreme latitudes where biogenic silica is rich, where the lack of commercial or scientific drilling means that no other prior information on porosity-depth functions is available.

The recognition of silica diagenetic boundaries on seismic data has the potential to be an important aspect of basin analysis and hydrocarbon exploration. The diagenetic boundaries have a substantial effect on the surrounding stratigraphy through the generation of high-amplitude cross-cutting boundaries with varied frontal morphologies, the generation of fractures together with other fluid flow-related features and the development of differential deformation in the overburden. The precise diagenetic processes governing the development of silica diagenetic boundaries cannot be accurately determined using seismic reflection data alone and should be combined with other sources of available data. However, the visualisation of diagenetic boundaries within a basin using seismic reflection data can be a very useful analytical tool at this large regional scale.

References

Andrews-Speed, C.P., Oxburgh, E.R. & Cooper, B.A. 1984. Temperatures and depth-dependent heat flow in Western North Sea. *American Association of Petroleum Geologists Bulletin,* **68**, 1764-1781.

Barenblatt, G.I., Patzek, T.W., Prostokishin, V.M. & Slin, D.B. 2002. Oil deposits in diatomites: A new challenge for subterranean mechanics. *Society of Petroleum Engineers,* **75230**, 1-9.

Berndt, C., Bunz, S., Clayton, T., Mienert, J. & Saunders, M. 2004. Seismic character of bottom simulating reflectors: examples from the mid-Norwegian margin. *Marine and Petroleum Geology*, **21**, 723-733.

Bjørlykke, K. & Høeg, K. 1997. Effects of burial diagenesis on stresses, compaction and fluid flow in sedimentary basins. *Marine and Petroleum Geology,* **14**, 267-276.

Bohrmann, G., Abelmann, A., Gersonde, R., Hubberten, H. & Kuhn, G. 1994. Pure siliceous ooze, a diagenetic environment for early chert formation. *Geology,* **22**, 207-210.

Braaksma, H., Drijkoningen, G.G., Filippidou, N., Kenter, J.A.M. & Proust, J.N. 2006. The origin and nature of seismic reflections of sharp-based shoreface deposits (upper Jurassic siliciclastics, northern France). *Geophysical Prospecting,* **54**, 211-236.

Brekke, H., Dahlgren, S., Nyland, B. & Magnus, C. 1999. The prospectivity of the Voring and More basins on the Norwegian Sea continental margin. *In*: Fleet, A.J. & Boldy, S.A.R. (eds) *Petroleum Geology of Northwest Europe: Proceedings of the 5th Conference.* Geological Society, London, 261-274.

References

Brekke, H. 2002. The tectonic evolution of the Norwegian Sea Continental Margin with emphasis on the Vøring and Møre Basins. *In*: Nøttvedt, A. *et al.* (eds) *Dynamics of the Norwegian Margin.* Geological Society, London, Special Publications, **167,** 327-378.

Brettle, M. & Bessa, J. 2006. Eastern Sakhalin hydrocarbon systems analysis – the impact of uplift, erosion and bypass on reservoir distribution. In: *Oil and Gas Habitats of Russia and Surrounding Regions*, 8-9 February 2006. Geological Society of London, Burlington House, London.

Brown, A.R. 2003. *Interpretation of Three Dimensional Seismic Data (6th edn).* AAPG Memoir, **42,** Tulsa, OK.

Brown, R.J., Anderson, N.L. & Cederwall, D.A. 1996. A seismic analysis of differential compaction in the Frasnian Duhamel reef, south-central Alberta. *Computers and Geosciences,* **22,** 345-354.

Cartwright, J. & Huuse, M. 2005. 3D seismic technology: the geological 'Hubble'. *Basin Research,* **17,** 1-20.

Chaika, C. & Dvorkin, J. 2000. Porosity reduction during diagenesis of diatomaceous rocks. *American Association of Petroleum Geologists Bulletin,* **84,** 1173-1184.

Chaika, C. & Williams, L.A. 2001. Density and mineralogy variations as a function of porosity in Miocene Monterey formation oil and gas reservoirs in California. *American Association of Petroleum Geologists Bulletin*, **85,** 149-167.

Compton, J.S. 1991. Porosity reduction and burial history of siliceous rocks from the Monterey and Sisquoc Formations, Point Pedernales area, California. *Geological Society of America Bulletin*, **103,** 625-636.

Davies, D.J., McInalley, A. & Barclay, F. 2003. Lithology and fluid prediction from amplitude versus offset (AVO) seismic data. *Geofluids*, **3,** 219-232.

Davies, R.J. 2005. Differential compaction and subsidence in sedimentary basins due to silica diagenesis: A case study. *Geological Society of America Bulletin,* **117,** 1146-1155.

Davies, R.J. & Cartwright, J., 2002. A fossilized Opal A to Opal C/T transformation on the northeast Atlantic margin: Support for a significantly elevated palaeogeothermal gradient during the Neogene? *Basin Research,* **14,** 467-486.

Davies, R.J. & Cartwright, J. 2007. Kilometer-scale chemical reaction boundary patterns and deformation in sedimentary rocks. *Earth and Planetary Science Letters,* **262,** 125-137.

Davies, R.J. & Clark, I. 2006. Continental slope failures primed and triggered by silica diagenesis: A case study based upon 3D seismic data analysis. *Basin Research.* **18,** 339-550.

Davies, R.J., Cartwright J. & Rana, J. 1999. Giant hummocks in deep-water marine sediments: Evidence for large-scale differential compaction and density inversion during early burial. *Geology*, **27**, 907-910.

Davies, R.J., Huuse, M., Hirst, P., Cartwright J. & Yang, Y. 2006. Giant clastic intrusions primed by silica diagenesis. *Geology*, **34**, 917-920.

Davies, R.J., Goulty, N.R. & Meadows, D. 2008. Fluid flow due to the advance of basin-scale silica reaction zones. *Geological Society of America Bulletin*, **120**, 195-206.

Decker, K. 1991. Rhythmic bedding in siliceous sediments; an overview. *In*: Einsele, G., Ricken, W. & Seilacher, A. (eds) *Cycles and Events in Stratigraphy*: Springer-Verlag, Berlin, 464-479.

Diaz, J.I., Nelson, C.H., Barber, J.H. & Giro, S. 1990. Late Pleistocene and Holocene sedimentary facies on the Ebro continental-shelf. *Marine Geology*, **95**, 333-352.

Dzevanshir, R.D., Buryakovskiy, L.A. & Chilingarian, G.V. 1986. Simple quantitative evaluation of porosity of argillaceous sediments at various depths of burial. *Sedimentary Geology*, **46**, 169-175.

Eichhubl, P. 2004. Growth of ductile opening-mode fractures in geomaterials. *In*: Cosgrove, J.W. & Engelder, T. (eds) *The Initiation, Propagation, and Arrest of Joints and Other Fractures*. Geological Society, London, Special Publications, **231**, 11-24.

Eichhubl, P. & Behl, R.J. 1998. Diagenesis, deformation, and fluid flow in the Miocene Monterey Formation. *In*: Eichhubl, P. (ed) *Diagenesis, deformation, and fluid flow in the Miocene Monterey Formation*. Pacific Section SEPM, Special Publications, **83**, 5-13.

Eichhubl, P. & Boles, J.R. 1998. Vein formation in relation to burial diagenesis in the Miocene Monterey Formation, Arroyo Burro Beach, Santa Barbara, California. *In*: Eichhubl, P. (ed) *Diagenesis, deformation, and fluid flow in the Miocene Monterey Formation*. Pacific Section SEPM, Special Publications, **83**, 15-36.

Eldholm, O., Thiede, J., Taylor, E., et al., 1987. Proceedings of the Ocean Drilling Program, Initial Reports (Part A), **104**: College Station, Texas.

Emery, D. & Myers, K.J. 1996. *Sequence Stratigraphy.* Blackwell Publishing, Oxford.

Fournier, F., Dequirez, P.Y., Macrides, C.G. & Rademakers, M. 2002. Seismic data for characterisation of the Unayzah Formation in central Saudi Arabia. *Geophysics,* **67**, 1372-1381.

Gluyas, J. & Swarbrick, R. 2004. *Petroleum Geoscience*. Blackwell Publishing, Oxford.

Gross, M.R. 1995. Fracture partitioning: Failure mode as a function of lithology in the Monterey Formation of coastal California. *Geological Society of America Bulletin,* **107**, 779-792.

Guerin, G. & Goldberg, D. 1996. Acoustic and elastic properties of calcareous sediments across a siliceous diagenetic front on the eastern US continental slope. *Geophysical Research Letters,* **23**, 2697-2700.

Gutierrez-Alonso, G. & Gross, M.R. 1997. Geometry of inverted faults and related folds in the Monterey Formation: implications for the structural evolution of the southern Santa Maria basin, California. *Journal of Structural Geology*, **19**, 1303-1321.

Hein, J.R., Scholl, D.W., Barron, J.A., Jones, M.G. & Miller, J. 1978. Diagenesis of late Cenozoic diatomaceous deposits and formation of the bottom simulating reflector in the southern Bering Sea. *Sedimentology*, **25**, 155-181.

Hesse, R. 1990. Origin of chert: Diagenesis of biogenic siliceous sediments. *In*: McIlreath, I.A. & Morrow, D.W. (eds) *Diagenesis*. Geoscience Canada Reprint Series, **4**, 227-252.

Hinman, N.W. 1990. Chemical factors influencing the rates and sequences of silica phase transitions: Effects of organic constituents. *Geochimica et Cosmochimica Acta,* **54**, 1563-1574.

Hurd, D.C. 1972. Factors affecting solution rate of biogenic opal in seawater. *Earth and Planetary Science Letters,* **15**, 411-417.

Hurd, D.C. 1973. Interactions of biogenic opal, sediment and seawater in the Central Equatorial Pacific. *Geochimica et Cosmochimica Acta,* **37**, 2257-2282.

Isaacs, C. M. 1981. Porosity reduction during diagenesis of the Monterey Formation, Santa Barbara coastal area, California. *In*: Garrison, R. E. & Douglas, R. G. (eds) *The Monterey Formation and related siliceous rocks of California*. Los Angeles, SEPM Pacific Section, 257-271.

References

Isaacs, C.M. 1982. Influence of rock composition on kinetics of silica phase changes in the Monterey Formation, Santa Barbara area, California. *Geology,* **10**, 304-308.

Jones, J.B. & Segnit, E.R. 1971. The nature of opal: I. Nomenclature and constituent phases. *Journal of the Geological Society of Australia*, **18**, 57-68.

Karlo, J.F. & Gebhard, I. 2006. A screening view of prospectivity of the Northern Sea of Okhotsk. In: *Oil and Gas Habitats of Russia and Surrounding Regions*, 8-9 February 2006. Geological Society of London, Burlington House, London.

Kastner, M., Keene, J.B. & Gieskes, J.M. 1977. Diagenesis of siliceous oozes- I. Chemical controls on the rate of opal-A to opal-CT transformation- an experimental study. *Geochimica et Cosmochimica Acta*, **41**, 1041-1051.

Keller, M.A. & Isaacs, C.M. 1985. An evaluation of temperature scales for silica diagenesis in diatomaceous sequences including a new approach based on the Miocene Monterey Formation, California. *Geo-Marine Letters,* **5**, 31-35.

Khvedchuk, I. 1993. The petroleum basins of the Sea of Okhotsk. *American Association of Petroleum Geologists Bulletin* (abstract), **77**, 1637.

Kuramoto, S., Tamaki, K., Langseth, M.G., Nobes, D.C., Tokuyama, H., Pisciotto, K.A. & Taira, A. 1992. Can opal-A/opal-CT BSR be an indicator of the thermal structure of the Yamato Basin, Japan Sea. *Proceedings of the Ocean Drilling Program, Scientific Results,* **127/128**, 1145-1156.

Lancelot, Y. 1973. Chert and silica diagenesis in sediments from the central Pacific. *Initial Reports of the Deep Sea Drilling Project*, **17**, 377-405.

Langseth, M.G. & Tamaki, K. 1992. Geothermal measurements: Thermal evolution of the Japan Sea basins and sediments. *Proceedings of the Ocean Drilling Program, Scientific Results,* **127/128**, 1297-1309.

References

Lee, G.H., Kim, H., Jou, H. & Cho, H. 2003. Opal-A/opal-CT phase boundary inferred from bottom-simulating reflectors in the southern South Korea Plateau, East Sea (Sea of Japan). *Geophysical Research Letters,* **30**, 2238-2241.

Lindquist, S.J. 2000. The North Sakhalin Neogene Total Petroleum System of Eastern Russia. US Geological Survey Open-File Report **99-50-O**.

Lorenzo, J.M. & Hesselbo, S.P. 1996. Seismic-to-well correlation of seismic unconformities at Leg 150 continental slope sites. *Proceedings of the Ocean Drilling Program, Scientific Results,* **150**, 293-307.

Meadows, D. & Davies, R.J. 2007. Morphological development of basin-scale silica diagenetic fronts revealed with two-dimensional seismic reflection data: offshore Sakhalin, Russian Far East. *Journal of the Geological Society, London,* **164**, 1193-1206.

Mizutani, S. 1970. Silica minerals in the early stage of diagenesis. *Sedimentology*, **15**, 419-436.

Morse, J.W. & Casey, W.H. 1988. Ostwald processes and mineral paragenesis in sediments. *American Journal of Science,* **288**, 537-560.

Mountain, G.S., Miller, K.G., Blum, P., et al. 1994. Proceedings of the Ocean Drilling Program, Initial Reports, **150**: College Station, Texas.

Murata, K.J., Friedman, I. & Gleason, J.D. 1977. Oxygen isotope relations between diagenetic silica minerals in Monterey Shale, Temblor Range, California. *American Journal of Science,* **277**, 259-272.

Nobes, D.C., Murray, R.W., Kuramoto, S., Pisciotto, K.A. & Holler, P. 1992*a*. Impact of silica diagenesis on physical property variations. *Proceedings of the Ocean Drilling Program, Scientific Results,* **127/128**, 3-23.

Nobes, D.C., Langseth, M.G., Kuramoto, S., Holler, P. & Hirata, N. 1992*b*. Comparison and correlation of physical-property results from Japan Sea basin and rise sites, legs 127 and 128. *Proceedings of the Ocean Drilling Program, Scientific Results,* **127/128**, 1275-1296.

Pisciotto, K.A. 1981. Diagenetic trends in the siliceous facies of the Monterey Shale in the Santa Maria region, California. *Sedimentology*, **28**, 547-571.

Posamentier, H.W. & Kolla, V. 2003. Seismic geomorphology and stratigraphy of depositional elements in deep-water settings. *Journal of Sedimentary Research*, **73**, 367-388.

Ritchie, B., Birkeland, E., Hirst, P., Koblov, E., Salnikov, B. & Zharov, A. 2006. The Deriugin Basin, Offshore Sakhalin, discovery of a new play. In: *Oil and Gas Habitats of Russia and Surrounding Regions*, 8-9 February 2006. Geological Society of London, Burlington House, London.

Scott, S. K. 1994. *Oscillations, Waves and Chaos in Chemical Kinetics*. Oxford University Press, Oxford.

Simmons, J.L. & Backus, M.M. 1994. AVO modelling and the locally converted shear-wave. *Geophysics,* **59**, 1237-1248.

Spikes, K.T. & Dvorkin, J.P. 2003. Model-based prediction of porosity and reservoir quality from P- and S-wave data. *Geophysical Research Letters,* **30**, 2029-2032.

Tada, R. 1991. Compaction and cementation in siliceous rocks and their possible effect on bedding enhancement. *In*: Einsele, G., Ricken, W. & Seilacher, A. (eds) *Cycles and Events in Stratigraphy*: Springer-Verlag, Berlin, 480-491.

Tada, R. & Iijima, A. 1983. Petrology and diagenetic changes of Neogene siliceous rocks in Northern Japan. *Journal of Sedimentary Petrology*, **53**, 911-930.

Tamaki, K., Pisciotto, K., Allan, J., et al. 1990. Proceedings of the Ocean Drilling Program, Initial Reports, **127**: College Station, Texas.

Thein, J. & von Rad, U. 1987. Silica diagenesis in continental rise and slope sediments off eastern North America (Sites 603 and 605, Leg 93; Sites 612 and 613, Leg 95). *Initial Reports of the Deep Sea Drilling Project,* **95**, 501-513.

Tribble, J.S., Mackenzie, F.T., Urmos, J., O'Brien, D.K. & Manghnani, M.H. 1992. Effects of biogenic silica on acoustic and physical properties of clay-rich marine sediments. *American Association of Petroleum Geologists Bulletin*, **76**, 792-804.

Tull, S.J. 1997. The diversity of hydrocarbon habitat in Russia. *Petroleum Geoscience,* **3**, 315-325..

Volpi, V., Camerlenghi, A., Hillenbrand, C.-D., Rebesco, M. & Ivaldi, R. 2003. Effects of biogenic silica on sediment compaction and slope stability on the Pacific margin of the Antarctic Peninsula. *Basin Research,* **15**, 339-363.

Weaver, R., Roberts, A.P., Flecker, R. & Macdonald, D.I.M. 2004. Tertiary geodynamics of Sakhalin (NW Pacific) from anisotropy of magnetic susceptibility fabric and paleomagnetic data. *Tectonophysics,* **379**, 25-42.

Williams, L.A. & Crerar, D.A. 1985. Silica diagenesis: II. General mechanisms. *Journal of Sedimentary Petrology,* **55**, 312-321.

Williams, L.A., Parks, G.A. & Crerar, D.A. 1985. Silica diagenesis: I. Solubility controls. *Journal of Sedimentary Petrology,* **55**, 301-311.

References

Wilson, J.C.& McBride, E.F. 1988. Compaction and porosity evolution of Pliocene sandstones, Ventura Basin, California. *American Association of Petroleum Geologists Bulletin*, **72**, 664-681.

Worrall, D.M., Kruglyak, V., Kunst, F. & Kuznetsov, V. 1996. Tertiary tectonics of the Sea of Okhotsk, Russia: Far-field effects of the India-Eurasia collision. *Tectonics,* **15,** 813-826.

Yilmaz, O. 1987. *Seismic Data Processing.* Society of Exploration Geophysicists, Investigations in Geophysics, **2**, Tulsa, OK.

Appendix I: Seismic Interpretation and Processing Methodology

When studying the seismic data the following criteria were used to decide if a particular seismic horizon should be mapped: (1) is it important with respect to understanding the silica diagenetic processes, such as the diagenetic boundaries themselves; and/or (2) is it important to help understand the overall stratigraphy of the basin, such as the position of the top of the basement.

The following table shows a list of the seismic horizons mapped during the course of this project:

Horizon Name	Survey	Description
3d_dm_basement	3D	Top of the Cretaceous basement
3d_dm_ct	3D	Opal-A to opal-CT boundary
3d_dm_palaeosb	3D	Top of the Miocene strata (the Late Miocene unconformity)
3d_dm_qtz	3D	Opal-CT to quartz boundary
3d_dm_seabed	3D	Present day seabed
2d_dm_basement	2D	Top of the Cretaceous basement
2d_dm_ct	2D	Opal-A to opal-CT boundary
2d_dm_qtz	2D	Opal-CT to quartz boundary
2d_dm_seabed	2D	Present day seabed
2d_dm_uc	2D	Top of the Miocene strata (the Late Miocene unconformity)

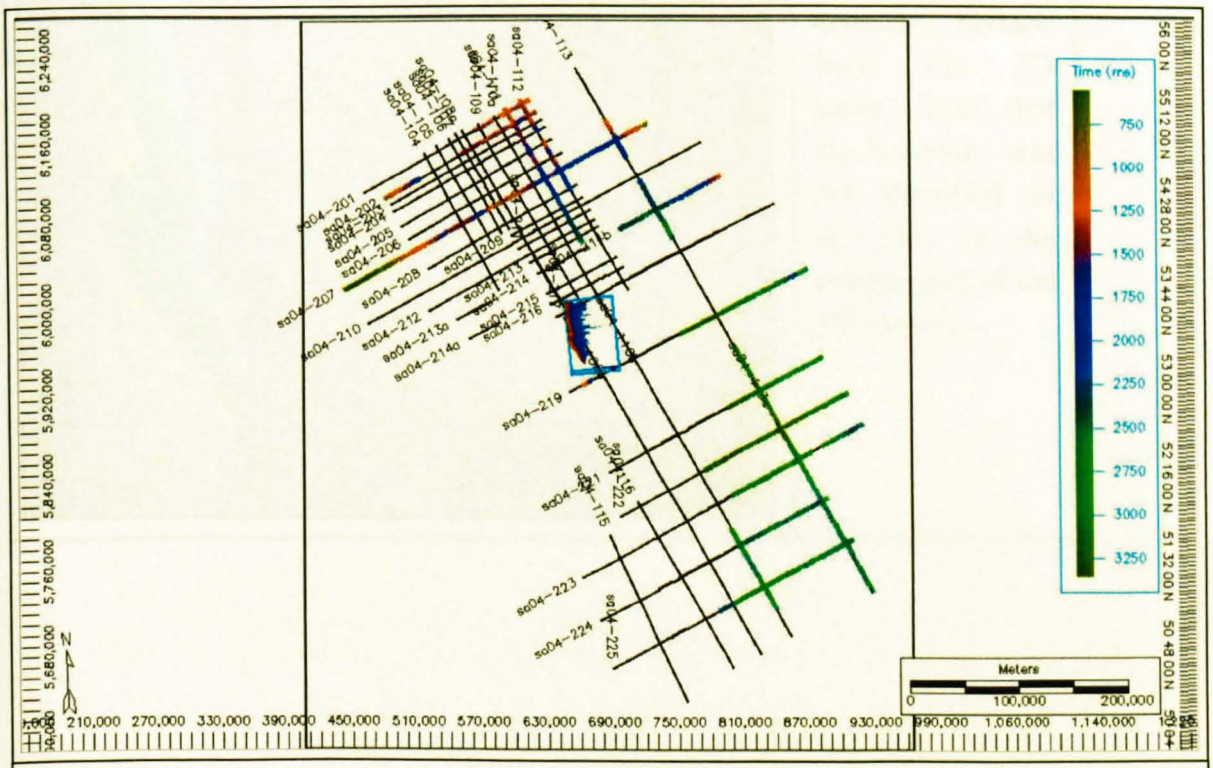

Fig. AI.1: Screenshot showing the positions of the seismic surveys in the NSB. The opal-A to opal-CT boundary interpretation is shown on this map. The blue rectangle on the map denotes the position of the 3D survey.

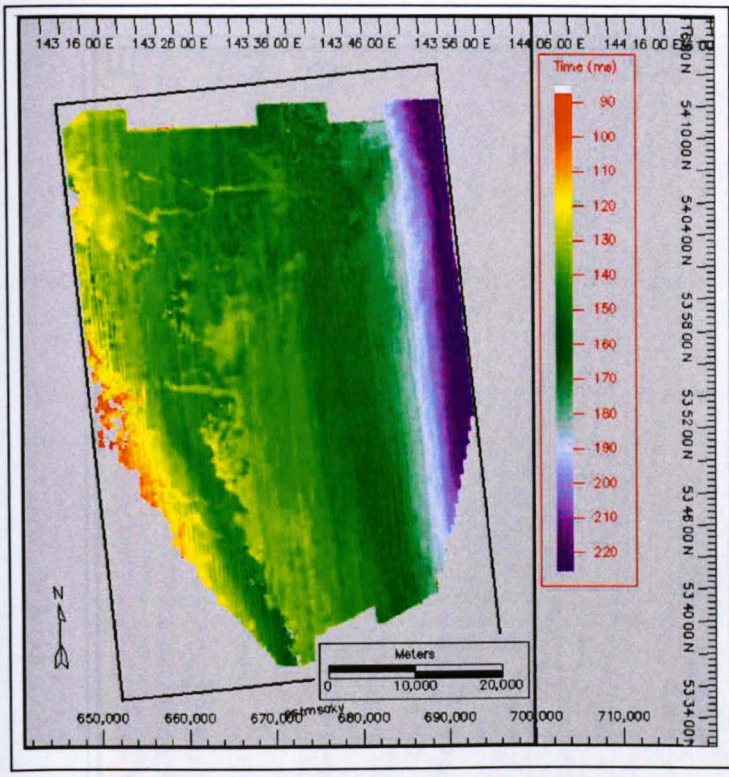

Fig. AI.2: Screenshot showing the interpreted seabed horizon from the 3D survey. Note that the seabed slopes away to the east, i.e. to the more distal parts of the NSB.

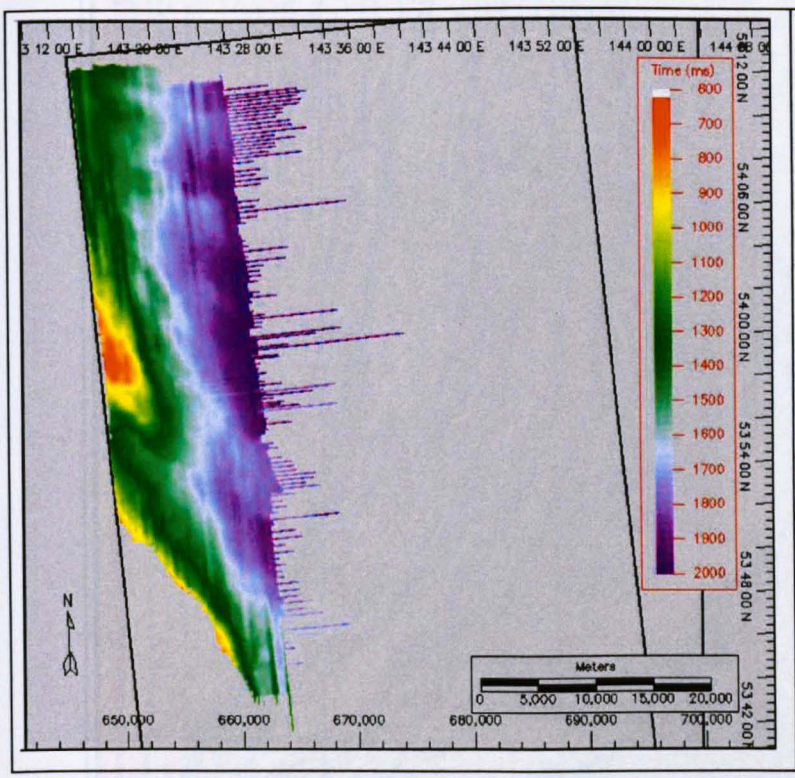

Fig. AI.3: Screenshot showing the interpreted opal-A to opal-CT boundary horizon from the 3D survey. Note that the boundary was not identified on the data in the eastern part of the 3D survey.

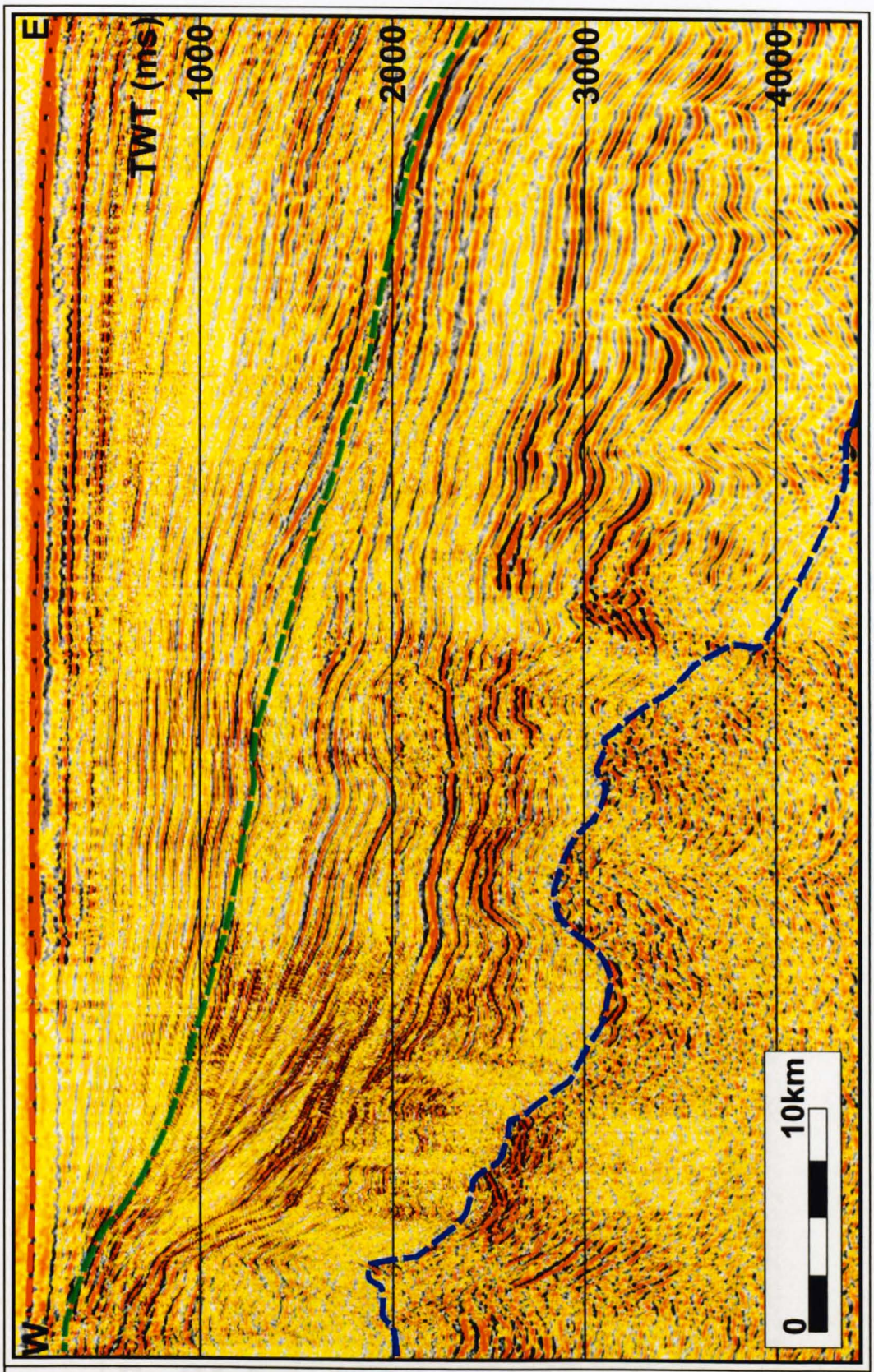

Fig. AI.4: Regional seismic line illustrating the tectono-stratigraphic setting of the NSB. The silica digenetic boundaries are not identifiable on this line. See figure 2.1 for the colour key to the stratigraphic subdivisions.

Fig. AI.5: Regional seismic line illustrating the tectono-stratigraphic setting of the NSB. Only the opal-A to opal-CT diagenetic boundary is identifiable on this line. See figure 2.1 for the colour key to the stratigraphic subdivisions.

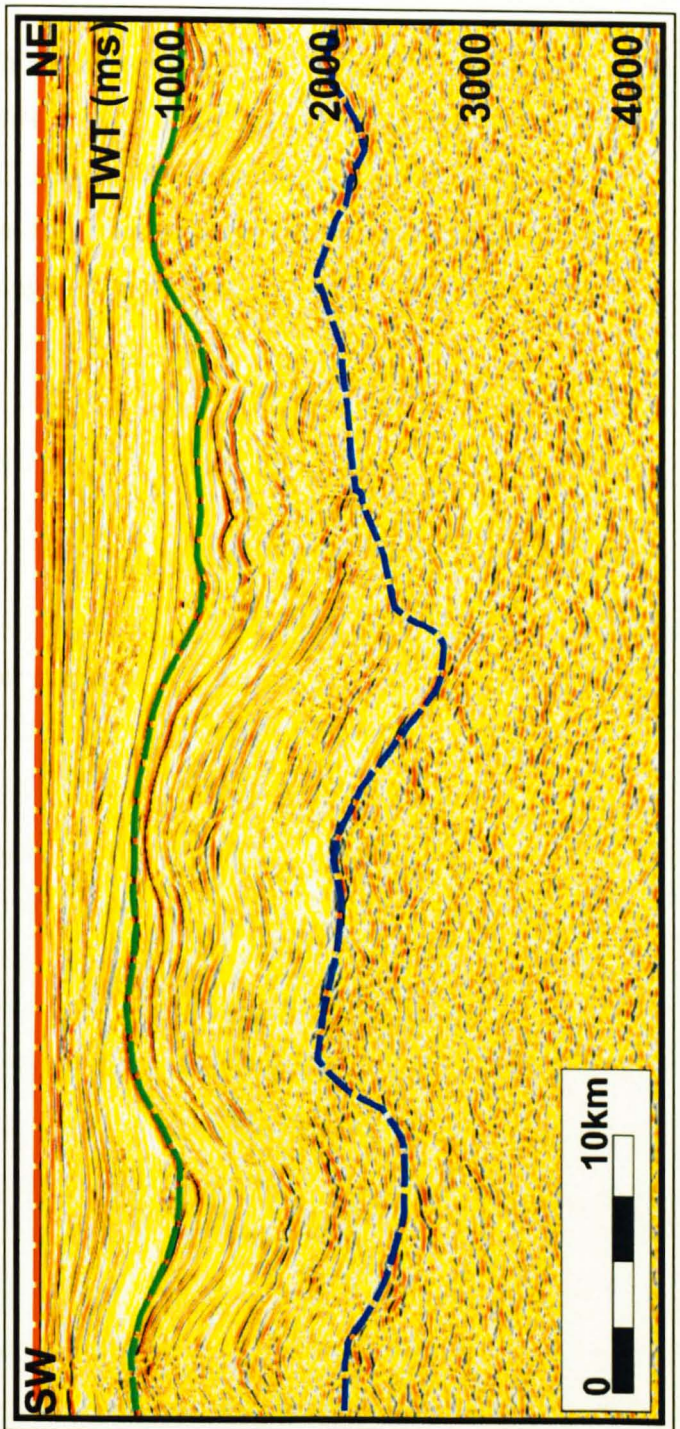

Fig. AI.6: Regional seismic line illustrating the tectono-stratigraphic setting of the NSB. The silica digenetic boundaries are not shown. See figure 2.1 for the colour key to the stratigraphic subdivisions.

Information regarding the seismic data:

Additional seismic parameter data associated with the NSB surveys:

Acquisition Date	Who	Depths: Source/Cable	Cable Length	Gun pressure	Near Offset	Filters	Sampling/Length
2004	DMNG/TGS	6m/8m	6000m	2000psi	125m	3-206Hz	2ms/8-12s

Field Recording *(This section is taken from a DMNG-TGS-NOPEC report on the seismic processing of the SA04 survey – permission to reproduce in this thesis granted by BP and DMNG-TGS-NOPEC. Report translated into English from Russian)*

Field seismic surveys for Project SA04 was carried by Seismic Vessel "Zephyr-1" in July-September 2004 using 120/80*-multiple CDP with end-on spread geometry and using hardware as follows:

Streamer

Streamer type	SYNTRAK RDA
Number of traces	480
Group length	12.5 m
Number of phones per group	16
Near trace	480
Near trace offset	125 m
Streamer depth	8 m

Seismic Source

Type	Tuned Bolt array
Gun volume	2940 cu in
Air pressure	2000 psi
Source depth	6 m
Shot point spacing	25/37.5* m

Recording details

Seismic Station		Syntrak 960-24
Filtering	Low Cut	3 Hz/12 dB
	High Cut	206 Hz/276 dB
Record length		8192/12288* msec
Sampling		2 msec
Record delay		60 msec
Tape format		SEG-D 8048

Note: * - characteristics for line SA04-110

Processing sequence *(This section is taken from a DMNG-TGS-NOPEC report on the seismic processing of the SA04 survey – permission to reproduce in this thesis granted by BP and DMNG-TGS-NOPEC. Report translated into English from Russian)*

Data processing was carried out on SUN Enterprise and IBM computers using processing packages GEOCLUSTER and PROMAX in September-December 2004. The processing sequence used on the seismic surveys is outlined in order below.

1. Data input, geometry

During data input SEG-D format was converted into Geovecteur format. Acquisition geometry was described in accordance with marine survey details and was entered into seismic trace headers. Raw data were amended with 60 sec owing to equipment delay.

2. Gain recovery/resampling

In the preprocessing stage, compensation of geometrical spreading effect was done using REFOR module with amplitude factor 1.5.

Thereafter, obtaining a final velocity model, dynamic compensations were reused with using SDICO module (subject to amendments for geometrical spreading as a function of velocity and offset) and EXPEN module for additional compensation of absorption and scattering effects.

Data resampling (from 2 msec to 4 msec) was carried out after band-pass minimum-phase filtering within 4-8-90-110 Hz frequency range.

3. Minimum phase deconvolution

Minimum phase deconvolution was carried out with using WAPCO module within 4-8-90-110 Hz frequency range. Deconvolution operator calculation was carried out as per signature calculated for actual used shot environments and seismic data recording.

4. First velocity analysis

Preliminary velocity analysis (VESPA module) was carried out discretely with line interval of 5000 m and creating super gathers from 15 CDP.

For Quality Control of the original wave field, control stacking was carried out with a 4 CDP increment.

5. F-K filtering and reduction

Suppression of low-velocity line interferences and partial removal of multiples was carried out using combined F-K filters as per seismograms SP (FKFIL module).

Filtering details are as follows:

Type of filter	Rejection filter
Filter details	EJ(-6000,-700,E99,P6)
	EJ(1000,2300,E99,P6)
Area of application	from seabed level
Tapering zone	500 msec
Filter details	EJ(1800,3100,E99,P6)
Area of application	500 msec lower than seabed level
Tapering zone	500 msec

Filtering was carried out with a frequency range of up to 110 Hz. All filters were used as an aliasing frequencies suppression option. Spatial smoothing of amplitude anomalies as shot point seismograms as well as a reduction/editing of reading with anomaly high amplitudes was carried out on statistical model basis using module SPASM.

6. Trace decimation

In order to eliminate random noise and non-coherent, near trace decimation was carried out in SP spacing with using MOSTA module. This procedure was carried out with using normal moveout corrections and subsequent redefinition of spread geometry.

7. F-K filtering

In order to suppress seabed multiple wave intensive background (waves with the velocity of 1470 m/sec) rejection filter was used (FKFIL module) as per CDP seismograms. Preliminary wrap around NMO with velocity of V=1470 m/sec were applied to seismograms. Filtering details:

Type of filter	Rejection filter
Filter details	EJ(-16500,-4500,E99,P6)
Area of application	T=LFD*1.7

Filtering was carried out with a frequency range of up to 100 Hz. Filter velocity details were defined after application of normal moveout corrections and apparent velocity correction V=10000m/sec.

8. Second velocity analysis

Second velocity analysis (VESPA) was carried out discretely with line interval of 2000 m. Stacking was carried out every 4 CDP for quality control. The results of velocity analysis were used for RADON-filtering procedure.

9. Predictive deconvolution

Predictive deconvolution was applied for recovery of higher frequencies, suppression of reverberation effect and short-period multiple waves. Deconvolution details were chosen on test basis as per the following procedure:

Prediction interval test	8-36 msec
Operator length test	120-600 msec
Operators calculation window test	1.5-4.0 s
and in running window with the space of 0.5 s.	
Combined multi-channel filter test	7-51 trace

As a result of testing deconvolution details accepted as follows:

Module	TRITA
Type	time-variant, multi-channel predictive deconvolution
Operator calculation windows	W 150 – W 2200 msec
	W 1700 – W 4500 msec
Operator length	L 360 / L 360 msec
Prediction interval	28 / 36 msec
Operator calculation base	31 trace
Calculation area	CDP

10. Multiple suppression

Suppression of multiple waves of different types as well as related circuit noises was carried out using RADON high-resolution parabolic transformation (RAMUR module). Details for calculation of primary and multiple waves model were chosen on basis of velocity model analysis.

Spatial parameters for filter using were tested:

NCX	30 – 120 traces
NCT	500 – 1200 msec

Processing parameters were accepted as follows:

Parabolas calculation zone	-960 / 6720 msec
Parabolas calculation space (DDT)	24 msec
Maximum band	100 Hz
Initial value of suppression zone (DTCUT)	100 msec
Basis of application (NCX, NCT)	60 traces / 1000 msec
Area of application	LFD * 1.5

11. DMO

DMO procedure was carried out using integral method (Kirchhoff) in KIDMO module.

12. Third velocity analysis

Velocity analysis (VESPA) after DMO procedure was carried out discretely with line interval 2000 m. The results of velocity analysis were used for seismic data migration.

13. Traces decimation

In order to decrease processing time the traces decimation was carried out within CDP (MOSTA module) before migration.

14. Prestack time migration

PSMIG module was used (realization of algorithm of phase shift) to perform prestack time migration. Migration was performed as per data with an application of normal moveout corrections with a frequency limitation in the range 4-100 Hz and conservable interface dip angle up to 70 degrees with the extrapolation spacing TAU 24 msec.

15. Fourth velocity analysis

After migration final velocity analysis (VESPA) was carried out with line interval 1000 m. Velocity details correction was carried out on basis of control stacking with changing of velocity data at range of +5% -5% with interval 2.5%. The results of velocity analysis were used to obtain final stacked sections as well as stacked sections on near and far trace offsets.

16. Stacking

Stacking was carried out on true-amplitude basis (ADPAM module) using external and internal muting (to suppress residual background of multiple waves). After moveout correction and directly before stacking the calculation and residual correction procedure was used for moveout curve correction (Time Varying Trim Statics – PROMAX) with search window 16 msec.

17. Demigration

Stacked time sections demigration was performed using PSMIG module - DEMIG option.

18. Migration

Time migration of seismic sections was performed using Kirchhoff algorithm (KIRCH module). Velocity details were primarily smoothed over on 160 CDP basis at the upper part of section and on 480 CDP basis at the lower part of section.

19. Multiple waves suppression

Suppression of residual background of multiple waves at the upper and middle parts of time seismic sections was performed using SPLAT module (in F-X area).

20. F-K filtering

Suppression of residual background of diffracted waves was performed using symmetrical rejection F-K filter at velocity range of 800-3300 m/sec. Sometimes additional F-K filter was used, in the variant of band-pass filter with velocity range of –4200/-2200 -- +2200/+4200 m/sec, with 40 Hz frequency limitation.

21. Band-pass filtering

Band-pass filters was chosen on test basis in the following consequence:

Enumeration of narrow-band filters

Enumeration of higher frequency filters with fixed lower frequency

Enumeration of lower frequency filters with fixed higher frequency

Enumeration of time-variant filters

Based on above test the following filtering details were accepted:

Filter 1

Frequency range (Hz)	Application window (msec)
4 – 7 – 80 – 85	0 – 700
4 – 7 – 50 – 55	2000 – 3000
4 – 7 – 25 – 30	5000 – 8000

Filter 2

Frequency range (Hz)	Application window (msec)
4 – 7 – 80 – 85	0 – 700
4 – 7 – 30 – 35	2000 – 3000
4 – 7 – 25 – 30	5000 – 8000

Filter 1 was used for line west ends;

Filter 2 was used for central and east parts.

Time sections filtering was carried out from seabed level.

22. Dynamic equalization

Time-variant dynamic equalization procedure was applied to final migrated time sections (DYNQU module) with the details as follows:

L – Operator length (msec)	Application window (msec)
L70	0-120
L 300	90 – 600
L 600	500 – 8000

23. Near/far trace stacking

Stacked sections of near/far trace offsets were obtained from migrated data using external and internal muting that provided division seismograms into two symmetrical (as per number of traces) parts. No further processing procedures were applied to these sections. All stacked time seismic sections are equated to sea level by application of static correction 10 msec.

Appendix II: Additional BP Data Relating to the NSB

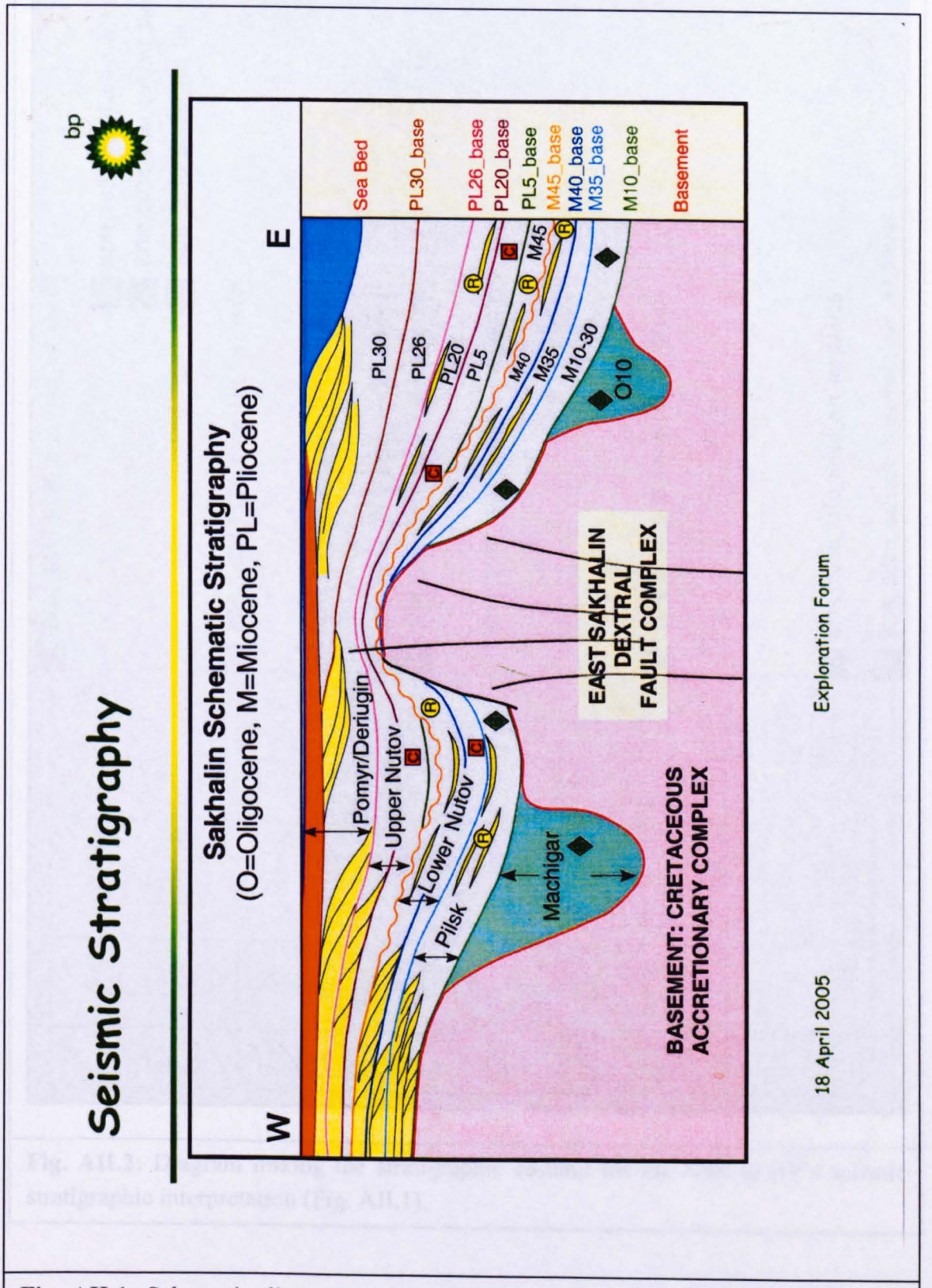

Fig. AII.1: Schematic diagram showing BP's seismic stratigraphic interpretation of the NSB, which the stratigraphic subdivisions in Chapters 2 and 3 were based upon.

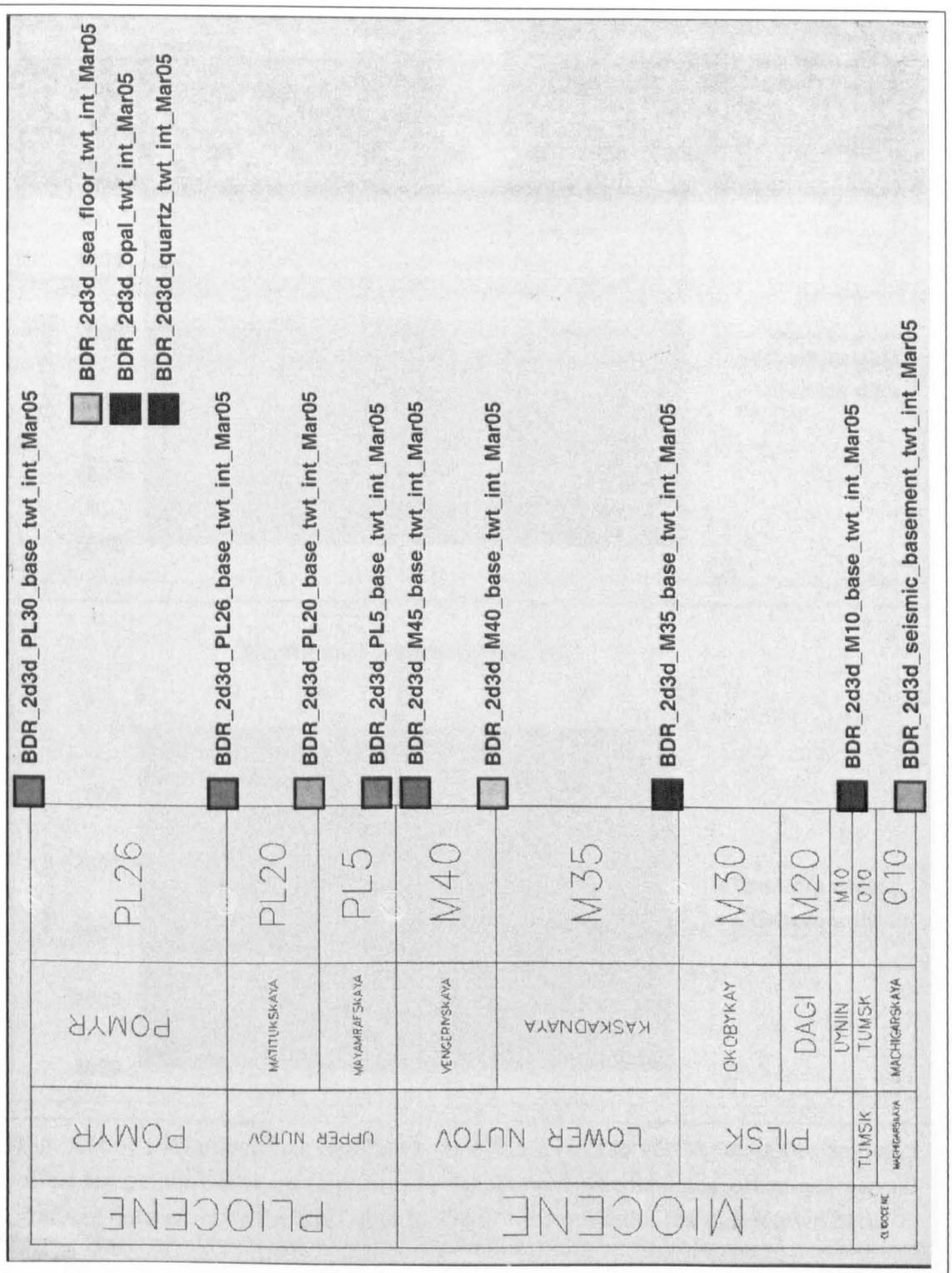

Fig. AII.2: Diagram linking the stratigraphic column for the NSB to BP's seismic stratigraphic interpretation (Fig. AII.1).

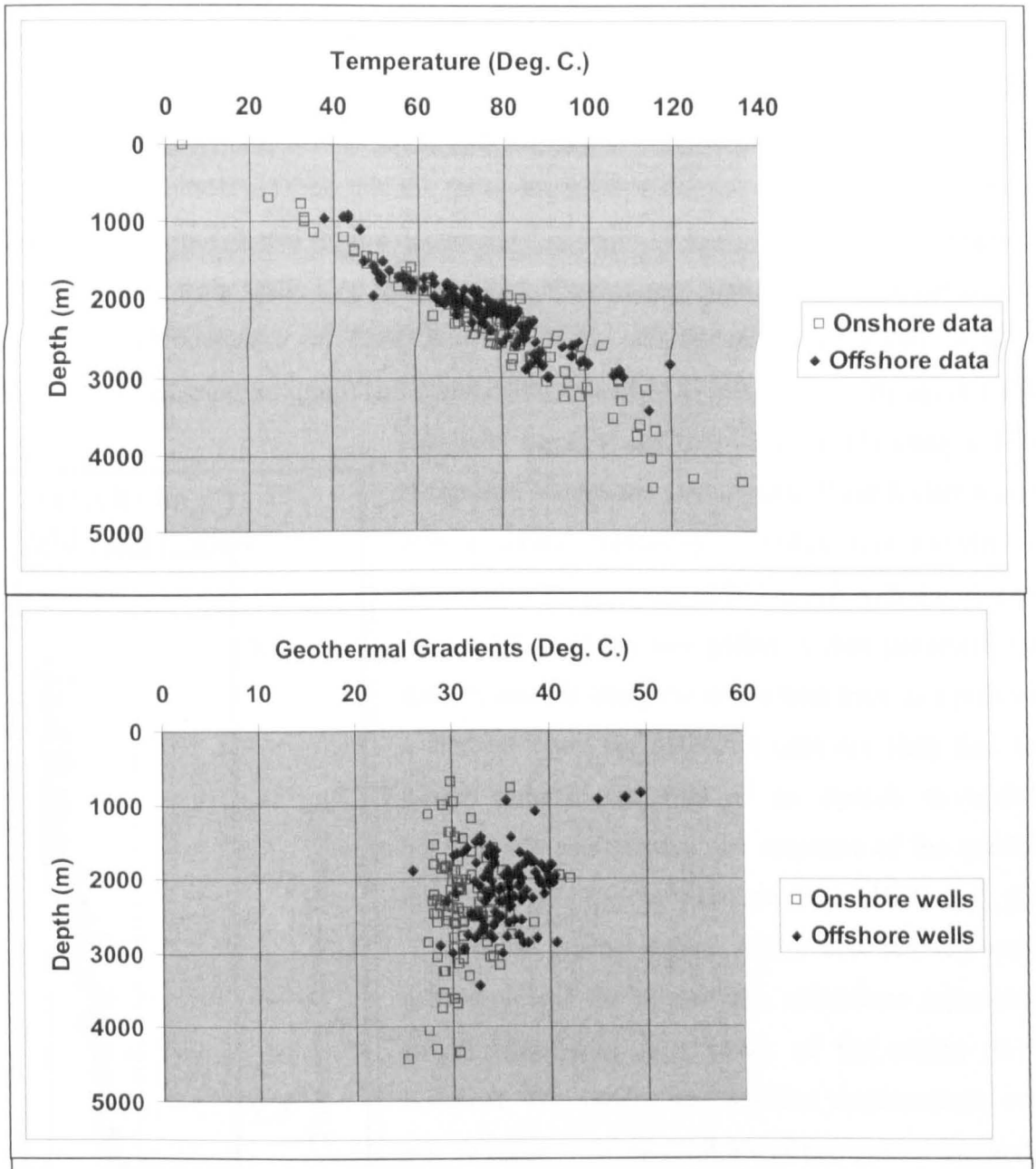

Fig. AII.3: BP temperature data from the NSB. **(Top)** Graph showing the Sakhalin offset temperature dataset. **(Bottom)** Graph showing the Sakhalin offset geothermal gradient dataset. Note the BHT data in Table 1.2 supersedes the data shown here.

Appendix III: Synthetic Seismic Modelling of Silica Diagenetic Reactions

In this section an attempt is made to replicate the seismic expression of the conversion of opal-A to opal-CT in seismic reflection data using physical property data to create a synthetic seismic shot gather, which will be compared to a real seismic example of an opal-A to opal-CT diagenetic boundary. To do this the following methodology is used: (1) P-wave velocity and density data are collated from a documented example of an opal-A to opal-CT boundary, in this case data from ODP Leg 150 Site 904, New Jersey continental slope, offshore NE United States (Mountain *et al.* 1994) is used; (2) the data are then loaded into *Promax* (a seismic data processing program) and converted into a table of interval velocity against TWT (two-way travel time) (Fig. AIII.1); (3) using a Finite Difference Model and a Minimum Phase Ricker wavelet with a central frequency of 60Hz, this wavelet was chosen as it gave an acceptable match with the observed data, a 1D synthetic shot gather is then generated (Fig. AIII.2); and (4) using the zero-offset trace as a proxy for a stacked trace the synthetic data are then tied to a nearby seismic example of an opal-A to opal-CT boundary to see whether the response of the synthetic matches that of the real example (Fig. AIII.3).

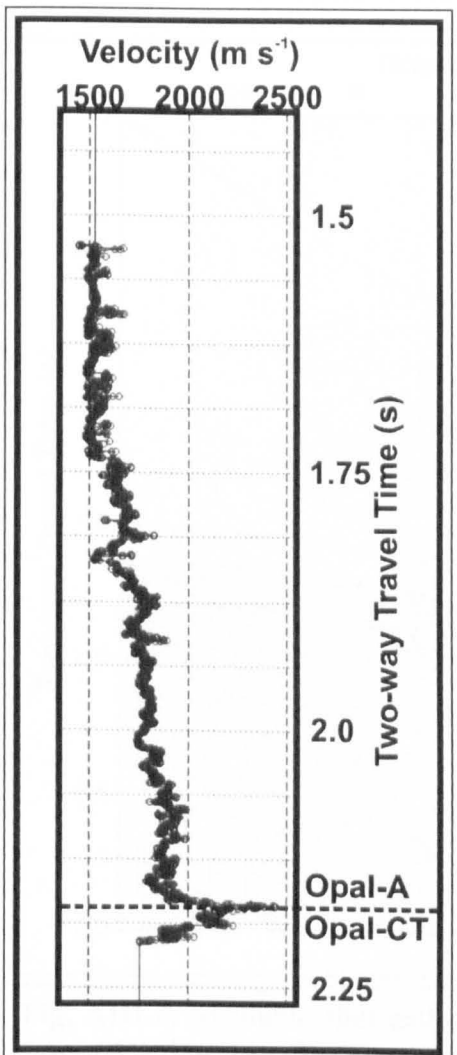

Fig. AIII.1: One-dimensional velocity diagram used to produce the synthetic shot gather (Fig. AIII.2).

The gap in figure AIII.2 between the seabed reflection and the rest of the reflections representing stratal boundaries is a result of the casing on the borehole. This means that wireline measurements could not be taken until the equipment had passed the bottom of the borehole casing. The depths were taken from information about Site 904 (see Mountain *et al.* 1994). The seabed is located at 1122.8 m below sea level with the bottom of the casing at 1216.7 m (93.9 m below the seabed). Generic values for P-wave velocity and density (1500 m s^{-1} and 1000 g cm^{-3}) were used to represent the layer between the seabed and the bottom of the casing in the synthetic model.

The synthetic shot gather in figure AIII.2 shows an event, which represents the opal-A to opal-CT boundary, located at a depth of ~2.18 s (in TWT). It is at this corresponding depth in the data where there is a sudden and dramatic increase in the P-wave velocity (Fig. AIII.1), which decreases slightly below the boundary. This velocity increase is a result of the physical property changes associated with the opal-A to opal-CT transition (Mountain *et al.* 1994). This event is slightly brighter in amplitude when compared to the rest of the synthetic seismogram (Figs. AIII.2 and AIII.3), i.e. the diagenetic boundary forms a distinct reflection with a positive polarity, which is commonly seen in other examples (e.g. the NSB).

The amplitude associated with the opal-A to opal-CT reflection on the synthetic seismogram gets larger with increasing offset (Fig. AIII.2). All the traces on the plot were scaled using a common gain so the increase of amplitude with offset at the opal-A to opal-CT reflection could be caused by an AVO (amplitude variation with offset) or interference of thin layers below the seismic resolution. However, the graph in figure AIII.4 suggests that the effect seen in figure AIII.2 is probably not an AVO. In figure AIII.4 the line representing the amplitude of the reflected P-wave (Rpp) generated from the Zoeppritz equations (e.g. Simmons & Backus 1994) is based on a simple interface between two layers above and below the opal-A to opal-CT transition, shows a slight decrease with increasing angle of incidence between 0° and 45°, where incidence angle is equivalent to offset. After 45° there is a rapid increase with increasing

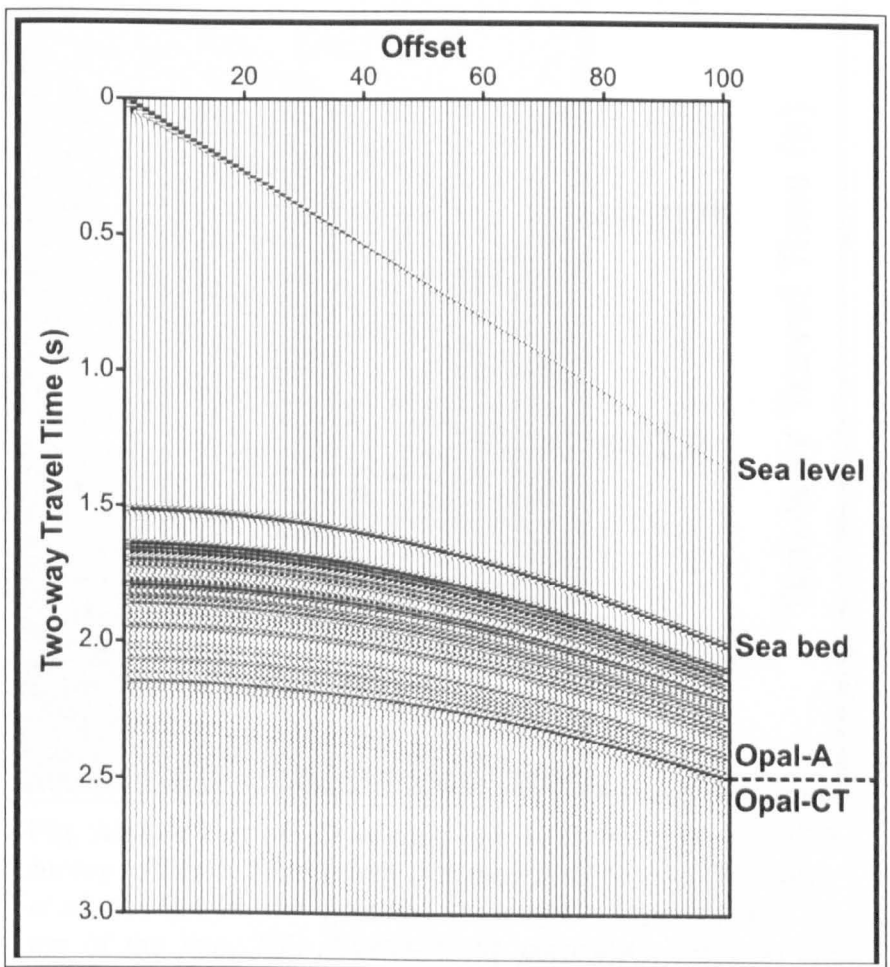

Fig. AIII.2: Synthetic shot gather generated using data collated from ODP Leg 150. The traces are approximately 20m apart, so the maximum offset is 2000 m.

angle of incidence until an angle of incidence of ~66° when it reaches the critical angle, i.e. the angle at which no P-wave energy is transmitted through the boundary. Therefore, for a simple interface you would not expect to observe a significant change in pulse of the silica transition reflection at limited amplitude offsets; hence it is likely that the apparent AVO on the synthetic seismogram is due to interference from reflections that form thin layers either side of the opal-A to opal-CT transition. The thin-scale layering either side of the diagenetic boundary is more geologically plausible (e.g. Fig. 1.8) than a simple two-layer model.

Figure AIII.3 shows a very good correlation between the synthetic seismogram and a 2D seismic line that is located next to Site 904. The correlation is fixed at the seabed and gives an excellent match at the reflector corresponding to the opal-A to opal-CT boundary. Some of the intermediate reflections do not match exactly, but this may be due to the location of the 2D seismic line and location of Site 904 not being a precise tie, errors in the generation of the synthetic seismogram or possibly a combination of these reasons. An attempt to correlate 2D seismic data to synthetic seismograms generated from well data at Leg 150 has been done before to correlate unconformities between sites (Lorenzo & Hesselbo 1996). Lorenzo & Hesselbo (1996) found that at Site 904 the diagenetic boundary created a strong reflection that could be mistaken for an unconformity. In conclusion, from these specific attempts to recreate the opal-A to opal-CT diagenetic boundary, the significant changes in physical properties, in this

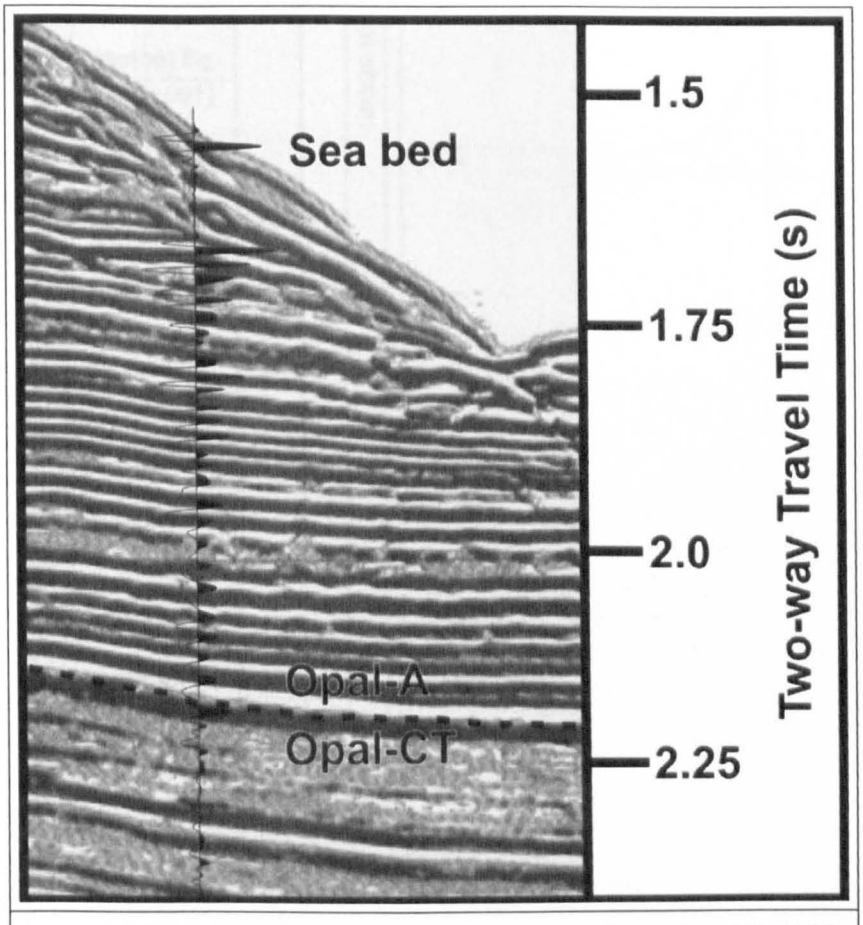

Fig. AIII.3: Part of 2D seismic line 1027 from the EW9009 survey (offshore New Jersey continental slope - see Mountain *et al.* 1994) with the synthetic seismogram superimposed on top of the line. This illustrates the correlation between the synthetic and actual seismic data with respect to the opal-A to opal-CT boundary.

case P-wave velocity and density that in turn relate to the dramatic reduction in porosity, produce a strong positive amplitude reflection on seismic data which represents the diagenetic transition of silica phases.

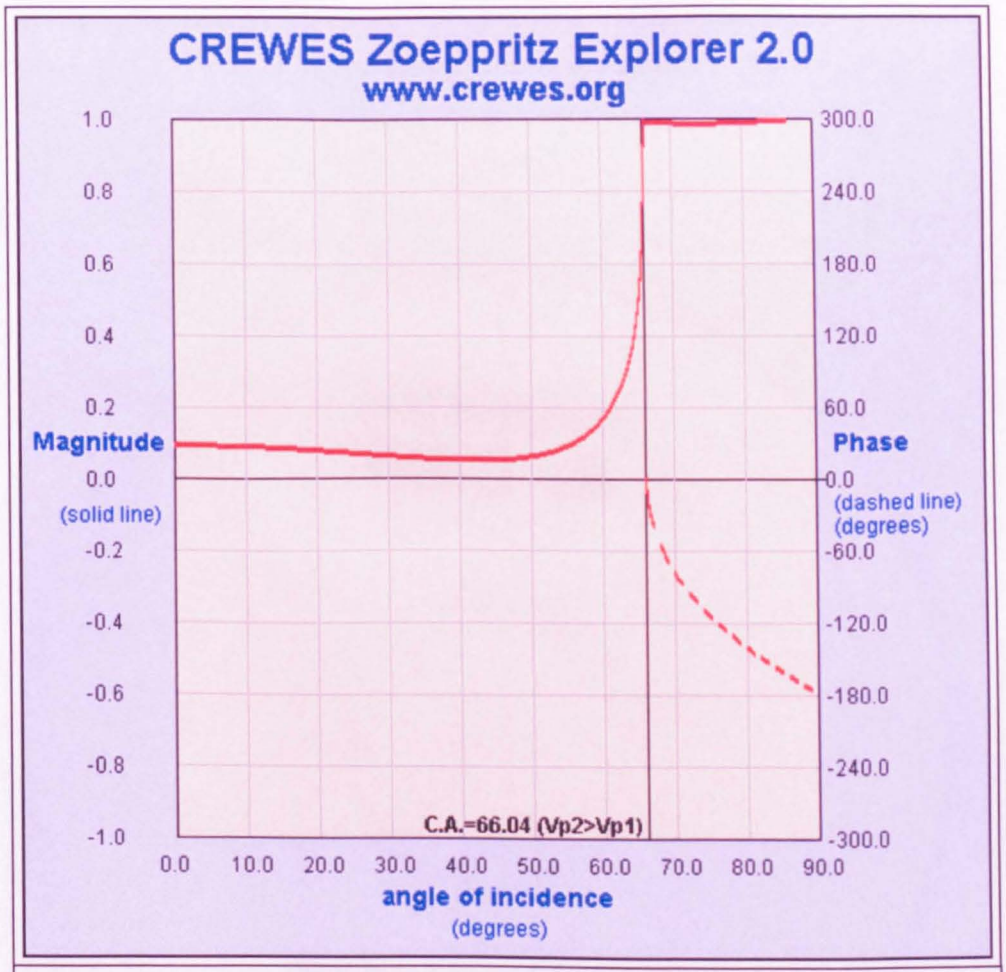

Fig. AIII.4: Screenshot of a graph (from www.crewes.org) for a Zoeppritz Equation solver. This can be used as a proxy for interpreting AVO effects. The red line represents the Rpp (reflected P-wave). The data that were input into the graph are shown in Table AIII.1.

	Density (kg cm^{-3})	P-wave Velocity (m s^{-1})	Estimated S-Wave Velocity (m s^{-1})
Upper layer	1772.6	1907.4	1101.2
Lower layer	1945.9	2087.2	1205.1

Table AIII.1: Table showing the data used to generate the graph in figure AIII.4. P-wave velocity and density were selected from one point just above and one point just below the opal-A to opal-CT boundary from the ODP Leg 150 Site 904 dataset (Mountain *et al.* 1994). The S-wave velocities were calculated using the following method: $Vs = Vp/\sqrt{3}$ (Richard Hobbs, pers. comm).